

Germline variants associated with immunotherapy-related adverse events

Stefan Groha^{1,2,13}, Sarah Abou Alaiwi³, Wenxin Xu⁵, Vivek Naranbhai⁵, Amin H. Nassar^{3,4}, Ziad Bakouny^{4,5}, Elio Adib^{3,4}, Pier V. Nuzzo^{3,6}, Andrew L. Schmidt⁵, Chris Labaki⁵, Talal El Zarif^{3,5}, Biagio Ricciuti⁸, Joao Victor Alessi⁸, David A. Braun³, Sachet A. Shukla^{2,5,7}, Tanya E. Keenan^{2,5,9}, Eliezer Van Allen^{2,5,10}, Mark M. Awad⁸, Michael Manos⁵, Osama Rahma^{4,5}, Leyre Zubiri¹¹, Alexandra-Chloe Villani^{2,12,13}, Christian Hammer¹⁷, Zia Khan¹⁷, Kerry Reynolds^{13,14}, Yevgeniy Semenov¹⁵, Deborah Schrag¹, Kenneth L. Kehl¹, Matthew L. Freedman^{2,5,*}, Toni K. Choueiri^{3-5,13,*}, Alexander Gusev^{1,2,13,16,*‡}

1. Division of Population Sciences, Department of Medical Oncology, Dana-Farber Cancer Institute, Boston, MA, USA
2. Broad Institute of Harvard & MIT, Cambridge, MA, USA
3. Lank Center for Genitourinary Oncology, Dana-Farber Cancer Institute, Boston, MA, USA
4. Department of Medicine, Brigham and Women's Hospital, Boston, MA, USA
5. Department of Medical Oncology, Dana-Farber Cancer Institute, Harvard Medical School, Boston, MA, USA
6. Department of Internal Medicine and Medical Specialties (DIMI), School of Medicine, University of Genoa, Genoa, Italy
7. Translational Immunogenomics Lab, Dana-Farber Cancer Institute, Boston, MA, USA
8. Lowe Center for Thoracic Oncology, Dana-Farber Cancer Institute, Boston, MA, USA
9. Breast Oncology Program, Dana-Farber/Brigham and Women's Cancer Center, Boston, MA, USA
10. Center for Cancer Precision Medicine, Dana-Farber Cancer Institute, Boston, MA, USA
11. Massachusetts General Hospital, Boston, MA, USA
12. Center for Immunology and Inflammatory Diseases, Department of Medicine, Massachusetts General Hospital, Boston, MA, USA
13. Harvard Medical School, Boston, MA, USA
14. Division of Medical Oncology, Bartlett, Massachusetts General Hospital, Boston, MA, USA
15. Department of Dermatology, Massachusetts General Hospital, Boston, MA, USA
16. Division of Genetics, Brigham and Women's Hospital, Boston, MA, USA
17. Genentech, South San Francisco, CA, USA

* Equal contribution

‡ Corresponding

Abstract

Immune checkpoint inhibitors (ICIs) have yielded remarkable responses in patients across multiple cancer types, but often lead to immune related adverse events (irAEs). Although a germline cause for irAEs has been hypothesized, no systematic genome wide association study (GWAS) has been performed and no individual variants associated with the overall likelihood of developing irAEs have yet been identified. We carried out a Genome-Wide Association Study (GWAS) of 1,751 patients on ICIs across 12 cancer types, with replication in an independent

cohort of 196 patients and independent clinical trial data from 2275 patients. We investigated two irAE phenotypes: (i) high-grade (3-5) events defined through manual curation and (ii) all detectable events (including high-grade) defined through electronic health record (EHR) diagnosis followed by manual confirmation. We identified three genome-wide significant associations ($p < 5 \times 10^{-8}$) in the discovery cohort associated with all-grade irAEs: rs16906115 near *IL7* (combined $p = 1.6 \times 10^{-11}$; hazard ratio (HR)=2.1), rs75824728 near *IL22RA1* (combined $p = 6.6 \times 10^{-9}$; HR=1.9), and rs113861051 on 4p15 (combined $p = 1.3 \times 10^{-8}$, HR=2.0); with rs16906115 replicating in two independent studies. The association near *IL7* colocalized with the gain of a novel cryptic exon for *IL7*, a critical regulator of lymphocyte homeostasis. Patients carrying the *IL7* germline variant exhibited significantly increased lymphocyte stability after ICI initiation than non-carriers, and this stability was predictive of downstream irAEs and improved survival.

Disclosures

D.A.B. reports nonfinancial support from Bristol Myers Squibb, honoraria from LM Education/Exchange Services, and personal fees from MDedge, Exelixis, Octane Global, Defined Health, Dedham Group, Adept Field Solutions, Slingshot Insights, Blueprint Partnerships, Charles River Associates, Trinity Group, and Insight Strategy, outside of the submitted work.

K.K. reports receiving honoraria from IBM and Roche.

M.M.A reports grants and personal fees from Genentech, grants and personal fees from Bristol-Myers Squibb, personal fees from Merck, grants and personal fees from AstraZeneca, grants from Lilly, personal fees from Maverick, personal fees from Blueprint Medicine, personal fees from Syndax, personal fees from Ariad, personal fees from Nektar, personal fees from Gritstone, personal fees from ArcherDX, personal fees from Mirati, personal fees from NextCure, personal fees from Novartis, personal fees from EMD Serono, personal fees from Panvaxal/NovaRx, outside the submitted work.

O.R. reports research support from Merck. Speaker for activities supported by educational grants from BMS and Merck. Consultant for Merck, Celgene, Five Prime, GSK, Bayer, Roche/Genentech, Puretech, Imvax, Sobi, Boehringer Ingelheim. Patent “Methods of using pembrolizumab and trebananib” pending.

S.A.S. reports nonfinancial support from Bristol-Myers Squibb, and equity in Agenus Inc., Agios Pharmaceuticals, Breakbio Corp., Bristol-Myers Squibb and Lumos Pharma.

T.K.C. reports research/advisory boards/consultancy/Honorarium (Institutional and personal, paid and unpaid): AstraZeneca, Aveo, Bayer, Bristol Myers-Squibb, Eisai, EMD Serono, Exelixis, GlaxoSmithKline, IQVA, Ipsen, Kanaph, Lilly, Merck, Nikang, Novartis, Pfizer, Roche, Sanofi/Aventis, Takeda, Tempest. Travel, accommodations, expenses, medical writing in relation to consulting, advisory roles, or honoraria. Stock options: Pionyr, Tempest. Other: Up-to-Date royalties, CME-related events (e.g.: OncLive, PVI, MJH Life Sciences) honorarium. NCI GU

Steering Committee. Patents filed, royalties or other intellectual properties (No income as of current date): related to biomarkers of immune checkpoint blockers and ctDNA. No speaker's bureau.

Z.B. reports research support from the imCORE Network on behalf of Genentech, Inc. and Bristol-Myers Squibb. Honoraria from UpToDate.

Introduction

Cancer immunotherapy has revolutionized cancer care by harnessing the patient's own immune system against tumors¹. However, because immune checkpoint inhibitors (ICIs) block the body's natural safeguards that prevent immune overactivation, treatment can also affect non-malignant tissues and cause autoimmune-like side effects²⁻⁵. Patients on ICIs thus commonly experience immune-related adverse events (irAEs)^{4,6,7}. High-grade irAEs can lead to hospitalization and treatment cessation in 15-30% of patients⁷, emphasizing the urgent need to understand mechanisms and predictors of irAEs. Recent studies have also shown that irAEs correlate with positive anticancer responses⁸, highlighting their relevance to broader therapy outcomes.

One hypothesis for the heterogeneity in irAE onset and severity is the impact of germline genetic determinants of immune activity⁶. Recent work has shown that polygenic germline risk for autoimmune conditions is correlated with onset of cutaneous and thyroid irAEs^{9,10}. Prior studies of response to ICIs have also highlighted both individual germline HLA alleles¹¹ and MHC diversity¹² as predictors of overall survival. However, no individual genetic variants associated with irAEs or response have so far been established. In this work, we hypothesized that individual germline variants may influence the broad spectrum of irAEs by modulating the general excitability of the immune system, as recently observed for somatic alterations^{13,14}. We carried out a Genome-Wide Association Study (GWAS) of irAEs for patients on ICIs at a single institution, followed by replication in patients treated at an independent institution and on clinical trials.

Results

Genome-wide Association Study of irAEs

We carried out a GWAS for two irAE phenotypes in 1,751 patients of European ancestry across 12 cancer types treated with ICIs at a single tertiary institution (DFCI cohort, Table 1, Figure S2). Two irAE outcomes were defined for each patient following treatment initiation: (1) "high-grade" irAEs (259 cases, 1375 controls) determined by manual curation of records following NCI CTCAE (v5) guidelines for grade 3-5 events, with attribution of AEs as being immune-related determined based on the clinical consensus of the patient's care team; (2) "all-grade" irAEs (339 cases, 1412 controls) algorithmically identified based on autoimmune-like EHR diagnosis codes (Supplementary Table S7) and including any high-grade irAEs, followed by manual review to exclude any events that were definitively linked to other causes. Detailed chart review in a subset of 44 patients found 85% of "all-grade" irAEs to be consistent with grade 2 or higher events (see Methods, Supplementary Table S10).

Three genome-wide significant loci ($p < 5 \times 10^{-8}$) were associated with all-grade irAEs: one near Interleukin 7 (*IL7*) at chr8q21, one near the Interleukin 22 Receptor Subunit Alpha 1 (*IL22RA1*) at chr1p36, and the third association at chr4p15 (Figure 1, Figure S3). No genome-wide significant associations were identified for high-grade irAEs. We tested each SNP for association with individual irAE subtypes and found that all three SNPs were nominally significant across multiple irAE subtypes with no clear outliers (Figure S13, Table S8), and were significant in the 80% of patients on PD-1 ICIs (with insufficient power to test differences by drug class; Figure S5). Neither variant was associated with overall survival nor with death without irAEs, even though all all-grade irAEs were associated with longer overall survival in a time-dependent analysis (HR=0.78 [0.65-0.94], $p = 8.6 \times 10^{-3}$; Table S6), consistent with previous findings.

The lead 8q21 SNP was rs16906115, a common variant in an intron of *IL7*, with a hazard ratio HR=2.0 [1.6-2.5] ($p = 3.8 \times 10^{-9}$, HR corrected for imputation error, see Supplementary Note; Figure 2, Figure S7). Within individual cancer types, a consistent sign was observed in 9 out of 11 cancer types ($p = 2.7 \times 10^{-2}$ by a one-sided binomial test) with nominal significance ($p < 0.05$) in Non-Small Cell Lung Cancer, Melanoma, RCC, Bladder Cancer, Cancer of Unknown Primary, as well as the collection of “other” less common cancer types (Figure 2). The lead 1p36 SNP was rs75824728, a common variant in an intron of *IL22RA1*, with a hazard ratio HR=1.9 [1.5-2.4] ($p = 8.4 \times 10^{-9}$; Figure S4). This SNP was also nominally significantly associated with high-grade irAEs with a comparable effect size (HR=1.5 [1.1-2.0], $p = 0.015$; Figure S9). Within individual cancer types, the association was nominally significant in Non-Small Cell Lung Cancer, Melanoma, Breast Cancer, as well as the collection of “other” less common cancer types (Figure 2). The lead 4p15 SNP was rs113861051 with a hazard ratio HR= 2.0 [1.6-2.6] ($p = 1.1 \times 10^{-8}$) (Figure S4). We carried out a broad scan for germline, clinical, and somatic features (including tumor mutational burden) associated with irAEs or interacting with the identified SNPs but observed no significant associations after multiple test correction (Table S2), underscoring the contribution of these germline findings to irAEs.

We evaluated potential modifiers or interactions of the discovered associations. First, using a normative cohort of >23,000 non-ICI patients at DFCI, no significant association between any of the three SNPs and the time from sequencing to the first code-based “all-grade” event was observed (Figure S10), indicating that the SNP effects were highly specific to the ICI setting. Likewise, none of the three lead SNPs were significantly associated with prior autoimmune disease defined based on ICD codes, nor with a polygenic risk score (PRS) for autoimmune disease (see Supplementary Methods) either in the ICI cohort or in the non-ICI patients. Though ICD-based autoimmune disease definitions are likely to be incomplete, we verified that our prior autoimmune disease phenotype was significantly associated with irAEs (Figure S2) and germline polygenic risk for autoimmune disease ($p = 8.8 \times 10^{-4}$ in the ICI cohort, see Supplementary Note). Finally, we investigated various adjustments for the competing risk of death, immortal time bias, as well as inclusion/exclusion of individuals with immune-related diagnoses at the start of treatment and observed no significant impact on these associations (Supplementary Note, Figure S6).

Independent replication of the *IL7* variant

We evaluated the three discovery SNPs in two independent cohorts for replication (see Methods for cohort details). The rs16906115 variant near *IL7* replicated significantly (HR=3.6 [1.8-7.1], $p=2.8 \times 10^{-4}$) in an independent cohort of 196 patients on ICIs treated at Mass General Hospital (MGH cohort) with severe irAEs requiring hospitalization and confirmed by chart review (Figure 2, Figure S11, Figure S12). rs16906115 also replicated nominally (HR=1.2 [1.0-1.5], $p=0.05$) in a second cohort of 2,275 patients on clinical trials (CT cohort) for ICIs with grade 2-5 irAEs recorded as part the trial (Figure 2c). Although no significant outliers were observed, a test for heterogeneity of effect sizes across trials was nominally significant ($p=0.02$), primarily driven by the IMpassion130 triple-negative breast cancer study. Sub-analyses did not show significant associations with any other event grade (Figure S15, S16, S17) or irAE subtype (Figure S15, S18). The other two associations, rs75824728 near *IL22RA1* and rs113861051 at 4p15, did not replicate in either independent cohorts; although all three associations remained significant in a meta-analysis with the MGH cohort (due to data constraints, we could not perform a genome-wide meta-analysis with the CT cohort). Lastly, while this manuscript was in preparation, the variant near *IL7* was independently replicated in a third cohort of 214 melanoma patients on ICIs in the UK with severe (grade 3 or above) irAEs requiring corticosteroids, which was further molecularly characterized in parallel work⁴². Thus, the *IL7* associated variant replicated in three independent cohorts (Supplementary Table S5).

Colocalization of *IL7* GWAS variant with a novel *IL7* cryptic exon

We sought to identify a putative mechanism for the *IL7* locus by integrating our GWAS with molecular data. In tissue-specific expression quantitative trait loci (eQTLs) mapped by the GTEx consortium²⁰, the lead irAE SNP was significantly associated with *IL7* exon junction usage in testis for the chr8:78740082:78749524 junction (which we call *IL7*_{unc}) and had an R^2 of 0.98 to the lead *IL7*_{unc} QTL (rs7816685), which was also in the irAE GWAS credible set (Supplementary Table S3, Supplementary Figure S8) (Figure S20). By inspection of the raw RNA-seq coverage and junction plots, we observed that carriers of the risk allele exhibited splicing and activation of a novel 250bp cryptic exon (spanning chr8:78746500-78746750, which we call *IL7*_{ce} for “cryptic exon”) that was entirely absent from all homozygous non-carriers (Figure 3a). The SNP had a stronger effect on *IL7*_{ce} and explained the association with *IL7*_{unc} in a conditional analysis, consistent with *IL7*_{ce} being the causal mediator (Figure S20). The lead *IL7*_{ce} QTL, rs7816685, was the only QTL located in the splice region of *IL7*_{ce} and was predicted to be -1bp from an Acceptor Gain region for *IL7* (delta score = 0.19 by SpliceAI²⁷) further implicating rs7816685 as the likely causal variant. Despite the increased expression in Testis, we did not find any association between sex and irAEs (Figure S25) nor any sex interaction ($p=0.28$), and we hypothesize that the effect was observed in Testis incidentally as this tissue contributes disproportionately to both cis and trans eQTLs identified in GTEx²⁰.

Considering *IL7*_{ce} as the putative functional mechanism, we next quantified its activity in a broader set of tissues and cell-types. Across the GTEx tissues, *IL7*_{ce} expression was generally low, with Testis and Lymphoblastoid Cell Lines (LCLs) exhibiting clear high outlier expression (Figure S21), the latter consistent with the role of *IL7* in lymphoid cell development. LCLs uniquely exhibited

significant correlation between $IL7_{ce}$ and total $IL7$ expression (Figure 3c) as well as significantly higher $IL7:IL7R$ co-expression in the presence of $IL7_{ce}$ ($P=3.4\times 10^{-3}$; Figure S21), suggesting that $IL7_{ce}$ may stabilize $IL7$ expression or increase $IL7R$ binding in lymphocytes. To better understand the precise cell-type of action, we mapped $IL7_{ce}$ in publicly available RNA-seq from sorted immune-related cells from patients with autoimmune diseases: $IL7_{ce}$ was highly expressed in B-cells and moderately expressed in CD4 T-cells, with no observable expression in the other immune cell types (Figure S22). Across 11,284 tumors from TCGA, $IL7_{ce}$ was associated with 13/61 previously defined immune landscape features¹⁴ (Bonferroni corrected $p<0.05$ after adjusting for cancer type and overall $IL7$ expression; Table S1) including: lymphocyte infiltration, BCR/TCR diversity, IFN-gamma response, and the “Wound Healing” immune cluster. In parallel work, the B cell specific effect of rs16906115 on $IL7$ was confirmed in melanoma patients receiving ICIs and its influence on T cell development further characterized⁴².

Association of $IL7$ variant with lymphocyte homeostasis

Due to the known role of $IL7$ in lymphocyte homeostasis²⁸, we explored whether the influence of rs16906115 on irAEs was reflected in peripheral blood lymphocyte count from clinical laboratory data. As a surrogate for lymphocyte expansion/homeostasis, we defined the change in lymphocyte count (δ_{LC}^{ICI}) using measurements 30 days before/after ICI initiation for patients in the DFCI and MGH cohorts. In the DFCI cohort, carriers of the risk allele exhibited no significant change in lymphocytes (median $\delta_{LC}^{ICI}=0.20$ [-0.80-1.2], $p=0.69$) whereas non-carriers had significantly reduced δ_{LC}^{ICI} (median $\delta_{LC}^{ICI}=-0.90$ [-1.3--0.50], $p=2.3\times 10^{-6}$ by paired Wilcoxon test); which replicated in the MGH cohort (median $\delta_{LC}^{ICI}=-5.1$ [-6.9--3.4] $p=4.1\times 10^{-8}$ for non-carriers; median $\delta_{LC}^{ICI}=0.05$ [-4.2,4.3], $p=0.99$ for carriers). The difference in δ_{LC}^{ICI} between carriers and non-carriers was significant in both the Profile cohort (difference in mean $\delta_{LC}^{ICI}=-1.1$ [-2, 0.0], $p=0.040$) and the MGH cohort ($\delta_{LC}^{ICI}=-5.4$ [-9.6,-1.0], $p=0.017$; Figure 4), as well as the independent analysis of melanoma patients receiving immune checkpoint inhibitors⁴². Similarly, δ_{LC}^{irAE} defined 30 days before vs. after irAEs was stable for carriers ($p=0.49$) but not for non-carriers ($p=2.2\times 10^{-3}$), though this association may be complicated by steroid usage (Figure S19). The $IL7$ variant thus had a consistent stabilizing effect on lymphocyte counts at the initiation of ICI therapy and at the onset of irAE. Results were similar when using absolute lymphocyte count (Supplementary Note). Lastly, we investigated whether this phenomenon pointed to broader lymphocyte dynamics irrespective of genotype status. Indeed, higher δ_{LC}^{ICI} was nominally associated with increased irAE incidence (HR=1.2 per s.d., $p=0.018$) and a concomitant increase in overall survival for those patients not experiencing any irAE (HR=0.87, $p=1.6\times 10^{-3}$) in the DFCI cohort.

Discussion

We conducted a GWAS of irAEs in an observational pan-cancer setting, identifying three novel genome-wide significant associations, with replication of a variant near $IL7$ in three independent cohorts. For the $IL7$ locus, we nominated rs7816685 as the likely causal variant, residing in the splice junction of a novel cryptic exon of $IL7$ and associated with broad differences in the tumor immune landscape.

Although the putative *IL7* mechanism identified in this work has not previously been linked to irAEs, *IL7* has been extensively studied for its involvement in immune response and auto-immune disease. *IL7* has a critical role in the development and maturation of T cells, limits organ toxicity during antiviral immune response, and supports aberrant immune activity in autoimmune disease²⁹. There is evidence that *IL7* expression blocks PD-1, leading to type 1 diabetes³⁰, as well as involvement in the development of chronic colitis³¹; functioning like a natural checkpoint inhibitor³². The administration of *IL7* in patients with cancer results in increased lymphocyte counts (particularly CD4+ and CD8+ T-cell counts) and reduced regulatory T-cell counts²⁸. It is therefore plausible that the *IL7* risk variant results in a more facilitatory milieu for autoimmune/autoreactive immune responses in patients on ICIs, explaining its association with irAEs. Several studies have shown that *IL7* receptor blockade can reverse autoimmune response^{30,33}, offering a potential therapeutic avenue for managing *IL7* mediated irAEs. These findings motivate further investigation into the influence of the *IL7* SNP and *IL7* splicing on ICI response, particularly for combination treatments.

Our study has several limitations. First, the heterogeneity of irAE presentation and severity led us to define two, partially overlapping outcomes. In the discovery GWAS, irAEs were manually abstracted from clinical notes as well as algorithmically inferred using EHR data (followed by manual quality control), and may have thus included some events with ambiguous causes, especially for irAEs that were observed well after the treatment was administered. This heterogeneity was highlighted by different associations with downstream survival, where DFCI all-grade irAEs were protective, DFCI high-grade irAEs were not associated with survival, and MGH high-grade irAEs were hazardous. The observational nature of the DFCI/MGH populations also limited the homogeneity of the cohort. Although we attempted to control for common covariates, most patients had a complex treatment history that could not be modelled. However, we expect this heterogeneity to primarily influence power and generalizability, as germline genetic variation cannot be *caused* by unmodelled confounders. Second, the influence of irAEs in risk allele carriers on downstream treatment decisions and the potential for germline-guided “decision support” is of great interest. While we attempted to annotate treatment discontinuation and steroid administration in carriers of the *IL7* risk allele (see Methods and Supplementary Table S9) we could not draw clear conclusions due to the limited data and high baseline rates of both outcomes. Ideally this relationship could be investigated in a prospective follow-up with strict monitoring of clinical decisions. Third, we restricted our study to individuals of European ancestry to mitigate possible population stratification, but further studies in non-European are warranted to understand the generalizability of these associations. In particular, the associated variant rs7816685 near *IL7* has an allele frequency of 0.31 in East Asian populations (compared to 0.065 in Europeans) and may thus explain more variance in irAEs in Asian patients. Lastly, the use of imputation from tumor-only panel sequencing for the discovery GWAS produced imputed variants with more noise than direct genotyping and likely excluded some difficult-to-impute or rare polymorphisms. This limitation also offers an opportunity for further analysis of this variant in existing panel sequencing datasets³⁴.

The identification of genetic variants associated with irAEs is consistent with a hypothesized patient-specific immunological set point and opens avenues for future analysis to inform the

genetic architecture of irAEs including: genetic correlation with other complex traits³⁵, polygenic risk scores for patient stratification³⁶, and Mendelian Randomization to estimate the causal influence of irAEs on other cancer outcomes³⁷. Larger studies will enable polygenic heritability analyses to uncover the cell types, gene sets, and pathways that drive these outcomes. Ultimately, the utility of these associations to identify high-risk patients for early monitoring or treatment modifications must be evaluated in prospective, randomized trials in conjunction with their influence on anti-tumor response.

Methods

Cohort definition, consent, and genotyping

Analyses were carried out across three cohorts with genotyping and clinical information (additional genotyping and phenotyping information provided in the Supplementary Note):

Dana-Farber Cancer Institute (DFCI) cohort: 1,751 patients of European ancestry (to avoid any confounding from population stratification) treated with ICIs (90% with PD-1/PD-L1) at DFCI from 2013 to 2020 (Table 1), across 12 cancer types. Patients were biopsied and sequenced on the OncoPanel tumor sequencing platform¹⁵ targeting 275-447 cancer genes and germline single nucleotide polymorphisms (SNPs) were imputed using ultra low-coverage off-target reads¹⁶ with imputation accuracy evaluated using a partially overlapping set of directly genotyped individuals (Figure S1). For normative comparisons, a pan-cancer control cohort of 23,763 individuals treated with non-ICI therapies at DFCI was similarly sequenced and imputed through the same pipeline. Patients provided informed consent for research and IRB approval was obtained (protocol #19-033 and #19-025).

MGH cohort: An independent pan-cancer cohort of 196 patients on ICIs at Massachusetts General Hospital (MGH) with direct germline genotyping on the Illumina Multi-Ethnic Genotyping Array (MEGA) (Table 1). Occurrence of high-grade irAEs (33 cases, 163 controls) was obtained through the Severe Immunotherapy Complications Program at MGH, for inpatient management of high-grade irAEs. Each high-grade irAE was clinically confirmed by an oncology team with expertise in diagnosing and managing irAEs and secondarily verified by organ-specific clinical irAE experts at the corresponding disease center. Secondary analyses of previously collected data were performed with approval from the Partners IRB (IRB protocol 2020P002307).

Clinical Trial (CT) replication cohort: A second replication analysis of individual associations was carried out in 2275 patients that were treated with atezolizumab (anti-PD-L1) and were of European ancestry and met sample and genetic data quality control from 12 previously published clinical trials sponsored by F. Hoffmann–La Roche/Genentech (Table S4). Studies included trials of atezolizumab in renal cell carcinoma (IMmotion, imm), lung cancer (IMpower, imp), triple-negative breast cancer (IMpassion, impas), urothelial cancer (IMvigor, imv), and advanced cancers (IDO; majority lung, breast, or ovarian). All patients provided informed consent for the respective main study. A subset of patients signed an optional Research Biosample Repository

(RBR) Informed Consent Form (ICF) to provide whole blood samples for future research, including study of inherited and non-inherited genetic variation from these whole blood samples. Ethics Committees (EC) and Institutional Review Boards (IRB) at each study site for each clinical trial approved the clinical trial protocol, the main study ICF, and the RBR ICF. Whole-genome sequencing data was collected from whole blood (as previously described⁹) and used to compute individual variant association statistics.

Statistical analysis

GWAS was carried out across all variants in the DFCI and MGH cohorts for association with time to irAE separately for each irAE definition. In all cohorts, individuals were restricted to European ancestry. Due to the competing risk of death while on treatment, a cause-specific hazard rate was computed for every SNP using a mixed-effects model¹⁷, equivalent to censoring on death or loss-to-follow-up. In each cohort, covariates were included for ancestry, age, gender, line/type of treatment (Supplementary Note). Statistical fine-mapping of genome-wide significant loci was carried out using the SuSIE software¹⁸. irAE probabilities and cumulative incidence were quantified using the Aalen–Johansen estimator, a non-parametric estimator that accounts for competing risks¹⁹. Associations between irAEs and overall survival were evaluated using a time-dependent covariate coded as 0 for controls and as 1 starting from the time of first irAE.

Analysis of molecular data

Associations were functionally characterized using publicly available gene expression and splicing data from multiple resources. Variants were connected to putative target genes using gene expression and splicing QTLs across 44 tissues from the GTEx consortium²⁰. RNA-seq BAM files were downloaded from the GTEx repository and splice junction usage was analyzed using ggsashimi²¹. Cell sorted data across 6 immune cell subsets from individuals with autoimmune diseases and healthy controls were accessed from ref.²² and GEO (SRP045500). Pan-cancer RNA-seq BAM files from TCGA were used to quantify expression across tumor sites²³ and correlated against previously defined immune populations and signals¹⁴. Analyses of read-level activity and cryptic splicing were carried out using the recount2 framework²⁴. Clinical lab measurements were extracted from EHR data via the Oncology Data Retrieval System²⁵ framework for the DFCI cohort and the Research Patient Data Registry (RPDR)²⁶ for the MGH cohort.

Acknowledgements

We thank all the patients who consented to participate in this study as well as the institutional data collection efforts that made this study possible. We would like to acknowledge Michael Hassett, Neil Lindeman, David Liu, Pieter Lukasse, Laura MacConnail, Paz Polak, Scott Rodig, Noah Zaitlen, and Elad Ziv for helpful discussions; the DFCI Oncology Data Retrieval System (OncDRS) for the aggregation, management, and delivery of the clinical and operational research data used in this project; and the DFCI/BWH Data Sharing Group for the aggregation, management, and delivery of the clinical and genomics data used in this project.

AG is supported by NIH R01CA227237, NIH R01CA244569, NIH R21HG010748, the Claudia Adams Barr Foundation, the Louis B. Mayer Foundation, and the Doris Duke Charitable Foundation. SAS acknowledges support by the NCI (R50RCA211482). SG was supported by NIH R01CA227237 and a DFCI Trustee Fellowship. TKC is supported in part by the Dana-Farber/Harvard Cancer Center Kidney SPORE and Program, the Kohlberg Chair at Harvard Medical School and the Trust Family, Michael Brigham, and Loker Pinard Funds for Kidney Cancer Research at DFCI. TEK acknowledges grant support from the National Institutes of Health (T32CA009172).

Supplementary Note

Sample collection, genotype imputation, and quality control

DFCI cohort

The DFCI cohort was sequenced as part of the *Profile* project, a prospective clinical sequencing effort for consented patients undergoing routine treatment at the Dana-Farber Cancer Institute and affiliated hospitals. A custom targeted hybrid capture sequencing platform (OncoPanel) was used to assay genomic variation from tumor biopsies. Each sample was sequenced on one of three panel versions targeting the exons of 275, 300, and 447 genes respectively. Samples meet a minimum of 30X coverage for 80% of targets for analysis. Somatic variation (including single nucleotide variants, insertions/deletions, and copy number variation) was called by the Profile clinical bioinformatics pipeline and signed out by a pathologist at Brigham & Women's Hospital after technical review, as previously described¹⁵. Off-target and on-target reads from the sequenced BAMs were imputed using the STITCH imputation software^{16,38}. Imputed variants were restricted to minor allele frequency >1% and imputation INFO score >0.4. Genetic ancestry was inferred using principal component projection with the SNPWEIGHTS software³⁹. Continental components were used to exclude non-European individuals, and within-Europe components were included as covariates.

A partly overlapping cohort of 833 individuals (126 overlapping patients on ICIs) with both OncoPanel tumor sequencing and direct germline SNP array genotyping (on the Illumina Multi-Ethnic Genotyping Array (MEGA)) was used to benchmark the imputation accuracy. Pearson correlation for each SNP was computed between the tumor-imputed and germline genotyped individuals. Mean imputed SNP correlation was 0.86 after variant quality control and highly uniform across the genome (Figure S1). Detailed analysis of variant imputation accuracy have been described separately and the imputation workflow is publicly available¹⁶. For visualizations where imputed patients were stratified by variant carrier/non-carrier status, the decision boundary was determined using logistic regression of carrier status on imputed dosage in the samples with both tumor sequencing and SNP array data.

MGH cohort

Blood samples were collected from MGH patients and genotyped on the Illumina MEGA array. Data was imputed to the 1000 Genomes reference panel using the Haplotype Reference Consortium imputation server, followed by quality control removing variants with minor allele frequency <1% and INFO score <0.9. Genetic ancestry was inferred using in-sample principal components and restricted to Europeans.

CT cohort

A subset of patients signed an optional Research Biosample Repository (RBR) Informed Consent Form (ICF) to provide whole blood samples for future research, including study of inherited and non-inherited genetic variation from these whole blood samples. Whole-genome sequencing data

was collected from whole blood as previously described⁹. Genetic ancestry was inferred using ADMIXTURE and restricted to Europeans (ancestry >0.7). In-sample principal components were also computed to account for any remaining population structure.

Outcome definitions in the DFCI cohort

Mortality was collected using linkage to the National Death Index (NDI) through 2019. For patients who died after 2019, a clinical death index from the electronic health record (EHR) was used (which captured 86% of occurred deaths when evaluated for patients before 12/31/2019).

The “all-grade” event definition was obtained by algorithmic abstraction using EHR diagnosis codes. A list of predefined relevant diagnosis codes was used to filter all available codes for potential adverse events after treatment start and up to 60 days after receiving the last ICI dose. Diagnosis codes, which were present in the EHR of the respective patient before treatment start were excluded. Evident false positives were excluded by inspection of the diagnosis code and manual review of the patient chart at the event date, to exclude events that did not occur or were clearly linked to non-ICI causes. The used search terms and manual exclusion list of search terms is shown in Supplementary table S7.

Prior autoimmune disease and polygenic risk score

We investigated relationships between the identified risk variants and prior autoimmune disease and autoimmune disease risk. We defined patients with prior autoimmune disease based on the occurrence of an autoimmune related ICD10 code before ICI treatment start. Each irAE lead SNP was then tested for association with prior autoimmune disease, while adjusting for age, gender, treatment year, panel version of the sequencing panel, treatment type, line of treatment, as well as cancer type. As an alternative measure of autoimmune disease risk, we also inferred a polygenic risk score (PRS) for any autoimmune disease from a recent UK Biobank GWAS study (see Data Availability). We confirmed that the PRS was significantly associated with the previous ICD-based autoimmune disease definition in the ICI cohort ($p=8.8 \times 10^{-4}$). Each irAE lead SNP was again tested for association with the PRS, adjusting for cancer type, age, gender, panel version, as well as the first two principal components to control for ancestry.

Termination of treatment and steroid administration

For a subset of 44 patients, which were selected based on highest dosage of the lead IL7 SNP, information on continuation of treatment after irAE as well as steroid administration was manually annotated through chart review.

Survival analysis

GWAS discovery

In the DFCI discovery cohort, discovery of GWAS variants associated with risk of irAEs was performed using a multivariate multi-state survival framework modelling with irAE as the primary outcome and death as a competing risk. Direct modelling of competing risks is important for

incidence computation and to account for potential survivor bias⁴⁰, where individuals who live longer may develop more irAEs by chance. Due to computational constraints, the mixed-effects survival GWAS methodology did not allow for stratified covariates and flexible truncation. We thus re-estimated the top associations ($p < 5 \times 10^{-6}$) by fixed-effect meta-analysis over the cancer types with stratification of any covariates that exhibited a proportional hazards violation. Lastly, to account for error in the imputation, we rescaled the HR based on the imputed/genotyped relationship, though we note this is a linear rescaling that does not impact the significance of the association.

Additionally to account for immortal time bias, 422 patients who were sequenced after the start of ICI treatment were left-truncated until sequencing. Left-truncation and excluding patients with allograft surgery or immunosuppressants at treatment start did not influence any of the genome-wide significant associations (Figure S6).

In the replication cohorts (MGH and CT), cause-specific hazard ratios and p-values were estimated by conventional survival analysis with censoring on death or loss to follow-up. This cause specific hazard computation (our primary measure of effect-size) is equivalent to that estimated from the multi-state model.

Multi-state modelling of competing risks

We employed a time-to-event analysis with irAEs as the event of interest. However, as death precludes from experiencing an irAE, death events were addressed through an illness-death model, a special case of the class of multi-state survival models. In this model patients in the “Treatment” state can either experience a transition to “irAE” or to “Death” without having experienced an irAE. Furthermore, patients who have experienced an irAE can also transition to the “Death” state. For any transition in the multi-state survival model censoring due to loss to follow-up, as well as left-truncation due to delayed sequencing was employed.

In the setting of multi-state survival models, there are two possible hazard rates one might be interested in: the cause-specific hazard and the subdistribution hazard. While the subdistribution hazard quantifies the risk for the incidence of the event in the population, the cause-specific hazard quantifies the inherent risk of a patient experiencing an event conditioned on that patient being event-free. The cause-specific hazard rate, therefore, corresponds to the infinitesimal generator of transitions in a Markov Jump process with added censoring. As we are interested in the biological mechanism of experiencing an irAE, the primary quantity of interest is the cause-specific hazard rate (see further discussion in ref.⁴¹). The subdistribution hazard, which takes into account the risk of the competing death event given from the same covariate, is of secondary interest primarily from an epidemiological perspective.

To address the challenge of estimating the cumulative population-level incidence/probability of an irAE in the multi-state setting, we employed the Aalen-Johansen estimator¹⁹. We treated irAEs as a transient state to obtain the probability over time to have experienced an irAE but be alive, and irAEs as an absorbing state to obtain the cumulative incidence of irAEs over time.

Covariate adjustment

In the DFCI discovery cohort, covariates were included for: two within-Europe ancestry components (after restricting to European individuals, see above); age at treatment start; gender; line of treatment as determined from the EHR medication records; start year of treatment; type of treatment (PD1/PD-L1 or CTLA4 monotherapy, combination); concurrent alternate treatment (chemotherapy, targeted therapy); as well as two technical covariates adjusting for the version of the targeted panel and an indicator for sequencing after treatment start. Patients were grouped into cancer types with >30 individuals, and the analyses were stratified or meta-analyzed over cancer types (as indicated). In the MGH cohort, covariates were included for: cancer type, type of immune checkpoint inhibitor, age at treatment start, gender, and genetic ancestry. Cancer type was included as a covariate rather than a stratifying variable due to the relatively small sample size of each type and the assumption that common covariate effects could be better learned across all samples. In the CT cohort, covariates were included for five genetic ancestry components, and stratified on treatment arms (which also capture cancer types).

Data availability

Full summary association statistics for the discovery cohort will be made available upon publication.

UK Biobank association statistics for autoimmune disease were previously computed by BOLT-LMM v2.3 and used to estimate the autoimmune disease PRS (accessed from: https://data.broadinstitute.org/alkesgroup/UKBB/UKBB_409K/). RNA-seq data from GTEx and TCGA was accessed through the ReCount2 interface and API (<https://jhubiostatistics.shinyapps.io/recount/>).

Table 1

Profile cohort (discovery)		MGH cohort (replication)	
	Overall (N=1751)		Overall (N=196)
irAEs		irAEs	
Yes	339 (19.4%)	Yes	33 (16.8%)
No	1412 (80.6%)	No	163 (83.2%)
Cancer Type		Cancer Type	
Non-Small Cell Lung Cancer	539 (30.8%)	GU	31 (15.8%)
Melanoma	241 (13.8%)	Melanoma	44 (22.4%)
Other	236 (13.5%)	Other	72 (36.7%)
Glioma	112 (6.4%)	Thoracic	49 (25.0%)
Breast Carcinoma	111 (6.3%)		
Esophagogastric Carcinoma	111 (6.3%)		
Renal Cell Carcinoma	109 (6.2%)		
Bladder Cancer	94 (5.4%)		
Head and Neck Carcinoma	90 (5.1%)		
Ovarian Cancer	40 (2.3%)		
Cancer of Unknown Primary	34 (1.9%)		
Colorectal Cancer	34 (1.9%)		
Sex		Sex	
Female	814 (46.5%)	Female	82 (41.8%)
Male	937 (53.5%)	Male	114 (58.2%)
Age		Age	
Mean (SD)	63.0 (12.4)	Mean (SD)	64.2 (13.4)
Median [Min, Max]	63.9 [19.6, 102]	Median [Min, Max]	66.6 [22.3, 90.2]
Type of Treatment		Type of Treatment	
CTLA4	49 (2.8%)	CTLA4	17 (8.7%)
Combination Therapy	154 (8.8%)	Combination Therapy	16 (8.2%)
PD-1/PD-L1	1548 (88.4%)	PD-1/PD-L1	163 (83.2%)
Sequencing			
Prior to ICI initiation	1363 (77.8%)		
Following ICI initiation	388 (22.2%)		
Start year			
Before 2016	357 (20.4%)		

2016	416 (23.8%)		
2017	557 (31.8%)		
2018	305 (17.4%)		
After 2018	116 (6.6%)		

Figure Legends

Figure 1. Manhattan plot of GWAS associations. Associations in the DFCI discovery cohort for all-grade irAEs. Each dot represents and associated SNP, with position of the SNP (x-axis) and p-value of the association (y-axis, $-\log_{10}$ scale).

Figure 2. Discovery associations and replication in MGH and CT cohort. Forrest plot of genome-wide significant association (reference dosage) with all-grade irAEs at 8q21 (a) in the Profile cohort, (b) the MGH cohort and (c) in the CT cohort. Aalen-Johansen estimator for the cumulative incidence of adverse events following ICI initiation stratified on SNP dosage in the DFCI discovery cohort (d), in the MGH replication cohort (e) and using a Kaplan Meier estimator in the CT cohort (f).

Figure 3. Colocalization with IL7 cryptic exon. Sashimi plot of alternative splicing of *IL7* stratified on the lead splice QTL (a), with the putative causal variant shown below and the cryptic exon highlighted (*IL7_{ce}*). Cryptic exon activity stratified by lead splice QTL genotype (b). Significance of co-expression of *IL7* and *IL7_{ce}* across GTEx tissues (Pearson correlation) (c).

Figure 4. Lymphocyte counts up to 30 days before and after ICI initiation for cases and controls. Paired Wilcoxon test between time-points in carriers and non-carriers in the DFCI (a) and MGH (b) cohort. Wilcoxon test of the difference in lymphocyte counts prior versus following ICI initiation between carrier and non-carrier in the Profile (c) and MGH cohort (d). Paired Wilcoxon test between before and after first irAE in carriers and non-carriers in the DFCI cohort (e). Association between difference in lymphocyte counts before and following ICI initiation and developing and irAE (f) as well as death without an irAE (g).

Supplementary Figure S1. Distribution of SNP imputation accuracy (Pearson correlation) from panel sequencing for 833 samples with available direct germline genotyping.

Supplementary Figure S2. Cumulative number of patients experiencing high-grade irAEs (a) or all-grade irAEs (b) stratified by therapy class.

Supplementary Figure S3. QQ-Plot for all-grade adverse events.

Supplementary Figure S4. Discovery associations with rs75824728 (a) and rs113861051 (b) stratified by cancer type.

Supplementary Figure S5. Discovery associations with (a) rs16906115, (b) rs75824728 and (c) rs113861051 stratified by treatment class.

Supplementary Figure S6. Association of rs16906115 (a) without left-truncation of the patients and (b) excluding patients with previous allograft or on immunosuppressant drugs.

Supplementary Figure S7. Correlation to true genotype for the genome-wide significant SNPs rs16906115 (a) and rs75824728 (b) as well as rs113861051 (c) association in 833 patients where both panel and array sequencing was available.

Supplementary Figure S8. Finemapped 95% credible set of associations with at the 8q21 (rs16906115) locus.

Supplementary Figure S9. Forrest plot for the top all-grade irAE SNP association in 1p36 locus, tested against high-grade irAE definition.

Supplementary Figure S10. Incidence of all-grade irAEs over time for the DFCI ICI cohort (a) compared to incidence of the corresponding diagnosis codes in the DFCI non-ICI cohort (b).

Supplementary Figure S11. (a) Logarithmic hazard rates (effect sizes) and (b) p-values for association in the discovery DFCI cohort and the MGH cohort for the 8q21 locus, restricted to nominally significant associations in the discovery cohort ($p < 0.05$). (c) Comparison of the association strengths of variants around the top association locus in DFCI and MGH. The 95% credible set in the DFCI cohort is colored in blue. The upper red line signifies genome wide significance, the lower red line bonferroni corrected significance for SNPs tested in the MGH cohort.

Supplementary Figure S12. Aalen-Johansen estimator for the probability of adverse events following ICI initiation taking into account death (a), as well as cumulative incidence of irAEs following ICI initiation (b) in the DFCI cohort; and in the MGH cohort (c,d).

Supplementary Figure S13. Association of r(a) rs16906115, (b) rs75824728 and (c) rs113861051 by type of irAE in the Profile cohort.

Supplementary Figure S14. Association of rs16906115 by type of irAE in (a) Profile and (b) CT cohort.

Supplementary Figure S15. Recorded irAE event type distribution in CT cohort for (a) grade ≥ 1 , (b) grade ≥ 2 and (c) grade ≥ 3 .

Supplementary Figure S16. Cumulative irAE probability distributions for in CT cohort grade ≥ 1 , grade ≥ 2 and grade ≥ 3 irAEs for carriers and non-carriers of the (a) rs16906115, (b) rs75824728 and (c) rs113861051 reference allele.

Supplementary Figure S17. Forest plots over trial arms in CT cohort for association with grade ≥ 1 , grade ≥ 2 and grade ≥ 3 irAEs for carriers of the (a) rs16906115, (b) rs75824728 and (c) rs113861051 reference allele on the hazard scale.

Supplementary Figure S18. Association with irAE subtypes in CT cohort for grade ≥ 1 , grade ≥ 2 and grade ≥ 3 irAEs for carriers of the (a) rs16906115, (b) rs75824728 and (c) rs113861051 reference allele on the log-hazard scale.

Supplementary Figure S19. As steroids influence lymphocyte counts, we conditioned on the patient receiving steroids 30 days before or after irAE. We observed a significant effect for carriers when steroids were given ($p=0.012$) with no effect in non-carriers ($p=0.84$). There was no significant effect in either carriers ($p=0.23$) nor non-carriers ($p=0.63$) when no steroids were given.

Supplementary Figure S20. Association of 8q21 SNP with (a) $IL7_{junc}$ and (b) $IL7_{ce}$ in GTEx testis. The risk SNP was significantly associated with $IL7_{ce}$ ($P=1.2 \times 10^{-20}$, $R^2=0.63$) and remained significant after conditioning on $IL7_{junc}$ ($P_{cond}=4.6 \times 10^{-15}$), whereas the risk SNP had a much weaker association with $IL7_{junc}$ ($P=1.4 \times 10^{-9}$, $R^2=0.11$) that was no longer significant after conditioning on $IL7_{ce}$ ($P_{cond}=0.05$).

Supplementary Figure S21. Expression of $IL7_{ce}$ in GTEx tissues (a). $IL7$ - $IL7R$ co-expression as function of $IL7_{ce}$ in GTEx LCLs (b).

Supplementary Figure S22. Expression of $IL7_{ce}$ in cell sorted immune cell data.

Supplementary Figure S23. $IL7_{ce}$ expression in TCGA by site.

Supplementary Figure S24. Association between previous auto-immune disease as defined by auto-immune ICD-10 codes, and all-grade irAEs.

Supplementary Figure S25. Association between sex assigned at birth and irAEs.

Supplementary Table S1. Association of $IL7_{ce}$ expression with TCGA immune landscape features. TGF- β response, TCR diversity, BCR diversity, and proliferation were not significantly associated with overall $IL7$ expression but were significant for $IL7_{ce}$. In contrast, increases in Th1 and Th2 cells were highly significantly associated with total $IL7$ expression ($P < 10^{-30}$) but not with $IL7_{ce}$ ($P > 0.3$).

Supplementary Table S2. Hazard ratios and significance of interaction term in interaction analysis of germline, somatic and clinical features with 8q21 SNP and with irAE as outcome.

Supplementary Table S3. 95% credible set of fine-mapping the 8q21 locus.

Supplementary Table S4. Names and references for the clinical trial studies.

Supplementary Table S5. List of genome-wide significant loci in the discovery cohort with effect sizes and p-values in the replication cohort, as well as allele frequency of the reference SNP in both Profile and MGH cohorts.

Supplementary Table S6. Overall survival association of adverse events in the Profile and MGH cohort.

Supplementary Table S7. Search terms and exclusion criteria for “all-grade”, EHR based irAE outcome definition

Supplementary Table S8. Frequency of irAE for carriers and non-carriers of the risk alleles by type of irAE.

Supplementary Table S9. Frequency of termination of therapy and steroid administration after irAE in the carrier and non-carrier group. The patients were ascertained by highest dosage of rs16906115 for curation.

Supplementary Table S10. Frequency and number of grades of irAEs. The patients were ascertained by highest dosage of rs16906115 for curation.

Bibliography

1. Ribas A, Wolchok JD. Cancer immunotherapy using checkpoint blockade. *Science* 2018;359(6382):1350–5.
2. June CH, Warshauer JT, Bluestone JA. Corrigendum: Is autoimmunity the Achilles' heel of cancer immunotherapy? *Nat Med* 2017;23(8):1004.
3. Esfahani K, Elkrief A, Calabrese C, et al. Moving towards personalized treatments of immune-related adverse events. *Nat Rev Clin Oncol* 2020;17(8):504–15.
4. Boutros C, Tarhini A, Routier E, et al. Safety profiles of anti-CTLA-4 and anti-PD-1 antibodies alone and in combination. *Nat Rev Clin Oncol* 2016;13(8):473–86.
5. Koon H, Atkins M. Autoimmunity and immunotherapy for cancer. *N. Engl. J. Med.* 2006;354(7):758–60.
6. Postow MA, Sidlow R, Hellmann MD. Immune-Related Adverse Events Associated with Immune Checkpoint Blockade. *N Engl J Med* 2018;378(2):158–68.
7. Wang DY, Salem J-E, Cohen JV, et al. Fatal Toxic Effects Associated With Immune Checkpoint Inhibitors: A Systematic Review and Meta-analysis. *JAMA Oncol* 2018;4(12):1721–8.
8. Eggermont AMM, Kicinski M, Blank CU, et al. Association Between Immune-Related Adverse Events and Recurrence-Free Survival Among Patients With Stage III Melanoma Randomized to Receive Pembrolizumab or Placebo: A Secondary Analysis of a Randomized Clinical Trial. *JAMA Oncol* [Internet] 2020 [cited 2020 Jan 2]; Available from: <https://jamanetwork.com/journals/jamaoncology/fullarticle/2757843>
9. Khan Z, Hammer C, Carroll J, et al. Genetic variation associated with thyroid autoimmunity shapes the systemic immune response to PD-1 checkpoint blockade. *Nat Commun* 2021;12(1):3355.
10. Khan Z, Di Nucci F, Kwan A, et al. Polygenic risk for skin autoimmunity impacts immune checkpoint blockade in bladder cancer. *Proc Natl Acad Sci U S A* 2020;117(22):12288–94.
11. Chowell D, Morris LGT, Grigg CM, et al. Patient HLA class I genotype influences cancer response to checkpoint blockade immunotherapy. *Science* 2018;359(6375):582–7.
12. Chowell D, Krishna C, Pierini F, et al. Evolutionary divergence of HLA class I genotype impacts efficacy of cancer immunotherapy. *Nat Med* [Internet] 2019; Available from: <https://doi.org/10.1038/s41591-019-0639-4>
13. Cubas R, Khan Z, Gong Q, et al. Autoimmunity linked protein phosphatase PTPN22 as a target for cancer immunotherapy. *J Immunother Cancer* [Internet] 2020;8(2). Available from: <http://dx.doi.org/10.1136/jitc-2020-001439>
14. Thorsson V, Gibbs DL, Brown SD, et al. The Immune Landscape of Cancer. *Immunity* 2018;48(4):812–30.e14.
15. Garcia EP, Minkovsky A, Jia Y, et al. Validation of OncoPanel: A Targeted Next-Generation

- Sequencing Assay for the Detection of Somatic Variants in Cancer. *Arch Pathol Lab Med* 2017;141(6):751–8.
16. Gusev A, Groha S, Taraszka K, Semenov YR, Zaitlen N. Constructing germline research cohorts from the discarded reads of clinical tumor sequences [Internet]. Available from: <http://dx.doi.org/10.1101/2021.04.09.21255197>
 17. Fast Algorithms for Conducting Large-Scale GWAS of Age-at-Onset Traits Using Cox Mixed-Effects Models. *Genetics* 2020;215(4):1191.
 18. Wang G, Sarkar A, Carbonetto P, Stephens M. A simple new approach to variable selection in regression, with application to genetic fine mapping. *J R Stat Soc Series B Stat Methodol* 2020;82(5):1273–300.
 19. Aalen OO, Johansen S. An Empirical Transition Matrix for Non-Homogeneous Markov Chains Based on Censored Observations. *Scand Stat Theory Appl* 1978;5(3):141–50.
 20. Aguet F, Anand S, Ardlie KG, et al. The GTEx Consortium atlas of genetic regulatory effects across human tissues. *Science* [Internet] 2020 [cited 2021 Oct 16]; Available from: <https://science.sciencemag.org/content/369/6509/1318.abstract>
 21. Garrido-Martín D, Palumbo E, Guigó R, Breschi A. ggsashimi: Sashimi plot revised for browser- and annotation-independent splicing visualization. *PLoS Comput Biol* 2018;14(8):e1006360.
 22. Linsley PS, Speake C, Whalen E, Chaussabel D. Copy number loss of the interferon gene cluster in melanomas is linked to reduced T cell infiltrate and poor patient prognosis. *PLoS One* 2014;9(10):e109760.
 23. Hoadley KA, Yau C, Wolf DM, et al. Multiplatform analysis of 12 cancer types reveals molecular classification within and across tissues of origin. *Cell* 2014;158(4):929–44.
 24. Collado-Torres L, Nellore A, Kammers K, et al. Reproducible RNA-seq analysis using recount2. *Nat Biotechnol* 2017;35(4):319–21.
 25. Orechia J, Pathak A, Shi Y, et al. OncDRS: An integrative clinical and genomic data platform for enabling translational research and precision medicine. *Appl Transl Genom* 2015;6:18–25.
 26. Nalichowski R, Keogh D, Chueh HC, Murphy SN. Calculating the benefits of a Research Patient Data Repository. *AMIA Annu Symp Proc* 2006;1044.
 27. Jaganathan K, Kyriazopoulou Panagiotopoulou S, McRae JF, et al. Predicting Splicing from Primary Sequence with Deep Learning. *Cell* 2019;176(3):535–48.e24.
 28. Rosenberg SA, Sportès C, Ahmadzadeh M, et al. IL-7 administration to humans leads to expansion of CD8+ and CD4+ cells but a relative decrease of CD4+ T-regulatory cells. *J Immunother* 2006;29(3):313–9.
 29. Barata JT, Durum SK, Seddon B. Flip the coin: IL-7 and IL-7R in health and disease. *Nat Immunol* 2019;20(12):1584–93.
 30. Penaranda C, Kuswanto W, Hofmann J, et al. IL-7 receptor blockade reverses autoimmune

diabetes by promoting inhibition of effector/memory T cells. *Proc Natl Acad Sci U S A* 2012;109(31):12668–73.

31. Totsuka T, Kanai T, Nemoto Y, et al. IL-7 Is essential for the development and the persistence of chronic colitis. *The Journal of Immunology* 2007;178(8):4737–48.
32. Doms H. Interleukin-7: Fuel for the autoimmune attack. *J Autoimmun* 2013;45:40–8.
33. Belarif L, Mary C, Jacquemont L, et al. IL-7 receptor blockade blunts antigen-specific memory T cell responses and chronic inflammation in primates. *Nat Commun* 2018;9(1):4483.
34. AACR Project GENIE Consortium. AACR Project GENIE: Powering Precision Medicine through an International Consortium. *Cancer Discov* 2017;7(8):818–31.
35. van Rheenen W, Peyrot WJ, Schork AJ, Lee SH, Wray NR. Genetic correlations of polygenic disease traits: from theory to practice. *Nat Rev Genet* [Internet] 2019; Available from: <http://dx.doi.org/10.1038/s41576-019-0137-z>
36. Torkamani A, Wineinger NE, Topol EJ. The personal and clinical utility of polygenic risk scores. *Nat Rev Genet* 2018;19(9):581–90.
37. Emdin CA, Khera AV, Kathiresan S. Mendelian Randomization. *JAMA* 2017;318(19):1925–6.
38. Davies RW, Flint J, Myers S, Mott R. Rapid genotype imputation from sequence without reference panels. *Nat Genet* 2016;48(8):965–9.
39. Chen C-Y, Pollack S, Hunter DJ, Hirschhorn JN, Kraft P, Price AL. Improved ancestry inference using weights from external reference panels. *Bioinformatics* 2013;29(11):1399–406.
40. Anderson JR, Cain KC, Gelber RD. Analysis of Survival by Tumor Response and Other Comparisons of Time-to-Event by Outcome Variables [Internet]. *Journal of Clinical Oncology*. 2008;26(24):3913–5. Available from: <http://dx.doi.org/10.1200/jco.2008.16.1000>
41. Austin PC, Fine JP. Practical recommendations for reporting Fine-Gray model analyses for competing risk data. *Stat Med* 2017;36(27):4391–400.
42. Taylor CA, Watson RA, Tong O, et al. Genetic variation at *IL7* provides mechanistic insights into toxicity to immune checkpoint blockade. Submitted.

Figure 1

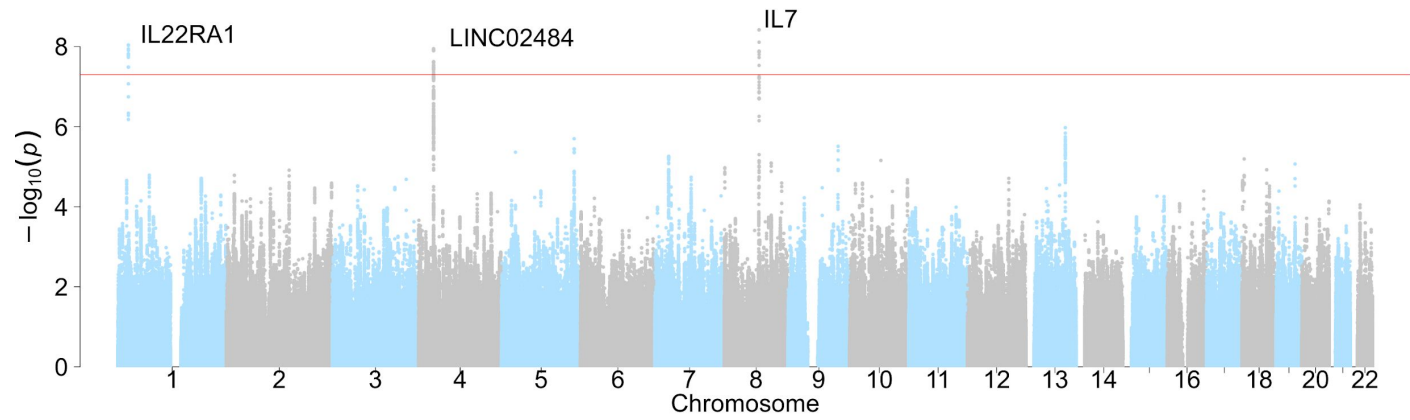
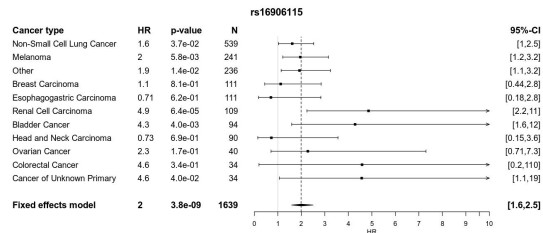
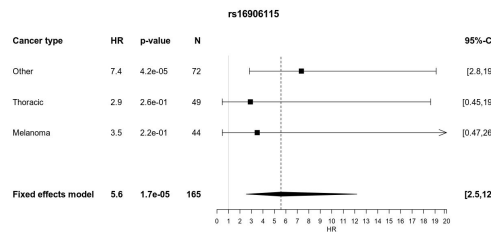


Figure 2

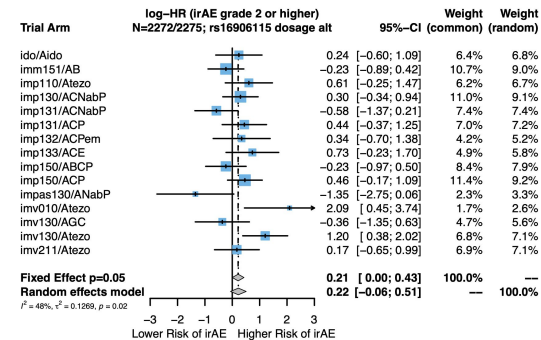
a.



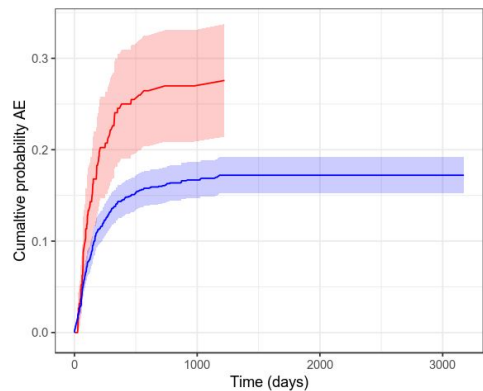
b.



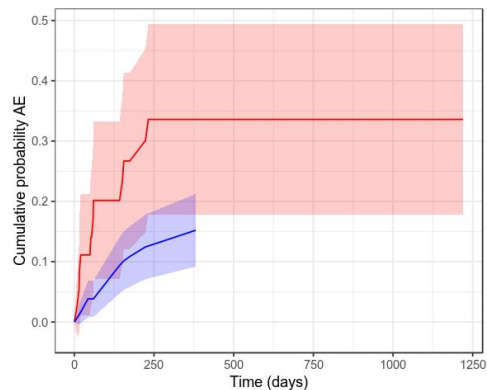
c.



d.



e.



f.

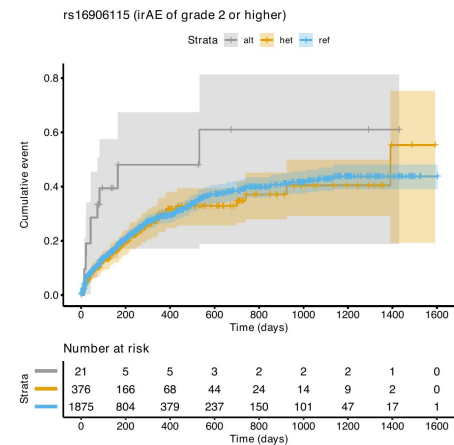
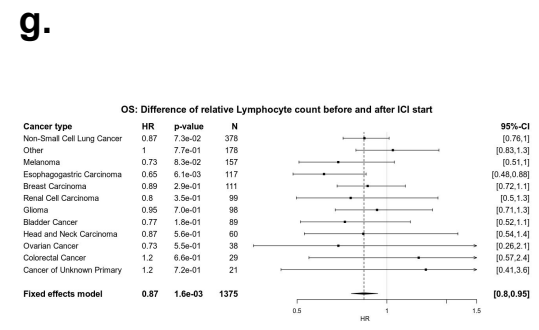
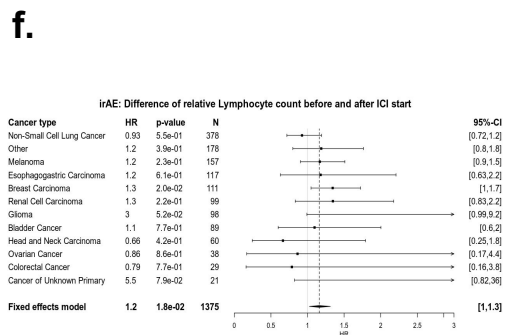
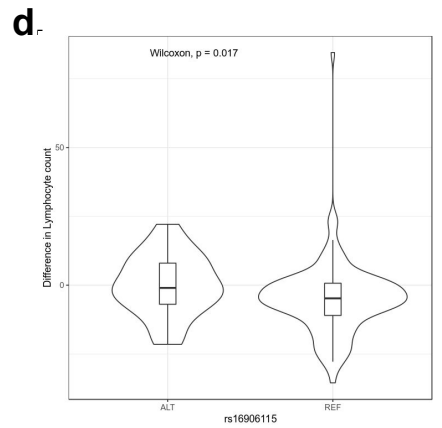
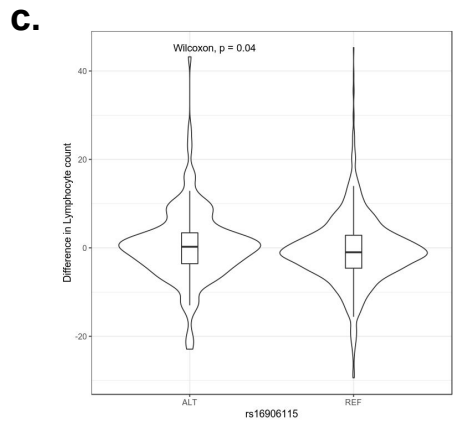
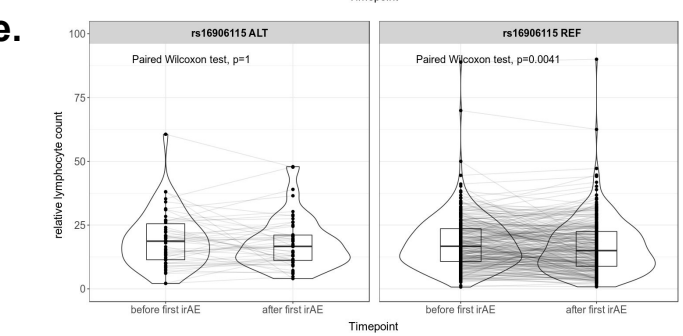
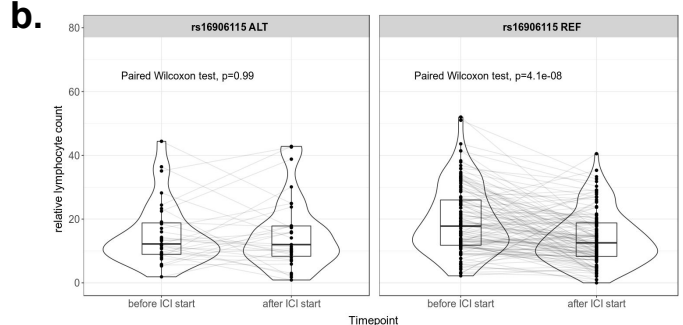
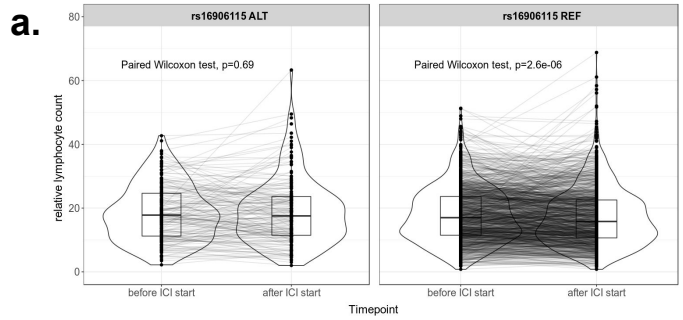


Figure 4



Supplemental Material

Figure S1

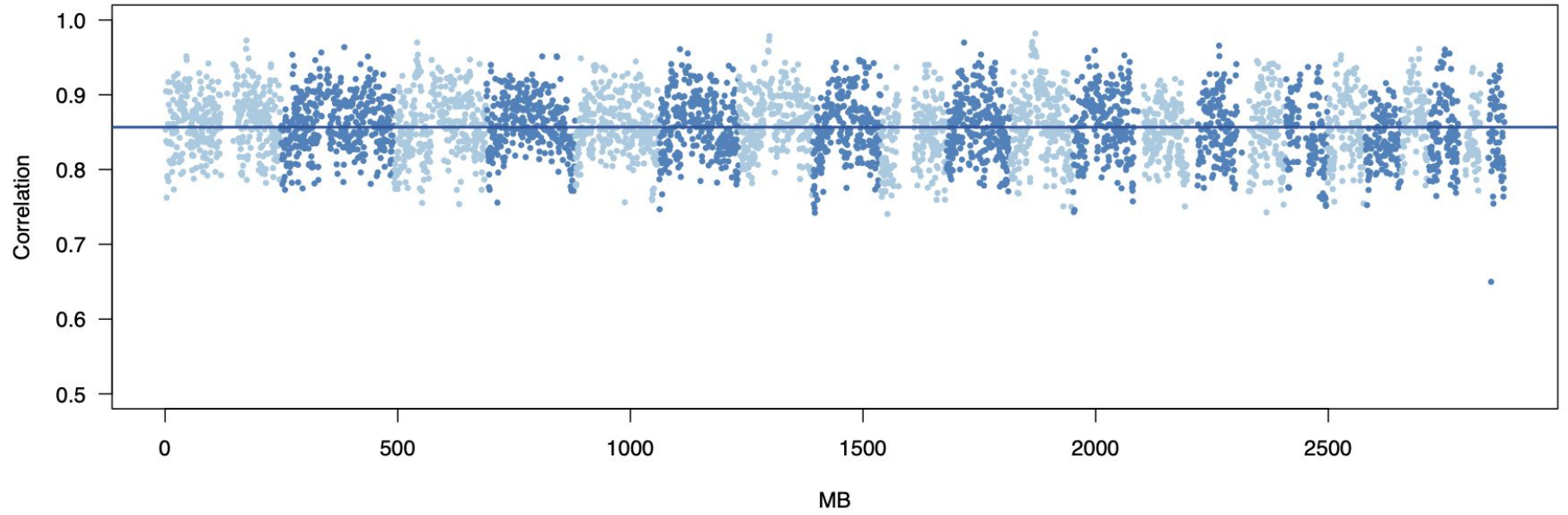


Figure S2

a. High-grade irAEs

b. All-grade irAEs

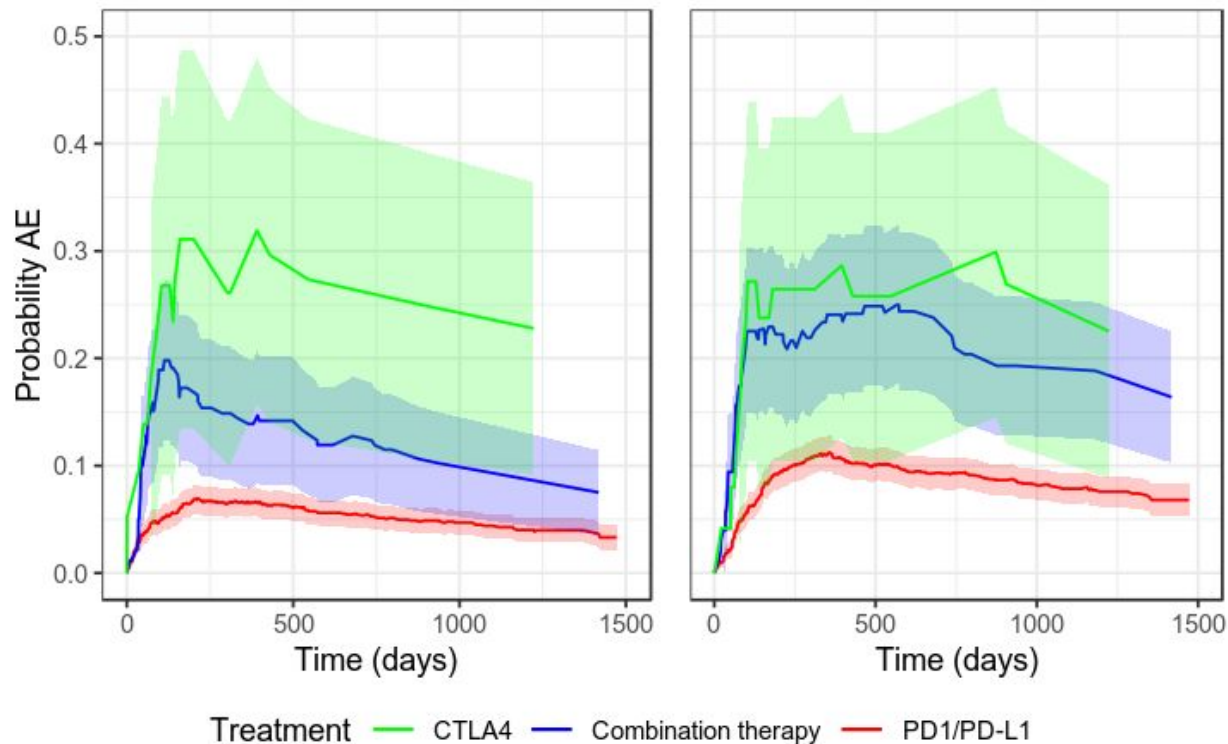


Figure S3

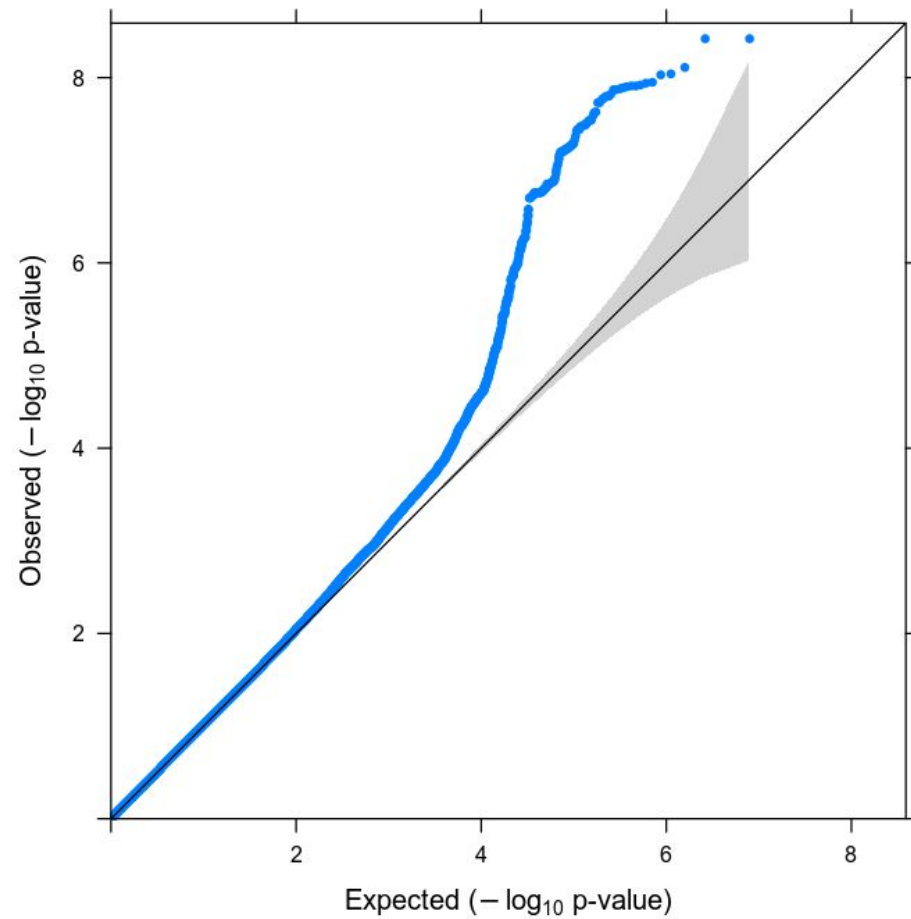
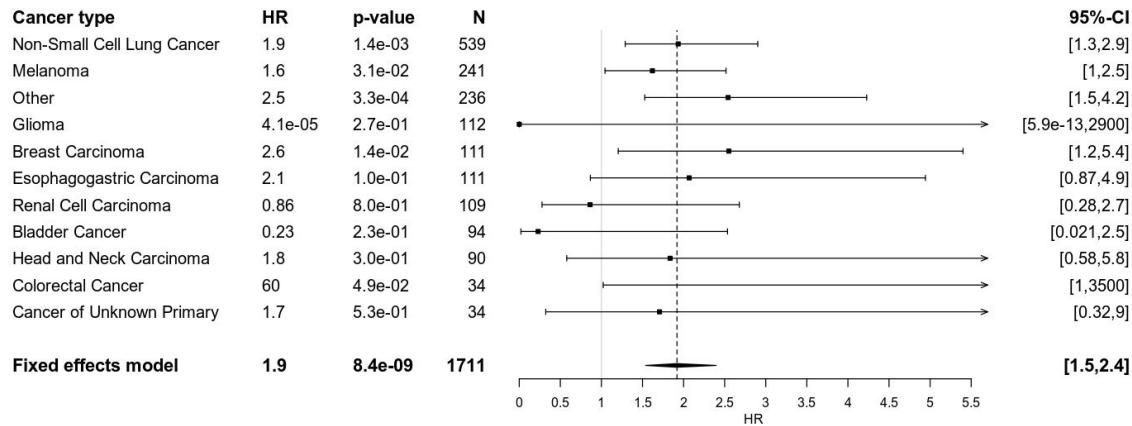


Figure S4

a.



b.

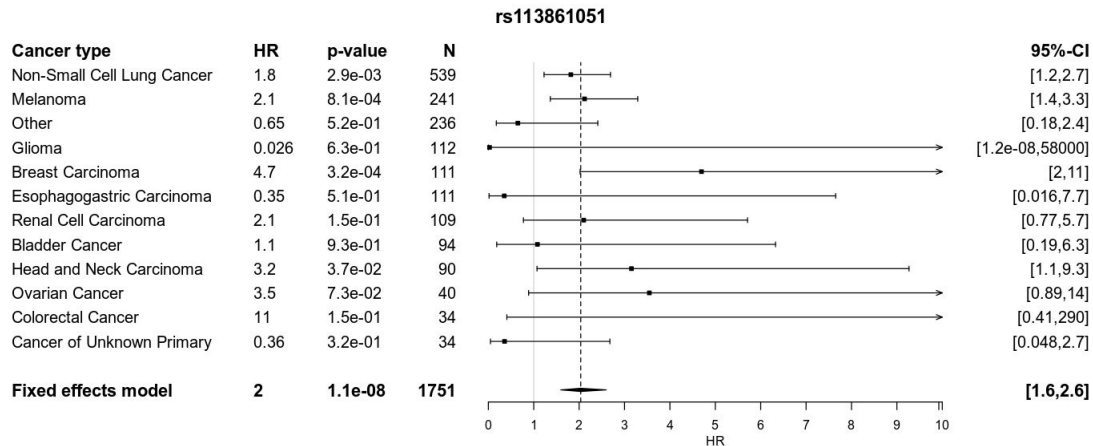
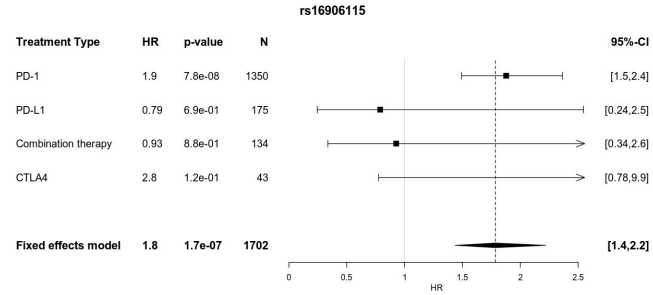
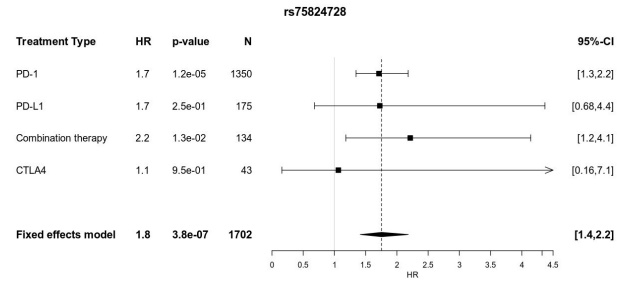


Figure S5

a.



b.



c.

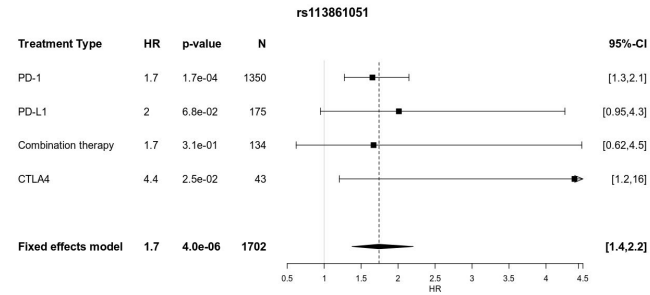
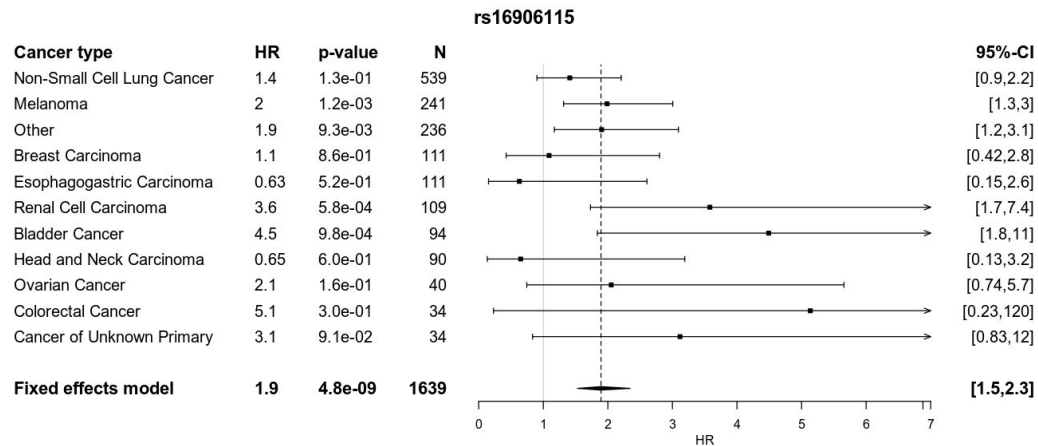


Figure S6

a.



b.

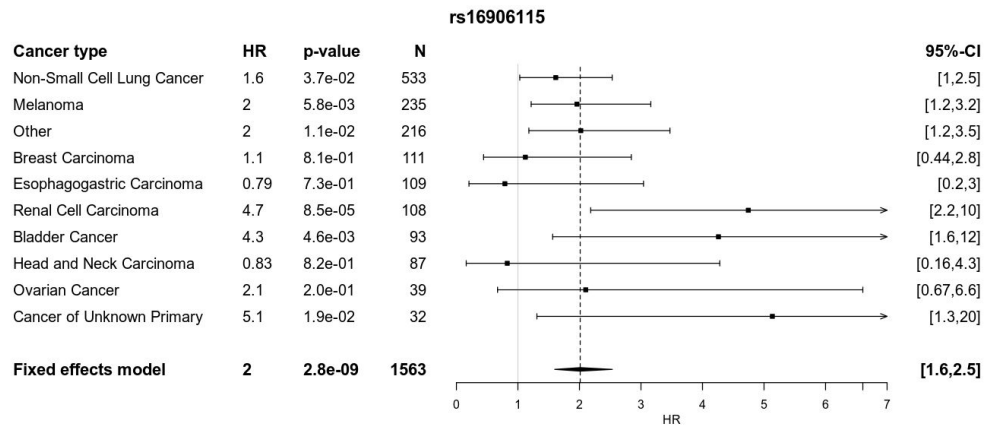
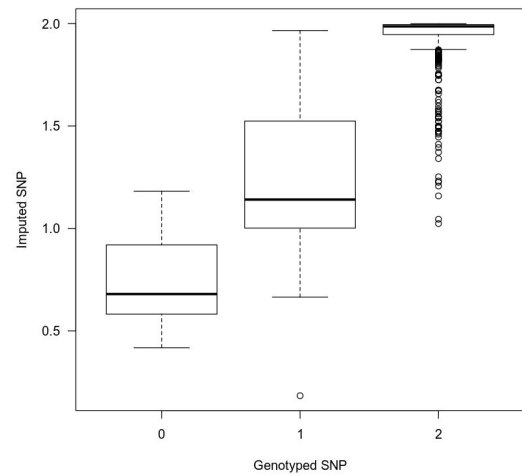
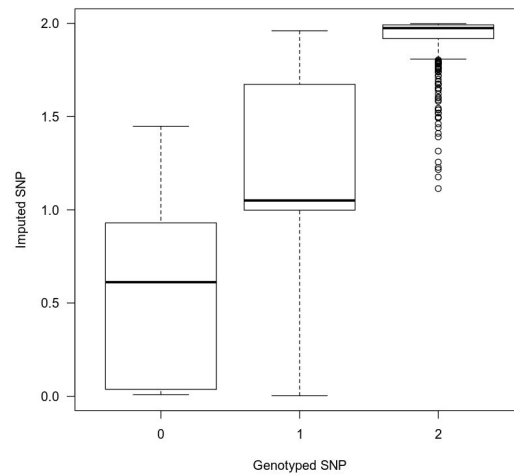


Figure S7

a.



b.



c.

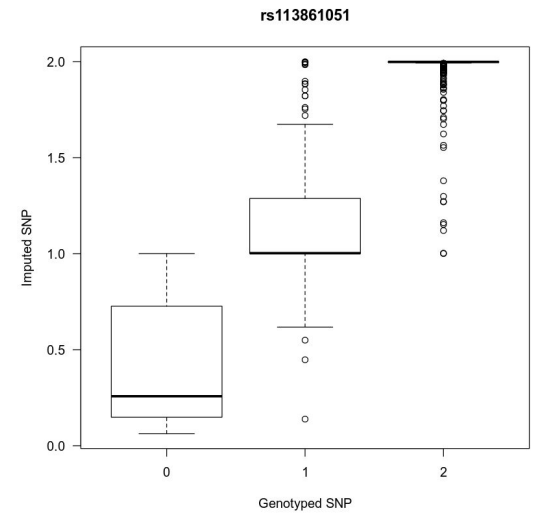


Figure S8

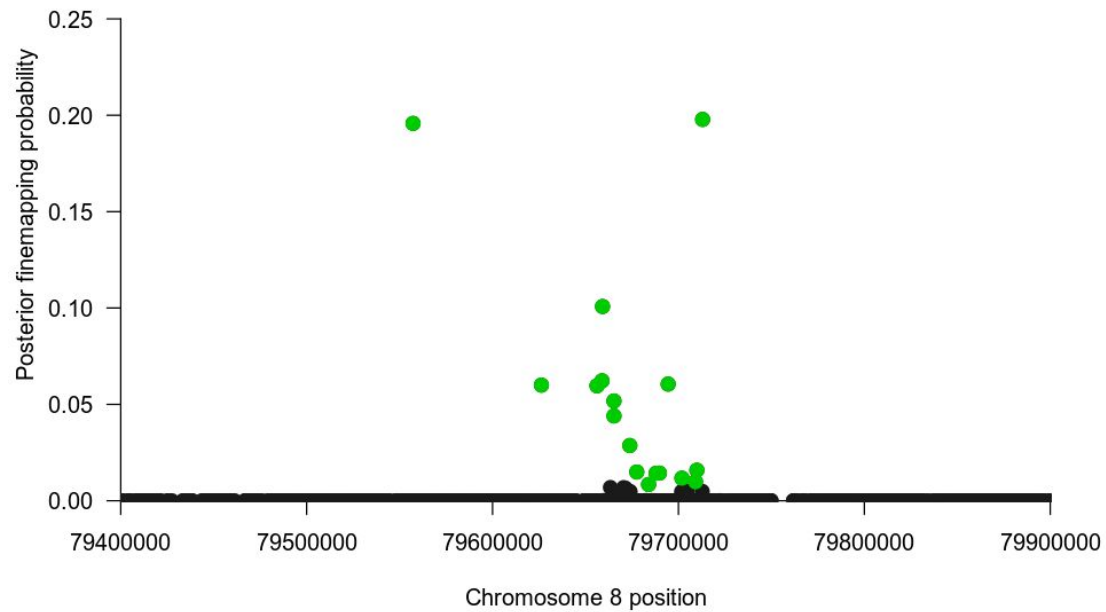


Figure S9

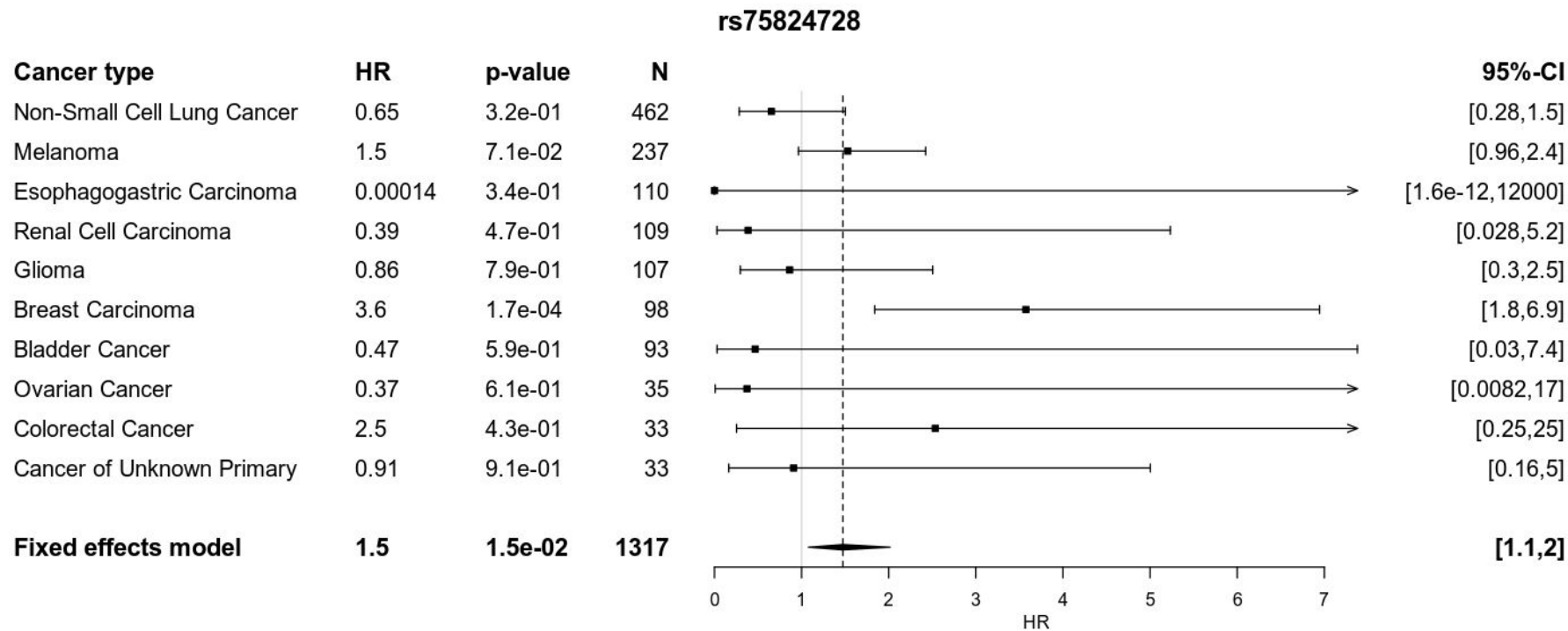


Figure S10

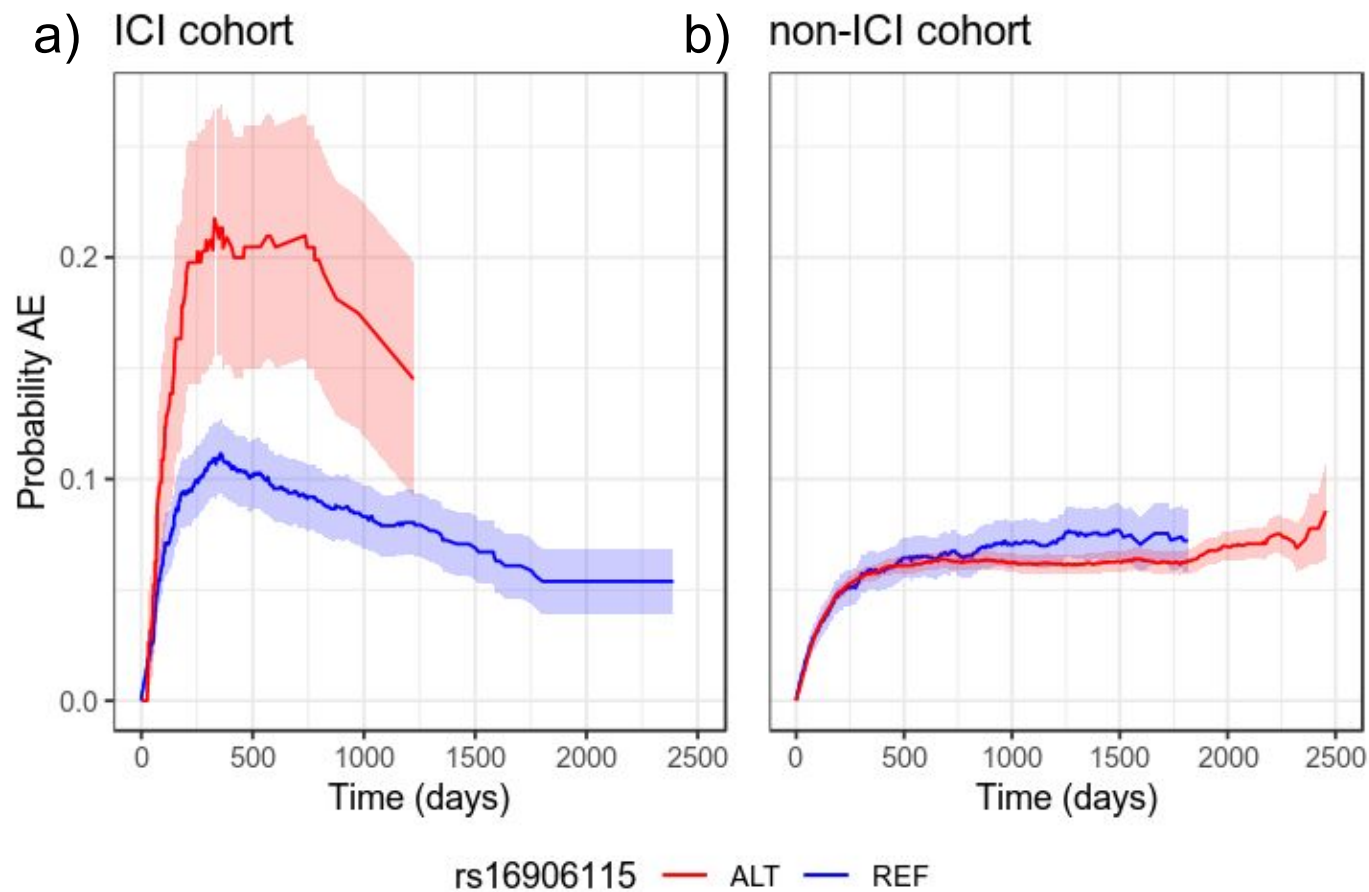
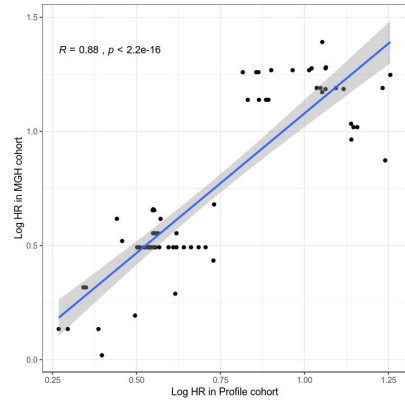
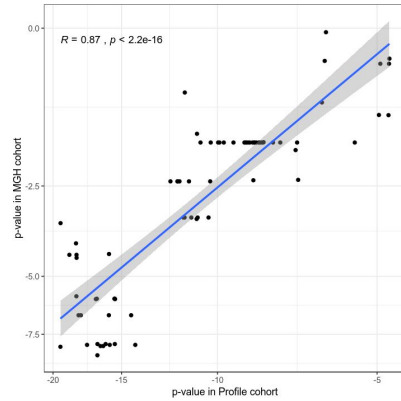


Figure S11

a.



b.



c.

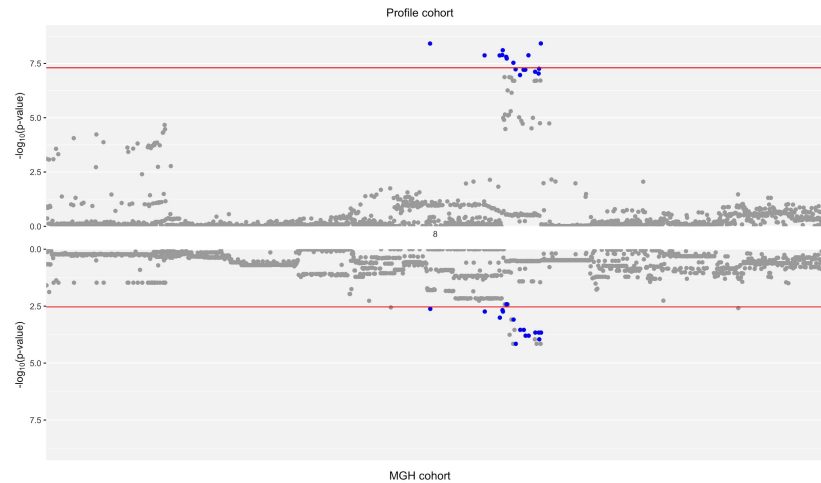
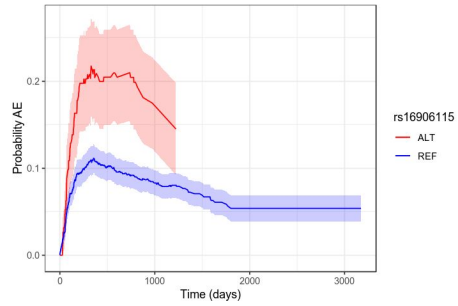
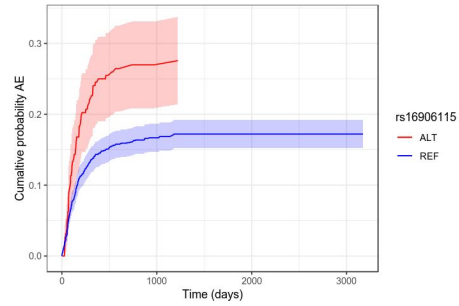


Figure S12

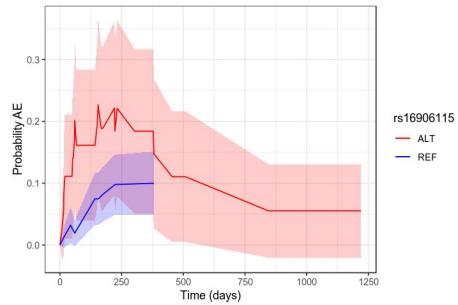
a.



b.



c.



d.

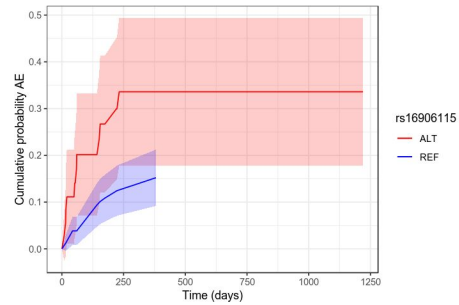
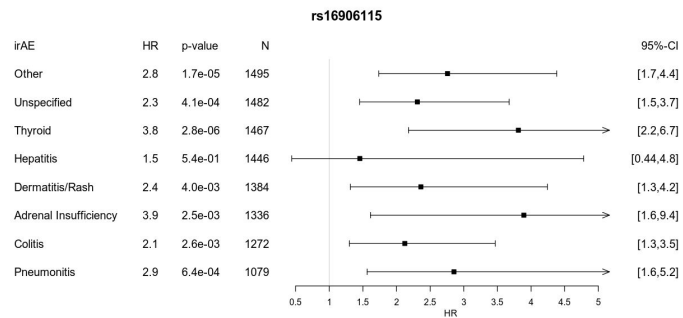
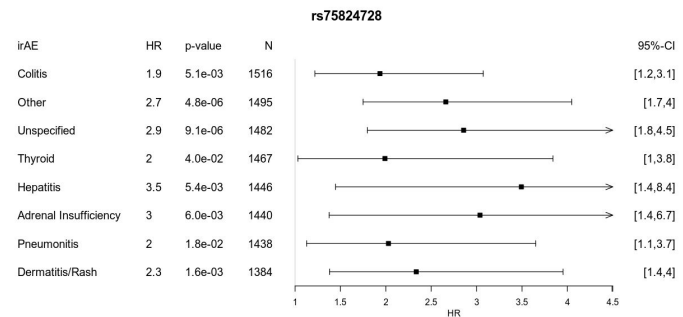


Figure S13

(a)



(b)



(c)

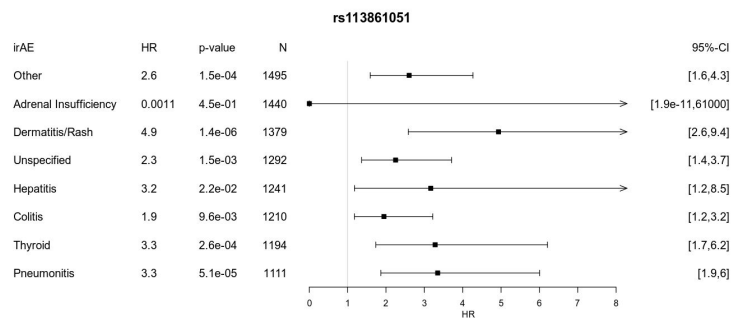
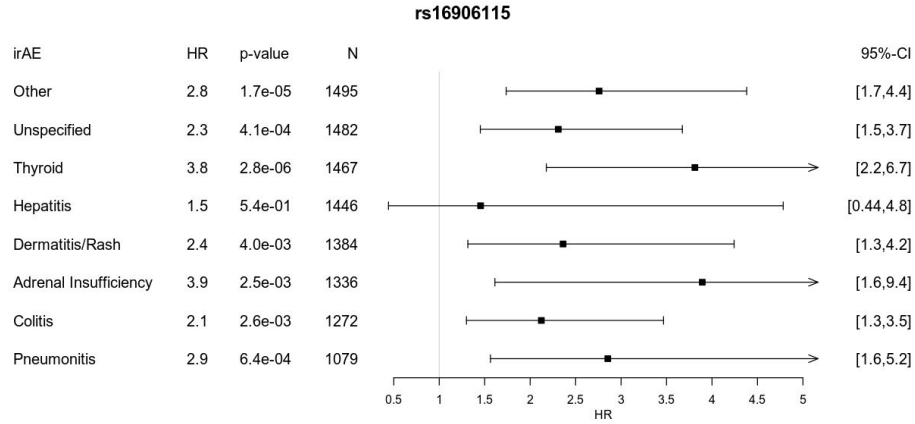


Figure S14

(a)



(b)

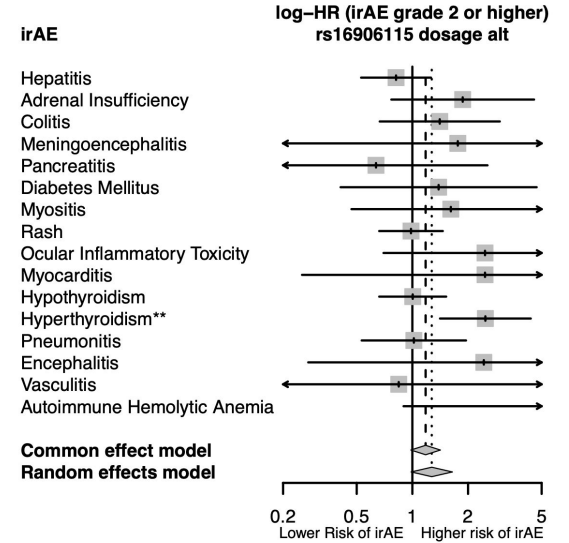
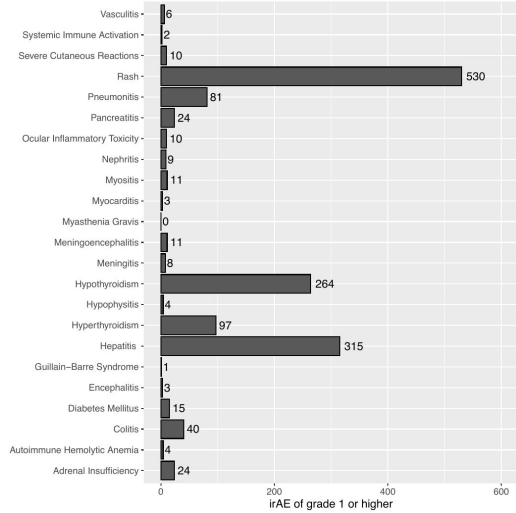
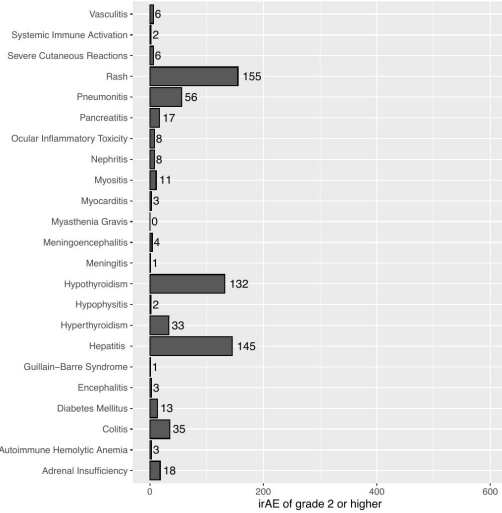


Figure S15

(a)



(b)



(c)

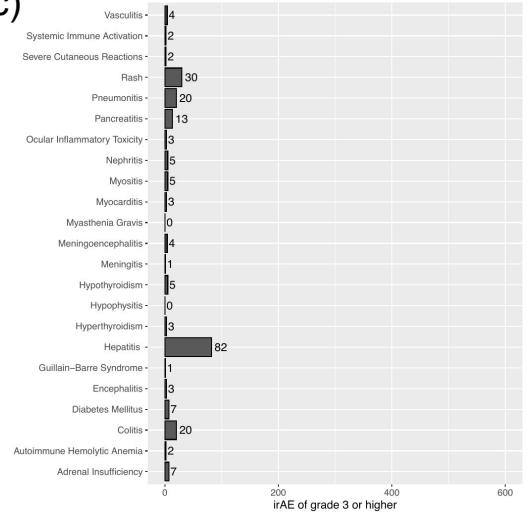
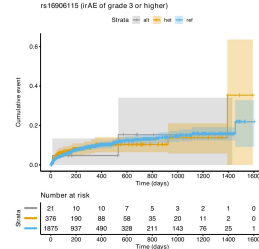
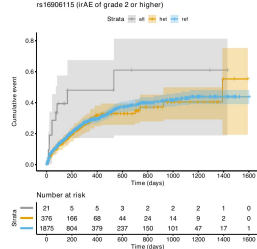
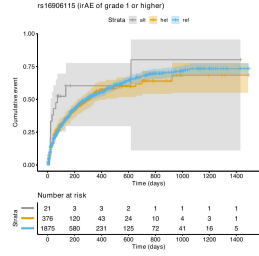
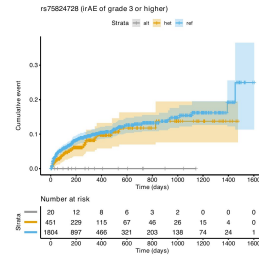
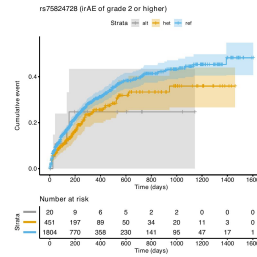
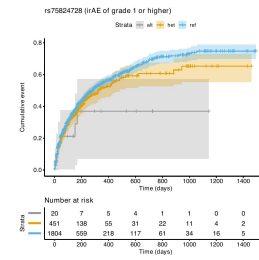


Figure S16

(a)



(b)



(c)

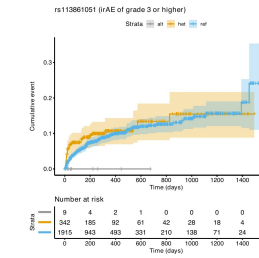
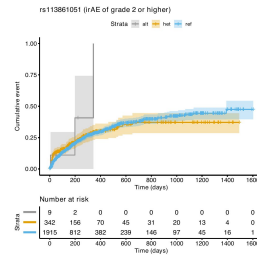
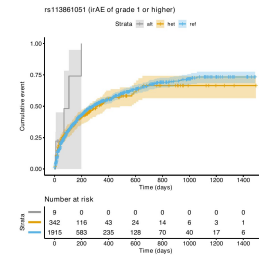
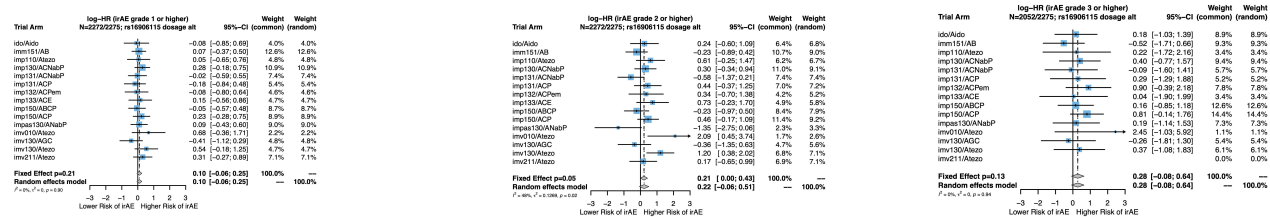
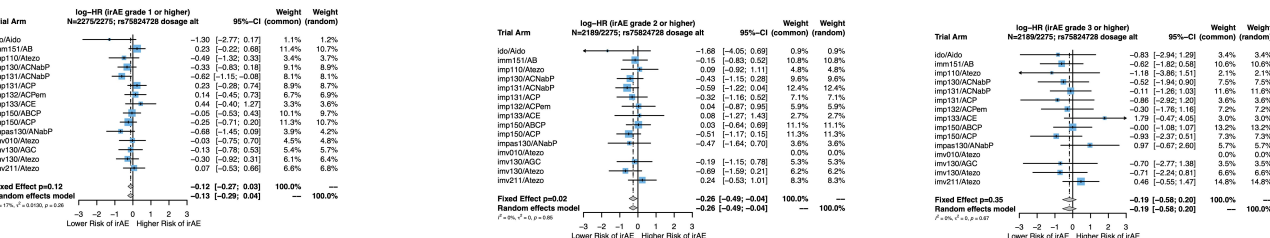


Figure S17

(a)



(b)



(c)

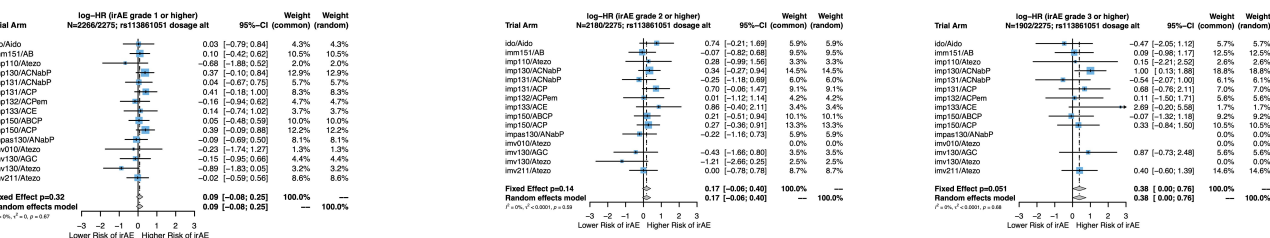
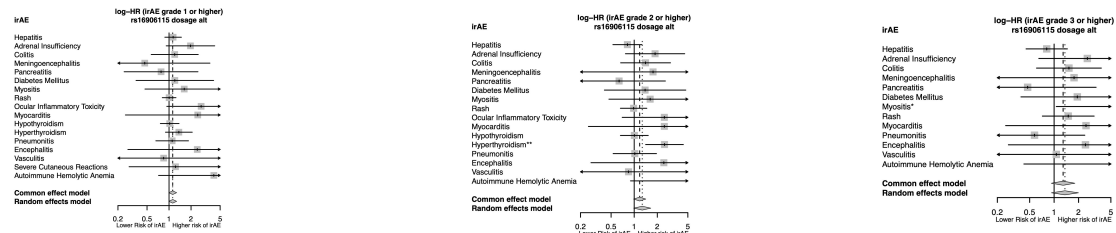
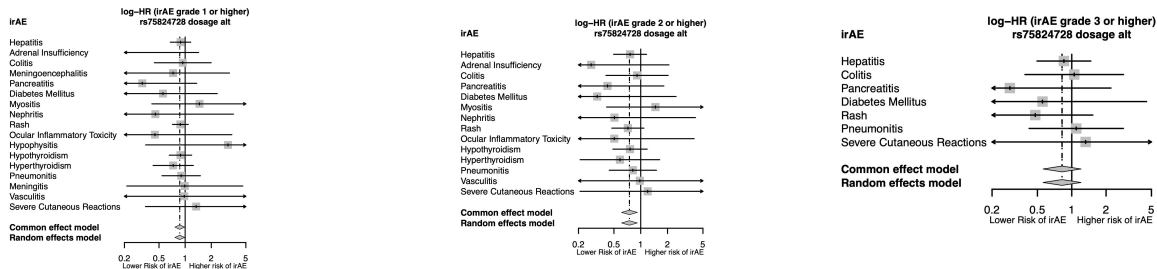


Figure S18

(a)



(b)



(c)

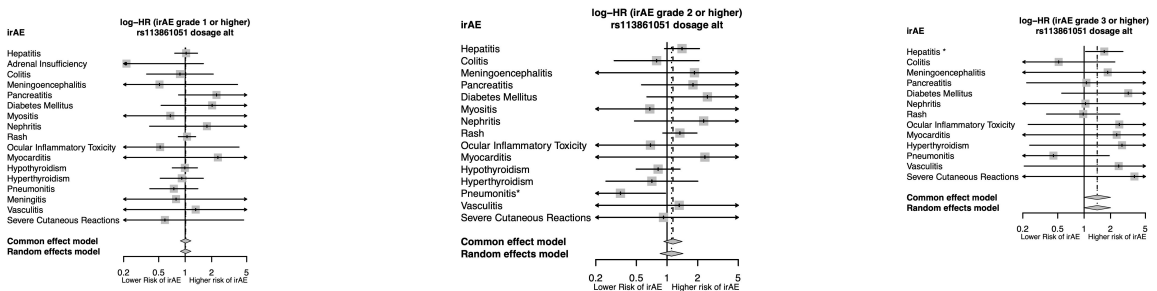
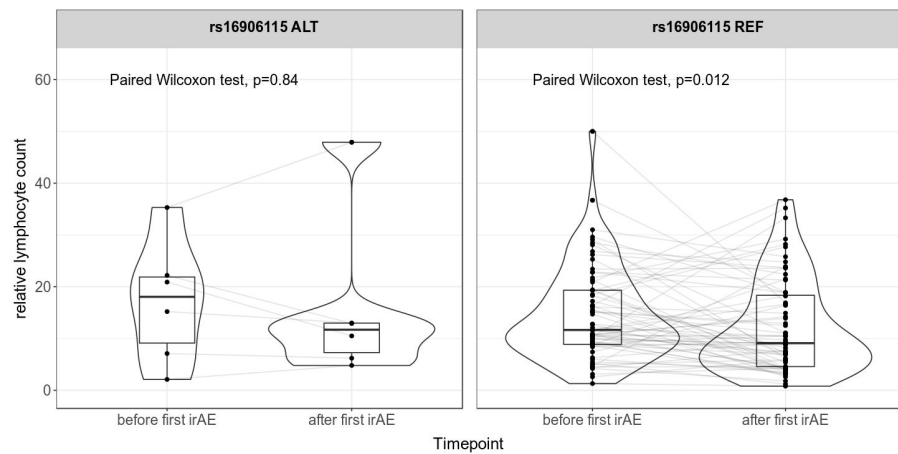


Figure S19

a.



b.

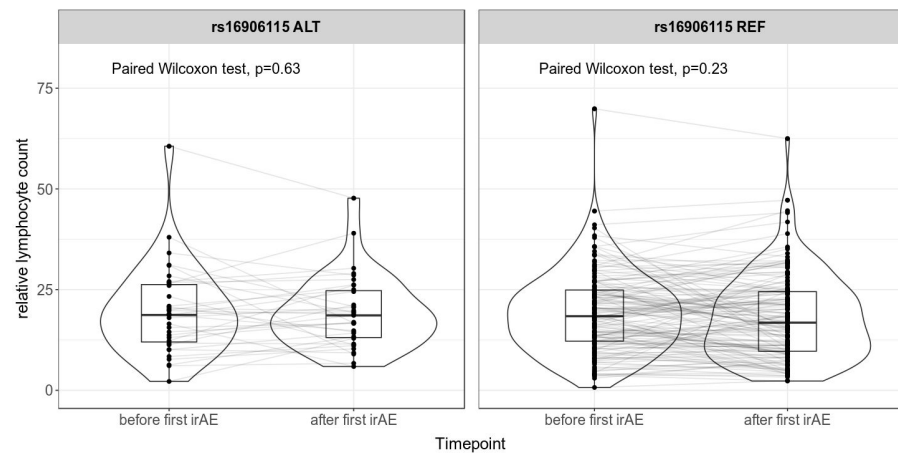
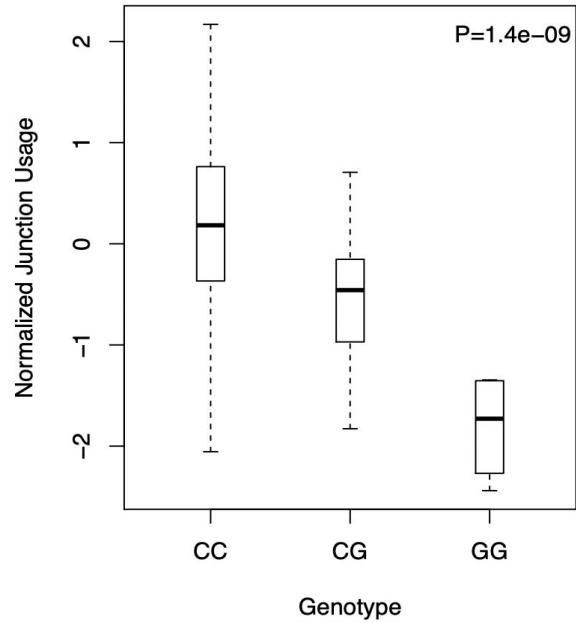


Figure S20

78740082:78749524 junction (Testis)



IL7 cryptic exon (Testis)

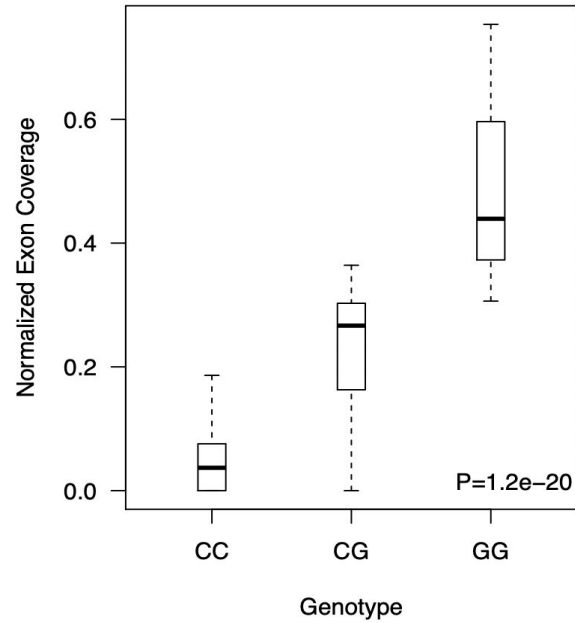
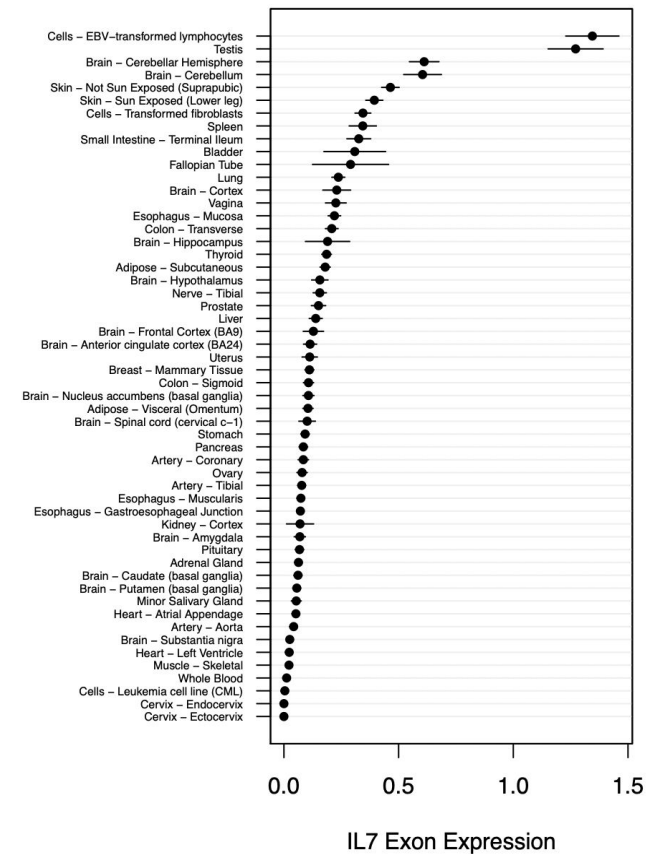


Figure S21

a.



b.

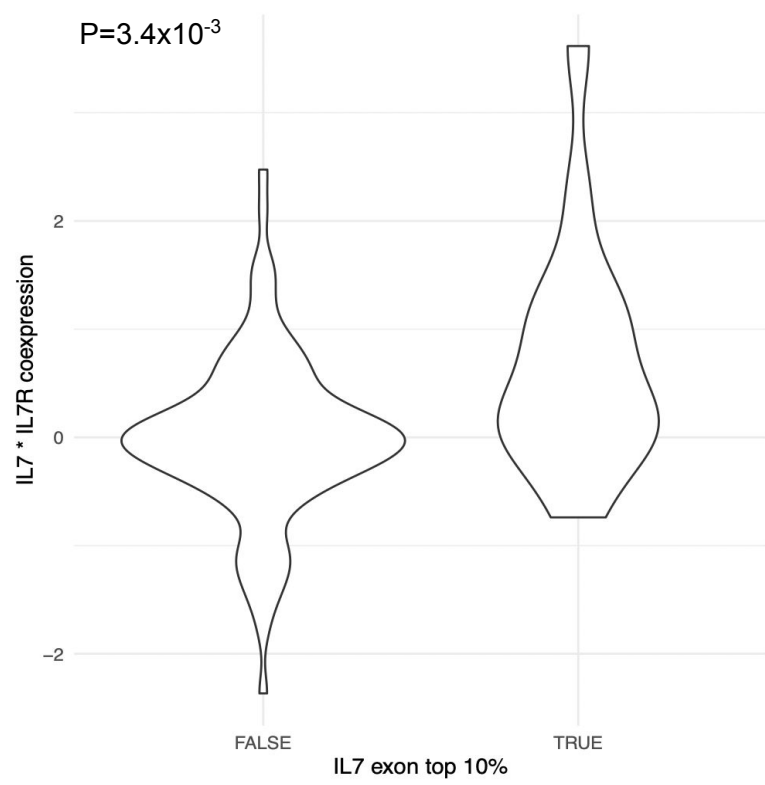


Figure S22

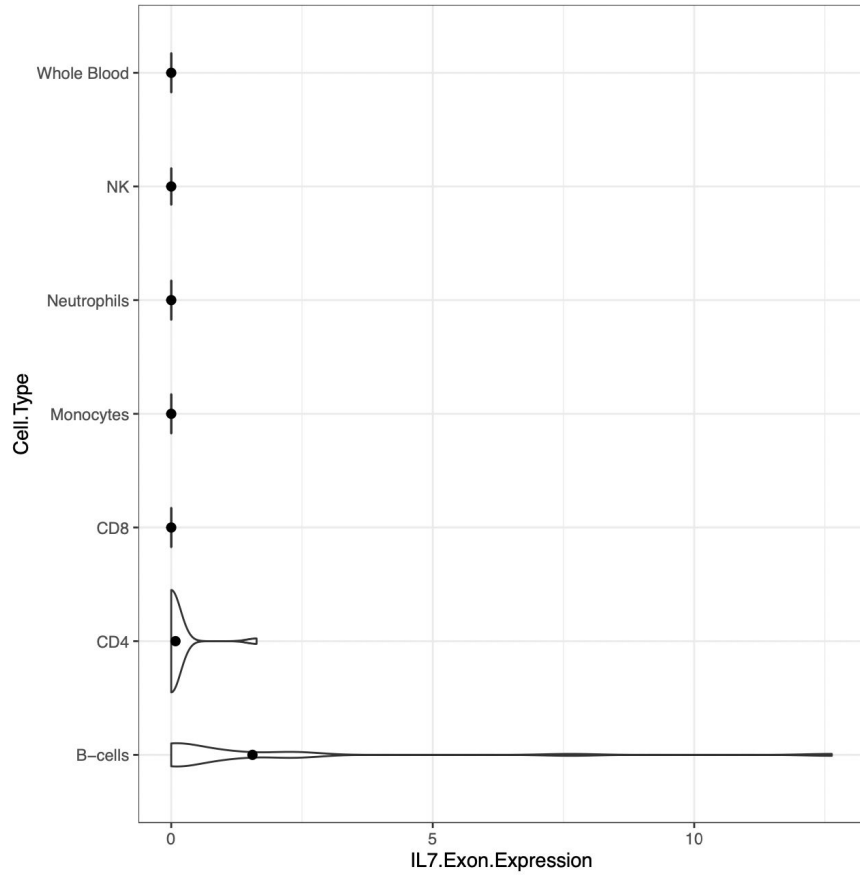
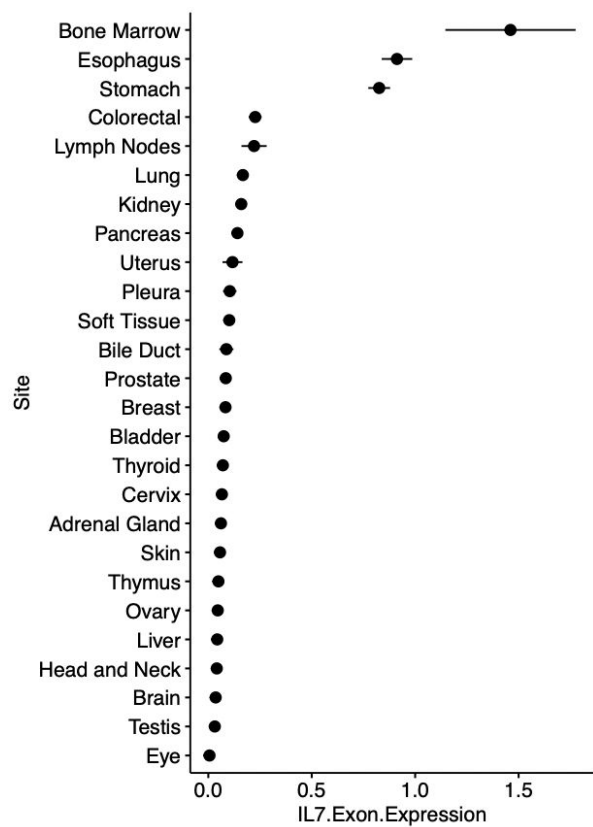


Figure S23



Previous autoimmune disease

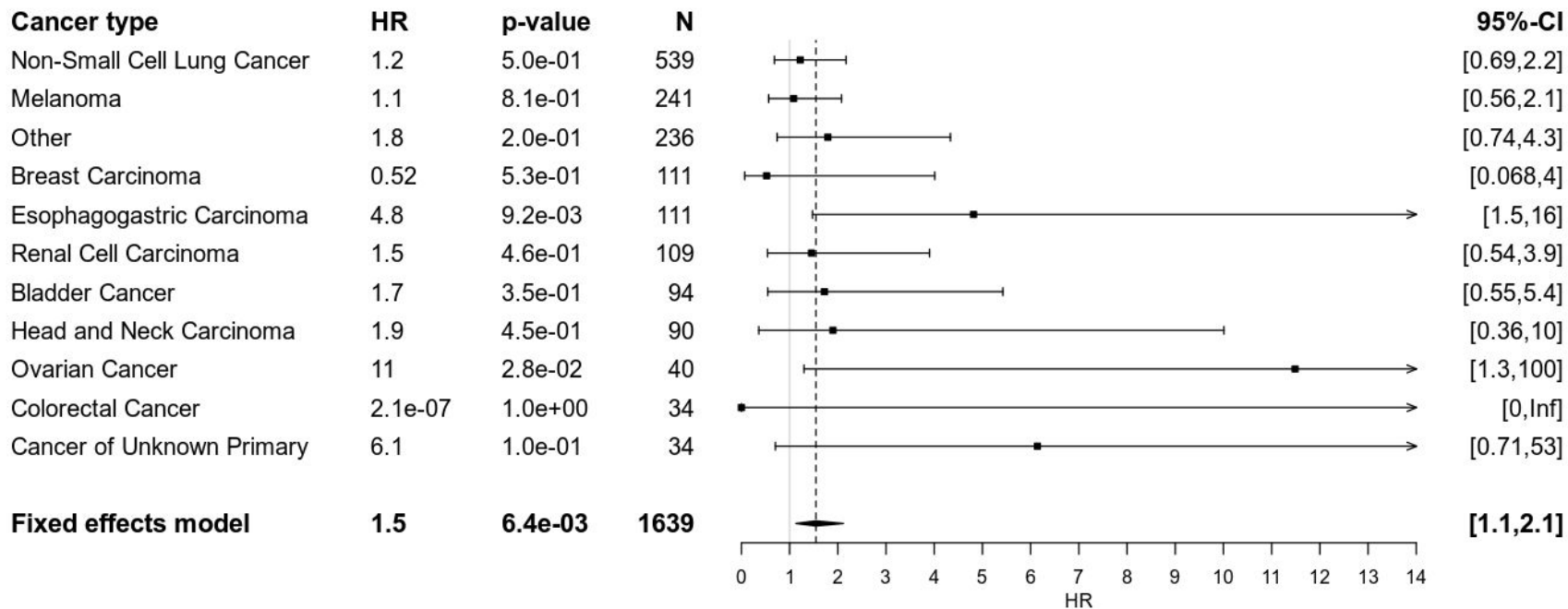


Figure S24: Previous autoimmune disease

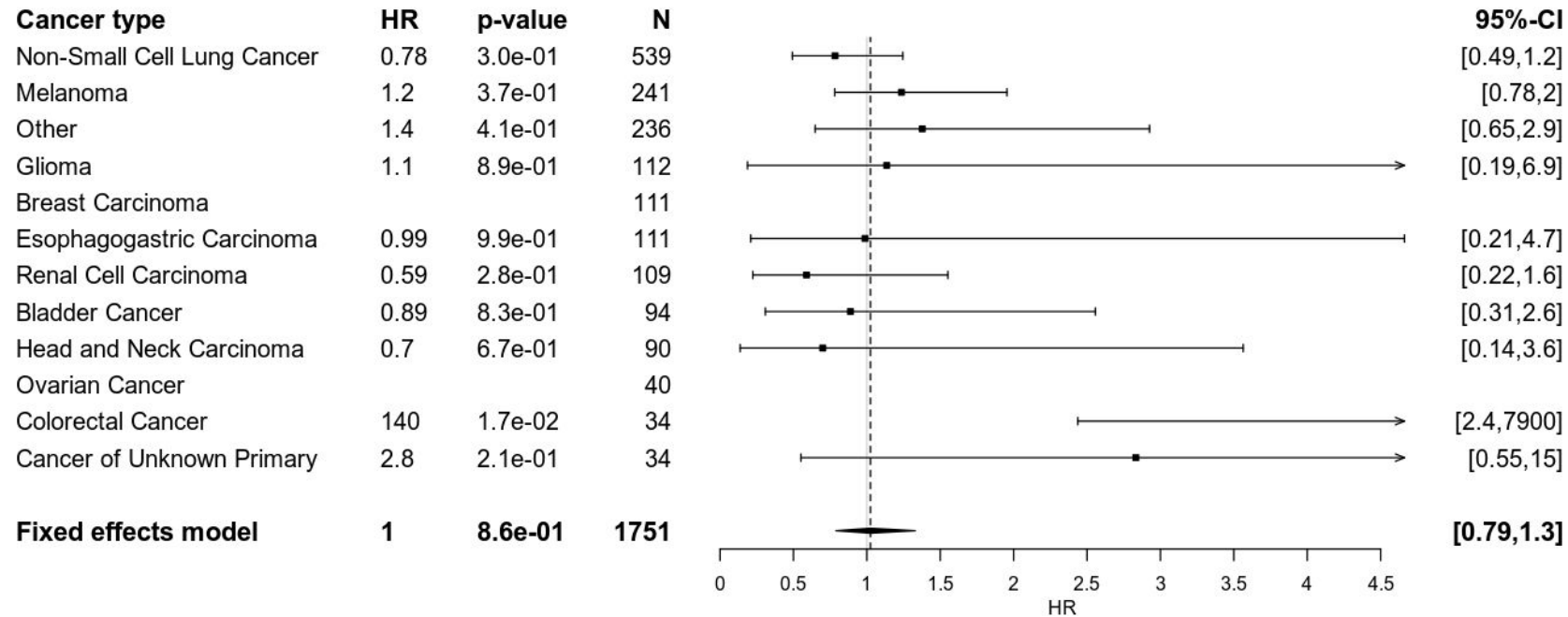



Figure S25: Sex difference

Table S1

Immune Feature	IL7 Exon Usage		IL7 Expression		IL7 Exon IL7 expression	
	Z-Score	P-value	Z-Score	P-value	Z-Score	P-value
Leukocyte.Fraction	9.2	7E-20	8.2	3E-16	7.7	2E-14
Stromal.Fraction	8.1	6E-16	3.4	7E-04	7.6	4E-14
Proliferation	7.2	5E-13	-1.4	2E-01	7.7	2E-14
Wound.Healing	7.1	1E-12	16.4	2E-59	4.0	6E-05
Macrophage.Regulation	7.1	1E-12	-5.2	2E-07	8.3	9E-17
Lymphocyte.Infiltration.Signature.Score	6.6	4E-11	4.1	4E-05	5.9	4E-09
IFN.gamma.Response	5.6	3E-08	7.2	9E-13	4.2	2E-05
TGF.beta.Response	5.5	4E-08	1.5	1E-01	5.3	1E-07
BCR.Shannon	5.3	1E-07	2.0	5E-02	5.0	8E-07
TCR.Shannon	4.0	7E-05	1.5	1E-01	3.8	2E-04
TCR.Richness	3.9	1E-04	7.7	2E-14	2.4	2E-02
CTA.Score	3.5	4E-04	1.8	8E-02	3.2	1E-03
Th1.Cells	3.3	1E-03	12.8	4E-37	0.8	4E-01
Th2.Cells	3.3	1E-03	21.8	5E-103	-1.0	3E-01
Th17.Cells	2.8	6E-03	-5.3	2E-07	3.9	8E-05
B.Cells.Naive	2.3	2E-02	4.0	6E-05	1.5	1E-01
Dendritic.Cells.Resting	1.0	3E-01	-3.9	1E-04	1.8	7E-02
Macrophages.M0	0.5	6E-01	-9.9	4E-23	2.6	9E-03
Macrophages.M1	0.4	7E-01	3.8	2E-04	-0.4	7E-01
Macrophages.M2	0.2	8E-01	-4.8	2E-06	1.2	2E-01
Mast.Cells.Activated	-0.1	1E+00	6.6	4E-11	-1.4	2E-01
NK.Cells.Activated	-0.6	5E-01	-4.2	3E-05	0.2	8E-01
Plasma.Cells	-0.7	5E-01	-11.5	3E-30	1.7	9E-02
T.Cells.CD4.Memory.Resting	-1.1	3E-01	-3.7	2E-04	-0.3	7E-01
T.Cells.CD8	-1.3	2E-01	-6.7	2E-11	0.1	1E+00
T.Cells.Follicular.Helper	-2.6	9E-03	-4.7	3E-06	-1.7	9E-02
T.Cells.Regulatory.Tregs	-3.6	3E-04	-1.2	2E-01	-3.4	7E-04
Lymphocytes	-3.6	3E-04	-6.6	4E-11	-2.3	2E-02
Macrophages	-4.2	2E-05	-2.8	5E-03	-3.8	2E-04

 Positive association


 Negative association

Table S2: Interaction Analysis

SNP	Chromosome	Position	Posterior probability	P-value in Profile cohort
rs16906115	8	79712998	0.1978415408	3.79E-09
rs7011565	8	79557237	0.1957790135	3.83E-09
rs16906062	8	79659182	0.1007706209	7.75E-09
rs7816685	8	79658906	0.06223026669	1.29E-08
rs73251644	8	79694464	0.06051930009	1.33E-08
rs73249933	8	79626275	0.05998693589	1.34E-08
rs74197776	8	79656182	0.05961872189	1.35E-08
rs117355070	8	79665307	0.05176578818	1.57E-08
rs116228140	8	79665329	0.04399633208	1.87E-08
rs141792902	8	79673847	0.02865189034	2.95E-08
rs4739139	8	79709926	0.01583309901	5.54E-08
rs59286098	8	79677592	0.01490514512	5.91E-08
rs16906090	8	79689755	0.01434440485	6.16E-08
rs10110519	8	79688026	0.01428458798	6.18E-08
rs2717536	8	79701876	0.01170948825	7.64E-08
rs9942766	8	79709182	0.009834019143	9.20E-08
rs2919935	8	79683948	0.008440074784	1.08E-07

Table S3: 95% credible set.

Study name	Reference
IDO inhibitor trial (ido)	Jung KH, LoRusso P, Burris H, et al., Clin Cancer Res, 2019
imm151 / IMmotion151	Rini BI, Powles T, Atkins MB, et al, Lancet, 2019
imp110 / IMpower110	Herbst RS, Giaccone G, de Marinis F, et al., N Engl J Med, 2020
imp130 / IMpower130	West H, McCleod M, Hussein M, et al., Lancet Oncol., 2019
imp131 / IMpower131	Jotte R, Cappuzzo F, Vynnychenko I, et al., J Thorac Oncol., 2020
imp132 / IMpower132	Nishio M, Barlesi F, West H, et al., J Thorac Oncol., 2021
imp133 / IMpower133	Horn L, Mansfield AS, Szczęśna A, et al., N Engl J Med., 2018
imp150 / IMpower150	Socinski MA, Jotte RM, Cappuzzo F, et al., N Engl J Med., 2018
impas130 /IMpassion130	Schmid P, Adams S, Rugo HS, et al., N Engl J Med., 2018 Schmid P, Rugo HS, Adams S, et al., Lancet Oncol., 2020
imv010 / IMvigora010	Bellmunt J, Hussain M, Gschwend JE, et al., Lancet Oncol., 2021
imv130 / IMvigora130	Galsky MD, Arija JÁA, Bamias A, et al., Lancet, 2020
imv211 / IMvigora211	Powles T, Durán I, van der Heijden MS, et al., Lancet, 2018

Table S4: Clinical trial replication cohorts

SNP	Ref>Alt	Profile cohort			MGH cohort			Clinical trial cohort	
		HR [95% conf int]	p-value	Frequency	HR [95% conf int]	p-value	Frequency	HR [95% conf int]	p-value
rs16906115	G>A	2.0 [1.6-2.5]	3.8x10 ⁻⁹	0.08	3.6 [1.8-7.1]	0.00028	0.10	1.2 [1.0-1.5]	0.05
rs75824728	G>A	1.9 [1.5-2.4]	8.4x10 ⁻⁹	0.10	1.49 [0.67-3.2]	0.4	0.08	0.77 [0.61-0.96]	0.02
rs113861051	A>(G/T)	2.0 [1.6-2.6]	1.1x10 ⁻⁸	0.07	1.4 [0.50-3.7]	0.55	0.08	1.18 [0.94-1.5]	0.14

Table S5: Genome wide significant loci

Cohort	Hazard ratio [95% conf int]	p-value
DFCI	1.2 [0.98,1.5]	0.083
MGH	1.3 [1.1-1.5]	0.007

Table S6: Overall survival association

Table S7: Search terms

irAE type	rs16906115		rs75824728		rs113861051	
	ALT	REF	ALT	REF	ALT	REF
Colitis	0.075	0.057	0.07	0.058	0.095	0.056
Other	0.086	0.042	0.11	0.039	0.11	0.04
Thyroid	0.08	0.025	0.042	0.03	0.061	0.029
Hepatitis	0.024	0.014	0.036	0.013	0.024	0.015
Adrenal insufficiency	0.024	0.016	0.036	0.015	0.008	0.018
Pneumonitis	0.042	0.031	0.048	0.03	0.11	0.024
Dermatitis/Rash	0.07	0.04	0.075	0.039	0.081	0.04

Table S8: irAE frequency in carriers and non-carriers by irAE type

		relative occurrence		absolute occurrence	
		Stopped therapy	Steroid given	Stopped therapy	Steroid given
rs16906115	ALT	0.45	0.48	20	21
	REF	0.5	0.5	1	1
rs75824728	ALT	0.36	0.36	4	4
	REF	0.49	0.51	17	18
rs113861051	ALT	0	0	0	0
	REF	0.54	0.56	21	22

Table S9: Occurrence of terminated therapy or steroid administration after irAE

grade of irAE	Number of events	Frequency
1	8	0.18
2	19	0.42
3	15	0.33
4	2	0.044
5	1	0.022

Table S10

test_name	HR	pval
ETV4 deletion	5.731719668	0.003699400454
PRS: PRSWEB_PHE	0.7550949468	0.01001543655
PRS: BRCA.ERPOS	0.7198298798	0.01044343632
SNV in PBRM1	3.785056795	0.01161673183
PRS: UKB_460K.bp	1.341783947	0.01183205383
FKBP9 deletion	23.06985775	0.01268981956
PRS: PRSWEB_PHE	0.7614820971	0.01491898934
RAD21 amplification	0.5100807525	0.01581436951
MYC amplification	0.5282454208	0.01641313591
EXT1 amplification	0.5224209595	0.01805440023
HLA_B_3502	0.1824060558	0.01885730417
TSC1 deletion	2.267507641	0.01910335487
RIT1 amplification	0.3546174109	0.02092329033
SNV in KEAP1	18.62636694	0.02224104713
PRS: UKB_460K.bp	1.297755261	0.02338238714
MYBL1 amplification	0.5130646042	0.02466486936
PRS: MEDS_P MID3	1.271415031	0.02550118264
SNV in BAP1	5.212250631	0.02665151397
SNV in KDM5C	8.984942194	0.02892369297
NBN amplification	0.5245835871	0.0290023963
MCL1 amplification	0.5476359034	0.02942844719
EED deletion	0.2025410208	0.02984498504
GLI3 deletion	20.15783465	0.03060921184
PRS: PRSWEB_PHE	0.8122150141	0.03282254513
JAK1 deletion	2.763798906	0.03376495058
PRS: UKB_460K.dis	1.301543093	0.03412615435
GBA amplification	0.3876058761	0.03639044686
PTCH1 deletion	2.058935475	0.03642655925
RSPO2 amplification	0.4444248628	0.03847852215
PRKDC amplification	0.5333109362	0.04039814261
Lab value: MPV	1.304653328	0.04075217595
SNV in DNMT3A	264.1946866	0.04083390644
PRDM1 deletion	0.4961774501	0.04085103024
FANCC deletion	1.998357002	0.04190215746
HLA_A_0101	0.6695153848	0.04210819356
NPRL2 amplification	8.530256906	0.04329046232
CDC73 deletion	11.65016524	0.04347320142
BCL2 amplification	0.2117517967	0.04408131728
FANCG amplification	0.1693113757	0.04820008356
BRCC3 amplification	7.221922411	0.04832622552
HLA_B_4403	1.801459696	0.04855363658
PRS: Stratified_rect	0.7949677598	0.04992908715

HLA_B_3503	2.854659263	0.05046039981
Lab value: GLOB	0.6540182794	0.05388394331
NTRK2 deletion	1.939829268	0.05388878251
NOTCH1 deletion	1.922227665	0.05456673281
PRS: MEDS_P MID3	1.226524685	0.05507243575
PRS: UKB_460K.blo	1.253378239	0.05557997345
RECQL4 amplificati	0.5551500377	0.05757071479
PRKDC deletion	2.82974404	0.05790906468
PRS: PMID27863252	0.8226974173	0.06043442068
KRAS deletion	2.959313964	0.06174435205
POLE amplification	3.146149137	0.06404531867
XPA deletion	1.895261676	0.0643297655
MPL amplification	0.2806639645	0.06455896714
FLT4 amplification	2.165435643	0.06551916053
PRS: PMID27863252	0.8276926911	0.06593843775
PRS: PMID27863252	1.203457168	0.06594616918
SNV in RBM10	3.912205743	0.06603365102
Lab value: CA	1.784857218	0.0660394233
RHOA deletion	2.631459671	0.0666891275
Lab value: MG	0.1760334704	0.06669127974
COL7A1 deletion	2.644680642	0.06756404418
KCNQ1 deletion	3.100325708	0.06863997054
RBBP8 deletion	2.949557127	0.06866020384
PRKCZ deletion	0.3210232092	0.06878303899
AURKA deletion	7.291338306	0.06880891996
BRAF amplification	0.5271258845	0.06907776553
GNAS deletion	5.565842771	0.06995396938
Lab value: LDH	1.001399607	0.07021888922
ZNF217 deletion	7.174919959	0.07176635775
PRS: GLIOMA	1.19285215	0.07249755917
PRKCI deletion	0.1842391603	0.07411007153
PRS: TRICL.sma_ns	1.269822053	0.07416063287
Lab value: PT	1.178014941	0.07510240999
PRS: PMID27863252	0.8339632996	0.07599485474
PRS: PRSWEB_PHE	0.8052972789	0.07704299224
CDKN2C amplificati	0.19279148	0.07822485453
PRS: PMID27863252	0.8344714008	0.07826029488
FANCG deletion	1.599678077	0.07850422435
GATA3 deletion	0.4902290496	0.07905322108
PRSS1 amplification	0.347412307	0.08135115968
LMO3 deletion	2.568873752	0.08185959706
PRKAR1A amplifica	0.5315628231	0.08349579877
PRS: UKB_460K.pig	1.243722681	0.08383145173

HLA_B_4901	2.308193489	0.08523468158
PTK2 amplification	0.4946650055	0.08544568222
AKT3 deletion	10.58248775	0.08609381146
HLA_DQA1_0101	1.448295165	0.08654387136
H3F3A deletion	10.16762276	0.08761854298
SNV in ATRX	5.329002489	0.08822866096
HLA_B_4402	1.741640375	0.08914783597
RET amplification	0.06368784432	0.08926650942
Lab value: PTI	4.806807542	0.08972257681
NFKBIZ deletion	0.3655016423	0.08977617148
GATA6 amplification	0.3664670786	0.08996892522
PRS: UKB_460K.pig	1.288058711	0.090142109
EZH2 amplification	0.557674872	0.09059778242
STAT6 amplification	1.602141793	0.09080937937
CDKN2B amplification	0.108056249	0.0914153669
UROD deletion	2.481003468	0.09345393877
PRS: MEDS_P MID3	1.209619647	0.09357057229
XRCC2 amplification	0.3724134655	0.09371341093
H19 deletion	2.831319992	0.094255384
CD79B amplification	0.5406625004	0.0950325489
RAD54B deletion	8.128090453	0.0961090609
PNKP deletion	3.738719085	0.0964542084
PAXIP1 amplification	0.3765426628	0.09651399535
SNV in PTEN	0.1095280502	0.09720108059
BRCA1 deletion	2.240355019	0.09808250266
Lab value: DMNEUT	0.9401686264	0.09962000499
FGFR4 amplification	1.856037611	0.100754695
PAX5 deletion	1.55975703	0.1013987112
NOTCH2 amplification	0.4384470419	0.1016554388
RAD54B amplification	0.5208354521	0.1017498174
SNV in SMARCA4	6.421912533	0.1030657903
PIK3CA deletion	0.248452819	0.1037086854
SS18 deletion	2.501580408	0.1044256229
ZNF708 deletion	2.485487631	0.1055731267
SOX2 deletion	0.2126715635	0.1062244564
TAL1 deletion	2.325867004	0.1062909055
SMARCE1 deletion	3.438469465	0.1068030433
SNV in CDKN2A	2.118233133	0.1073466443
Lab value: TRIG	1.012839638	0.1086882129
ARID1A amplification	0.001439682594	0.1097630862
MAP2K1 deletion	0.3839499477	0.109966931
MDM4 deletion	8.452981815	0.1110168502
SNV in BCORL1	11.55405179	0.1115742241

RNF8 amplification	0.4579930383	0.1125851536
UBE2T amplification	0.4993317583	0.1128806326
TMB_binned2	1.444272276	0.1152372152
PRS: PMID27863252	1.172975511	0.1167462006
HLA_B_0801	0.6811132887	0.1170249746
CDKN2A amplification	0.03431131703	0.1175979173
FANCA deletion	0.5427618478	0.1191636076
PRS: UKB_460K.bio	1.187820096	0.1194976189
SNV in ERBB4	2.734600831	0.1203804142
BRCA1 amplification	0.4365078861	0.1206084923
SNV in B2M	3.446887976	0.121491715
Lab value: AMY	1.014124515	0.1215101605
PRS: CKD_overall_E	1.43410216	0.1232957887
PRS: UKB_460K.lun	0.8415881278	0.123581724
FH deletion	8.971862957	0.1244166929
SNV in KDM6A	2.497325248	0.1248416694
BRAF deletion	0.2719016698	0.1257642374
HOXB13 deletion	4.113098928	0.1260492115
CYLD deletion	0.5469151155	0.1263361435
NFKBIA deletion	1.730224382	0.1277828652
TMB	1.023056694	0.1283360624
CTCF amplification	4.966895085	0.1283992483
totalper_genes	0.24529636	0.1302080162
PRS: PRSWEB_PHE	1.173344237	0.1309304075
RUNX1T1 amplification	0.5263056705	0.1309441763
DAXX amplification	0.4874495042	0.1328429064
ERBB3 amplification	1.526492431	0.1338525222
CBFB amplification	4.758534114	0.134543108
ABL1 deletion	1.669055611	0.1351306811
PRS: UKB_460K.rep	0.8629191045	0.1352651271
SDHAF2 amplification	0.08405596059	0.1357863283
MYCL deletion	2.336241655	0.1364824274
PRS: UKB_460K.bo	1.188626429	0.1366484401
ATR amplification	0.1338770307	0.1375638043
RMRP amplification	0.1882802466	0.1376978016
UROD amplification	0.03727998327	0.1389957678
NF2 amplification	0.2513317265	0.1390132213
POLQ deletion	0.3833246686	0.1391742322
RPTOR deletion	6.261418414	0.1398083995
PRS: PMID27863252	1.149336033	0.1399370578
POT1 amplification	0.4182666293	0.1402582878
CBLB deletion	0.4079493278	0.1406624059
PRS: UKB_460K.car	0.8819937605	0.1422306834

SPOP deletion	3.751507309	0.1424629366
RAD51D amplificati	0.3745611711	0.1430658689
ARID1A deletion	0.5502556849	0.1442037099
RET deletion	0.5770640521	0.1463767836
SMARCB1 amplifica	0.3782417814	0.1479160453
MAPK1 amplificatio	0.3301999589	0.1479672587
SMAD4 amplificatio	0.3532792711	0.1492929281
HLA_DQB1_0602	1.436659576	0.1504885309
ETV4 amplification	0.4714068449	0.1512499896
BRE amplification	0.06935156907	0.1517987489
ERBB2 amplificatio	0.5333844239	0.1523638703
MYB amplification	0.5020951577	0.15272354
TET1 deletion	0.4695766784	0.1532651135
IGF2 deletion	2.454389384	0.1537131707
SF1 deletion	0.3451128123	0.1537223208
MECOM deletion	0.03551938671	0.1537515815
PTEN amplification	0.00174013901	0.1541756847
KIF1B amplification	0.01334552323	0.1546832667
MBD4 deletion	0.2972238541	0.1554024385
PRF1 deletion	0.6179517029	0.1569198945
ARID2 amplification	1.575690127	0.1581922909
BCL6 deletion	0.3034331679	0.159388803
SMO deletion	0.3060760468	0.1605972785
TERC amplification	0.5571226539	0.1610564139
PVRL4 amplificatio	0.5508922656	0.1610579538
RHPN2 deletion	5.990116226	0.1637419224
RHEB amplification	0.6129913209	0.1639162892
PRS: TRICL.sma.HM	1.191992733	0.1647178931
CDK8 deletion	0.3796539909	0.165737541
CIC amplification	0.3556205111	0.1659536307
NRAS amplification	0.3504256822	0.1672004304
STAT3 amplification	0.5146224695	0.1672304665
GATA2 deletion	0.4043847955	0.1690481716
MLH1 amplification	2.321758929	0.1694052013
CDH1 deletion	0.5253432953	0.1700091104
PPP2R1A deletion	3.196683391	0.1709527724
IGF1R deletion	0.4502363783	0.1711090161
PRS: PRSWEB_PHE	0.8626338142	0.1712469011
TMB_rank	1.15356967	0.1716284338
MYCL amplification	0.3275646431	0.171919864
GEN1 amplification	0.2459840174	0.1744705073
YAP1 deletion	0.3925406233	0.176567283
RMRP deletion	1.680271351	0.1766908652

GATA6 deletion	1.693509709	0.1767138417
PTPN11 amplificatio	1.548353912	0.1773709269
KMT2D amplificatio	3.194497226	0.1776008002
GLI1 amplification	1.469259454	0.1798546336
XRCC1 amplificatio	0.3937971758	0.1798761458
MUTYH amplificatio	0.3035189172	0.1828414911
HLA_A_0201	1.256948489	0.1828729884
SOX9 amplification	0.6482161297	0.1829474575
HLA_DPB1_0101	0.5019007254	0.1833707199
HLA_C_0401	0.7308478156	0.1834704265
MAX deletion	2.494359067	0.1849259964
HLA_DQB1_0501	1.347249532	0.1867637441
CREBBP deletion	0.2479112195	0.1869932807
PRS: Stratified_left	0.8621703175	0.187391747
HLA_C_0701	0.761855325	0.1881304
STAG1 amplificator	1.518132386	0.1882544238
PRS: Stratified_rect	0.8711488284	0.1893136414
ETV5 deletion	0.3068740478	0.1898332532
HLA_DRB1_0101	1.529235284	0.1900012535
PRS: PMID27863252	0.858067108	0.1907018167
HLA_A_2902	1.528584742	0.1914934029
SUZ12 amplificator	0.5778248801	0.1916364931
GREM1 amplificatio	0.0110833975	0.1916433267
EME1 deletion	3.104781765	0.1920163715
TSC2 deletion	0.2707713445	0.1921472657
NTRK1 amplificatio	0.7060782426	0.1928150197
HLA_C_0202	1.598131492	0.1938864192
ROS1 deletion	0.630535872	0.194170538
DEPDC5 deletion	2.243914538	0.1941861839
RPA1 amplification	3.18729498	0.1947149283
FANCF amplificatio	0.1223561403	0.1947546752
PRS: TRICL.ade_ns	1.199567794	0.1955126656
NF1 deletion	1.838350842	0.1956465004
PRS: UKB_460K.dis	0.8683058343	0.196966171
ID3 amplification	0.4049863934	0.197104553
REL deletion	0.0006961226388	0.1989607591
ZNRF3 amplificator	0.2772878926	0.1990098328
PRPF8 amplificator	0.1857966635	0.199074343
HLA_B_1402	1.537832141	0.1993132769
TCEB1 amplificator	0.5998764381	0.1995888387
HLA_A_3101	1.824273385	0.2007150457
TERC deletion	0.05472630791	0.2017791731
PRS: PRSWEB_PHE	1.137170847	0.2019774698

RHEB deletion	0.3114108604	0.2022046408
FAM46C amplificati	0.3979824806	0.2023673531
Lab value: T3TM	0.9857927273	0.2030590469
PIM1 amplification	0.6362995815	0.2052771508
HLA_B_4002	6.558420527	0.2057575065
SETBP1 amplificati	0.4360019955	0.2067685785
EWSR1 amplificatio	0.3265596262	0.207130614
ALOX12B deletion	1.640316725	0.2087395263
CDK12 deletion	2.329741592	0.209885595
CHEK2 amplificatio	0.3903475662	0.2102713781
CEBPA amplificatio	0.6364926857	0.211004113
PRS: Stratified_LvR	1.144468058	0.2110229487
BRIP1 amplification	0.6482360311	0.2126890974
SMARCE1 amplifica	0.4332296015	0.2129823208
MEN1 amplification	0.1646257654	0.2130637651
B2M amplification	0.2756965046	0.2150508773
PMS2 deletion	2.777890087	0.2157152923
PRKAR1A deletion	3.915924132	0.2161219474
CBL deletion	0.6644547475	0.2166429075
CDKN1A amplificati	0.6364013107	0.2168012549
EGLN1 amplificatio	0.5876667692	0.2173660257
SRSF2 amplificatio	0.6393551259	0.2180862647
IL7R amplification	1.885445968	0.2196269938
PRS: Stratified_cold	0.8752067203	0.2200828657
HLA_DRB1_1501	1.429325806	0.2208034575
HLA_DQA1_0201	1.338722663	0.2210153176
CCND3 amplificatio	0.6909635657	0.2216589664
IDH2 deletion	0.5118885114	0.2218136641
BRCA2 amplificatio	0.3252875255	0.224431562
CCNE1 deletion	1.928305669	0.2266026489
PAX5 amplification	0.5061014664	0.2272899953
RPTOR amplificatio	0.5651866969	0.2286951223
GLI2 amplification	0.3622943525	0.2290398712
BLM deletion	0.5034632384	0.2291294737
PRPF40B amplificat	1.534085063	0.2292752899
MAF amplification	4.660794803	0.229486636
NTRK3 deletion	0.5122936381	0.2300958888
RAD51D deletion	2.307304709	0.2301724051
PRS: UKB_460K.car	0.878891924	0.2310632205
RICTOR amplificati	1.886558832	0.2316008528
TLR4 deletion	1.698800929	0.2319623216
CBFA2T3 amplificat	5.098910277	0.2323802381
Lab value: PBUN	1.016799899	0.2329235651

IDH1 deletion	1.478981464	0.2329833617
TAL1 amplification	0.01141605709	0.2337506271
PRS: BUN_overall_E	1.134236219	0.2341532018
PRS: PRSWEB_PHE	0.8667443347	0.2380879962
HLA_B_5001	3.619382843	0.2380911714
HIST1H3C amplifica	0.6136380626	0.2385385684
RAD52 deletion	0.2930095315	0.239925274
CRTC1 deletion	2.533768074	0.240197143
RICTOR deletion	0.4439647992	0.2408141677
Lab value: ALB	1.413414323	0.2415209581
WRN amplification	0.5140993137	0.2419333864
NTHL1 deletion	0.2156312892	0.2426035199
RPL26 deletion	1.638679588	0.2431393621
SS18 amplification	0.2324992802	0.2451459214
ZRSR2 deletion	0.1061392361	0.2459343389
KDM6B deletion	1.571125973	0.2474774695
CDK9 deletion	1.595215055	0.2475485482
ALK deletion	0.008833916945	0.2475749413
SDHB deletion	0.6447396782	0.2481693415
Lab value: PGLU	0.9954286728	0.2489313598
SMO amplification	0.6694423972	0.2509429359
HLA_C_0802	1.45584011	0.251034758
KAT6B deletion	0.5559874494	0.2511556602
BRD3 deletion	2.27918948	0.252654871
HLA_C_1601	1.771530996	0.252994078
TOPBP1 deletion	0.354448518	0.2531991572
ID3 deletion	0.6336896651	0.2536887536
GATA4 amplification	0.5051647277	0.2538558899
Lab value: AEOSM	28.1998513	0.2556530849
Lab value: CRE	1.20659424	0.2561325244
SYK deletion	1.582180625	0.2573261421
BARD1 deletion	2.033946718	0.2575302388
RBBP8 amplification	0.2322776158	0.2583919427
Lab value: VCRE	1.09072988	0.2603510649
XRCC5 deletion	2.021959034	0.260606871
CTNNA1 deletion	0.432869805	0.2618629417
POLQ amplification	0.2330523898	0.2622089858
POLE deletion	3.137214684	0.2628626173
SDHB amplification	0.3113225662	0.2648357295
HLA_B_3508	0.08878911836	0.2652012983
CDH4 deletion	3.772872799	0.2652429426
NFE2L2 deletion	0.5187649092	0.2655119898
SH2B3 amplification	1.450715537	0.2661680995

STAT3 deletion	1.697637791	0.2662446402
ERBB4 deletion	1.409914782	0.2668098865
TCF7L1 amplificatio	2.129294655	0.2675246938
PRS: UKB_460K.blo	0.8825458153	0.2679902502
ERCC1 amplificatio	0.4509665465	0.2689245489
PRS: UKB_460K.dis	1.136204967	0.269775985
PRS: TRICL.nonsmc	1.142426559	0.2703414859
EZH2 deletion	0.3292096985	0.2718160325
BMPR1A amplificati	0.05028226249	0.2724784332
PRS: MEDS_PMI3	0.8872572105	0.2735737476
TLX3 amplification	1.862480248	0.2751978934
SMAD2 amplificatio	0.4869679903	0.2756273123
HNF1A deletion	1.681430628	0.277234679
NPRL3 deletion	0.3156146521	0.2775444034
FAS amplification	0.002485563618	0.2776306504
CCND1 deletion	0.3209625121	0.2783781537
Lab value: TP	0.7870246319	0.2791211953
Lab value: EGFR	0.9917603753	0.2791809483
PRS: PRSWEB_PHE	1.120260115	0.2802865687
MET deletion	0.4098036097	0.2803308685
SNV in TSC1	5.949158491	0.2807935251
CADM2 deletion	0.5440864788	0.2810195963
FGFR1 deletion	1.373848304	0.2815100984
SQSTM1 deletion	1.872703081	0.2821977343
KDM6A amplificatio	0.06604511659	0.2823198986
JAK1 amplification	0.02660882724	0.2834691678
FANCE amplificatio	0.6808762457	0.2835410997
ERCC1 deletion	2.860465194	0.2835828134
CSF3R amplificatio	0.3919159337	0.2847950311
RINT1 amplification	0.5406436159	0.2855681872
NFKBIE amplificatio	0.6545895035	0.2859236807
NF1 amplification	0.5921352188	0.2862547481
DIS3L2 deletion	1.950025707	0.2864633189
RB1 deletion	0.6739276861	0.2889180468
TOPBP1 amplificati	0.2951863387	0.2900227785
ARHGEF12 amplific	0.1969998029	0.290443196
CDK6 amplification	0.7066298676	0.2905802368
HMBS amplification	0.1974054411	0.2910567662
BUB1B amplificatio	0.4054664182	0.2918036014
CDK2 amplification	1.481899589	0.2918657374
PRS: RCC	0.8779401163	0.2920411154
EPHA7 deletion	0.4346586675	0.2924940144
SLX1B deletion	2.416620278	0.2938313136

SNV in VHL	2.067500268	0.2939917781
SDHD deletion	0.7263936587	0.2942849462
SNV in BRCA2	2.323958942	0.2949855337
Lab value: MMONO	1.122978935	0.2950423369
PRS: UKB_460K.bl	0.8944796799	0.2956965045
MTOR deletion	0.675797022	0.2961210148
STAG2 amplificator	0.1345420099	0.29690737
H3F3B amplificator	0.6170508574	0.2974494248
CUX1 amplification	0.6902845296	0.2984116046
PALB2 deletion	0.3129717277	0.2989837108
PRS: PMID27863252	0.8871690128	0.2997668118
CCND1 amplificatio	0.6677919091	0.2997836927
DDR2 deletion	4.681141837	0.3007882406
SDHC deletion	4.681141837	0.3007882406
RARA amplification	0.6181391064	0.3029813357
PDGFRB deletion	0.6181919952	0.3040485368
ATR deletion	0.4085612464	0.3041494179
KIT deletion	1.476884354	0.3050158413
KLLN amplification	0.02941788368	0.305202283
CDKN1B deletion	1.443462893	0.305778283
QKI amplification	0.3106271335	0.3059936392
Lab value: UWBC	0.9531313778	0.306153542
SNV in MSH2	6.29106312	0.3076423905
SMC3 amplification	0.001200544225	0.3088032685
HRAS deletion	0.5946840595	0.3088775634
RHOT1 amplificatio	0.5862985839	0.3103892519
PRS: PMID27863252	0.8805437272	0.3107462782
PDGFRA deletion	1.47164388	0.3119178987
ELANE deletion	0.2334155325	0.3122181246
IL7R deletion	0.4888053919	0.3126295858
RAD50 deletion	0.4798768231	0.3142875441
CALR deletion	0.1025326734	0.3145532931
ARID1B amplificatio	0.3364351264	0.3145899358
ERCC6 amplificatio	0.1329991098	0.3148190819
GSTM5 deletion	0.533391705	0.3186599725
PHF6 deletion	0.1732884207	0.3196527458
PRS: PRSWEB_PHE	1.122051841	0.321794617
ETV1 deletion	2.328230441	0.3225713503
PARK2 amplificatio	0.3543322699	0.3226638322
CRLF2 deletion	0.2752381409	0.3234114981
RAD51C deletion	2.726166473	0.3235130846
SF3B1 amplificatio	0.6092216849	0.3239878237
SLC25A13 amplifica	0.59926649	0.3248894161

Lab value: MLYMPH	1.045190513	0.324920372
PTPN14 amplification	0.6728987111	0.3258147596
EME1 amplification	0.5803683583	0.3264963119
PTPN11 deletion	1.618525976	0.3266841724
MAP2K2 amplification	0.1717437309	0.3270023534
KLLN deletion	0.6251486351	0.3282794653
PPM1D deletion	2.879977866	0.3284965639
CDK1 deletion	0.559924387	0.3286557627
PDGFRB amplification	1.64441642	0.3287811128
PRS: MEDS_P MID3	1.112738751	0.329212862
STAG2 deletion	0.09880030443	0.3301297121
GALNT12 deletion	2.072150907	0.3303212548
Lab value: SGPT	0.9945987103	0.3304923334
SUFU amplification	0.002262188989	0.3306968549
PRS: UKB_460K.cov	0.8686280379	0.3308994821
ATM amplification	0.2640272499	0.3323108148
BUB1B deletion	0.7001504271	0.3328468371
POLH amplification	0.6835957882	0.3328521592
PRS: UKB_460K.bo	1.118670603	0.3332091459
POT1 deletion	0.3641115218	0.333529881
PRF1 amplification	0.1054682565	0.3337005788
KDR deletion	1.433292288	0.3340614753
CBL amplification	0.3652875708	0.335233964
Lab value: MONO	1.034242597	0.3357354663
SLX4 deletion	0.08374491936	0.335764289
BCORL1 deletion	0.1480888447	0.3360260228
SETD2 amplification	1.853584451	0.3366910022
FOXL2 amplification	0.358563273	0.3369025866
BRD3 amplification	0.4712079691	0.3370576533
NOTCH3 deletion	0.02247080579	0.3371118783
AR deletion	0.0534364609	0.3372021117
PRS: PRSWEB_PHE	1.113207603	0.33827655
MET amplification	0.7312530742	0.338780465
FAH deletion	0.3910636024	0.3389550694
PRS: Stratified_mak	0.9009270913	0.3405364733
HNF1A amplification	1.372195223	0.341072612
PNRC1 deletion	0.4590608012	0.3412096994
TRAF7 deletion	0.09000721047	0.3421471345
PMS2 amplification	0.772565303	0.3422495631
RSPO3 amplification	2.079740844	0.3428158115
TET2 deletion	1.347325682	0.3433967255
TRAF7 amplification	2.049248967	0.3436510248
PSMD13 deletion	0.01399546177	0.3439108357

PRS: PMID27863252	0.8911789398	0.344315832
HLA_DRB1_0701	1.256677366	0.3444227705
IDH2 amplification	0.5571700928	0.3444683195
FUS deletion	0.2494557579	0.345168764
HLA_C_0303	0.7012153858	0.3461249075
RHOH deletion	1.665784986	0.3462130756
PRS: PMID27863252	0.8917221619	0.3473208156
PRS: TRICL.ade1_n	1.132411648	0.3480398954
USP8 deletion	0.6131346343	0.3480618951
CDK12 amplification	0.5704370042	0.349327255
SNV in SMAD4	0.08730591715	0.350308733
SNV in ASXL1	1.984344666	0.3503791053
XRCC3 amplification	0.1547168152	0.3504840144
Lab value: PLT	0.9988997381	0.3514306569
RB1 amplification	0.4209950923	0.3517021565
EP300 amplification	0.6062135083	0.3523608262
PIK3C2B deletion	2.076009186	0.3523863044
NEIL1 deletion	0.4092816285	0.3525002001
FAM175A deletion	1.905151665	0.3527105366
USP28 amplification	0.2372668017	0.3528950819
NEGR1 deletion	0.4944538636	0.353010491
GNAQ deletion	1.345923348	0.3542108352
H3F3A amplification	0.7794786106	0.3547429855
RNF43 deletion	2.54695779	0.3551111576
NEIL1 amplification	2.127888014	0.3554772763
PRS: PRSWEB_PHE	0.9021185124	0.3561969058
ARID1B deletion	0.744572962	0.3563621008
KCNIP1 deletion	1.679275998	0.3574524124
PRS: UKB_460K.dis	0.8991843983	0.3580124024
PRS: UKB_460K.pig	1.10448834	0.3580569153
ITK deletion	0.4798005915	0.3591838549
PRS: Stratified_prox	0.9108582795	0.3594339847
JAK2 deletion	1.251844968	0.361054435
Lab value: ALK	0.9984385704	0.3618962762
PRS: UKB_460K.bo	0.9009687196	0.3622428533
KMT2A amplification	0.2748536636	0.3651064411
HLA_DQB1_0604	1.690715928	0.3652046691
EGFR deletion	2.00869932	0.3669390586
HLA_DQB1_0202	1.296332531	0.3684680889
MITF amplification	0.5890856881	0.3684910921
CRKL amplification	0.6550008539	0.370158984
PNKP amplification	0.2702876518	0.3701630769
SNV in NF1	1.280860456	0.3709328261

MUS81 amplificatio	0.202815878	0.371233371
SNV in FAT1	2.689319447	0.3716454742
PRS: BreastCancer	1.13369127	0.3719538599
RUNX1 amplificatio	0.658065282	0.3720964851
NT5C2 amplificatio	0.0005644113314	0.3732765211
BCOR amplificatio	0.05948357644	0.3740710261
RHBDF2 amplificati	0.6633978279	0.3770512829
NF2 deletion	1.415891946	0.3794566227
TNFAIP3 amplificati	0.5791024045	0.3795783835
SNV in RB1	0.005466486977	0.3810461751
ATRX deletion	0.03851494441	0.3811961853
MSH6 amplificatio	0.611499279	0.3814496967
ERCC4 deletion	0.1870204644	0.3815531807
SNV in ATM	0.4481498317	0.3815697178
SDHC amplificatio	0.8001153276	0.3844762656
ENG amplificatio	0.5006230055	0.384740901
TRIM37 amplificatio	0.6622151557	0.3850178853
Lab value: URBC	1.052878965	0.3872658724
SNV in NOTCH1	1.683567984	0.3877095166
EWSR1 deletion	1.404040823	0.3878222149
CHEK1 amplificatio	0.198978903	0.3882435318
XRCC5 amplificatio	2.222432095	0.3888452148
HLA_C_0304	1.30700056	0.3890380071
TMB_binned1	0.7945635592	0.3891970577
ATM deletion	0.7740987304	0.3899897666
NPRL2 deletion	0.6660915765	0.3906113755
CHEK1 deletion	0.6422445544	0.3911012826
ABL1 amplificatio	0.5745809104	0.391400854
Lab value: FRT4M	1.836621986	0.3915633938
TCEB1 deletion	0.1095071809	0.3922367004
BAP1 amplificatio	0.3625213029	0.3927812127
CUX1 deletion	0.4685070477	0.3929519332
SMAD4 deletion	1.299008154	0.3932266344
HLA_B_1401	0.001954841398	0.3935513531
PRS: PMID27863252	1.09104877	0.3936464434
TAZ amplificatio	0.2924534457	0.3942537966
HFE amplificatio	0.6852424438	0.3960193741
PRS: PRSWEB_PHE	0.9160719334	0.3961214369
ALK amplificatio	0.6100214266	0.3974065009
CD274 deletion	1.231691098	0.3988140039
CDK4 deletion	1.532835304	0.3988517438
RUNX1T1 deletion	2.505844971	0.3988817539
NOTCH3 amplificati	0.08782611136	0.3992809704

FBXW7 amplification	0.1933382885	0.3995237078
KDM5C amplification	0.1174761463	0.399606827
HLA_B_1501	0.6788343536	0.4006125205
GNB2L1 amplification	2.130413888	0.4008833981
PRS: UKB_460K.rep	1.120997356	0.4018209575
HLA_A_3001	1.802785869	0.402112953
PHF6 amplification	0.3238813775	0.4021393675
GPC3 deletion	0.2252503707	0.4021500569
UIMC1 deletion	0.5186771598	0.4022817606
Lab value: GGTL	0.974619683	0.4044061122
NFKBIA amplification	0.6007467402	0.4049122519
RPA1 deletion	0.731689467	0.405505163
ARAF amplification	0.04278916491	0.4067397699
BABAM1 deletion	0.1621573857	0.4069662194
DDR2 amplification	0.8074966432	0.4074347286
RBL2 amplification	0.08882347368	0.4096201724
HLA_B_5101	0.6932806766	0.4111056418
EGLN1 deletion	3.686610908	0.411434798
FAN1 amplification	0.06368745459	0.412569869
ESR1 amplification	0.5839646959	0.4133107683
PRS: PMID27863252	0.9177833805	0.413329351
NT5C2 deletion	0.6962823718	0.4141880874
PRS: PRSWEB_PHE	0.9135887825	0.4162859749
DCLRE1C deletion	0.6905082046	0.4164473131
PRS: PRSWEB_PHE	0.9149945921	0.4174516312
CCNE1 amplification	0.7629518488	0.4181365788
MTAP deletion	0.7529348518	0.4183534194
DDB1 amplification	0.1904520844	0.4184645698
VEGFA amplification	0.7331866978	0.4185727779
PRS: UKB_460K.rep	1.096308459	0.4203316194
SH2B3 deletion	1.489388922	0.4207050125
ARHGEF12 deletion	0.6402357939	0.4207592199
HABP2 deletion	0.682382063	0.4217549095
SMARCB1 deletion	1.383359224	0.4224957407
AXL deletion	1.691725521	0.4234140407
TAL2 deletion	1.831501005	0.4239990411
MITF deletion	0.7622300268	0.4241152659
SNV in SETD2	1.491993814	0.4247949476
EPHA3 deletion	0.6890039338	0.4249086486
EPCAM amplification	1.956253194	0.4249666301
U2AF1 amplification	0.6214195074	0.4262389044
TSC1 amplification	0.6076141682	0.4262779301
AKT2 deletion	1.66415995	0.4263864762

PRS: PMID27863252	0.9103739484	0.4277195902
CDK2 deletion	2.140105363	0.4284445577
RELA amplification	0.237530616	0.4285144717
PRS: PRSWEB_PHE	0.9106740424	0.4292077716
BRE deletion	0.0171086929	0.4299394471
APC amplification	1.603254505	0.4299457723
PRS: MEDS_P MID3	0.9163977161	0.430082262
CDC73 amplification	0.8164544443	0.4303360018
FLT3 deletion	0.7282594616	0.4326015241
IDH1 amplification	0.6125718233	0.4335419895
PRS: PMID27863252	0.923028857	0.4357013787
PRS: TRICL.ade.HM	0.9104779391	0.4361872281
Lab value: MEOS	1.297024852	0.4363400994
DDB2 amplification	0.2107723461	0.4365283618
KLF2 deletion	0.2290971297	0.4371737003
PRS: PMID27863252	0.9066257077	0.4374636943
HLA_DPB1_0402	0.7355995955	0.4376666465
MAP3K1 amplification	1.622631438	0.4380519526
SDHD amplification	0.4471520925	0.4381623349
NSD1 deletion	0.5459883718	0.4401778072
RNF43 amplification	0.6787395513	0.4412293962
PARK2 deletion	0.7908906934	0.4413157368
FAT1 deletion	0.5497951782	0.4413957966
CHEK2 deletion	1.351107475	0.4433811771
PRS: UKB_460K.bl	1.093824042	0.4433824886
CARD11 deletion	1.863307334	0.4439837028
MYD88 amplification	1.546763423	0.4455969153
EXO1 deletion	3.490069952	0.4458428552
TCF3 deletion	0.6112553247	0.4463586209
NFE2L2 amplification	0.6605335653	0.446680591
RAD51C amplification	0.6961043944	0.4469240525
PRS: PRSWEB_PHE	0.930056913	0.4478798625
NSD1 amplification	1.490597613	0.4485334012
BARD1 amplification	2.553053083	0.4488056368
ZNRF3 deletion	1.572331874	0.4488220997
SPOP amplification	0.6573359936	0.4505687428
Lab value: CEA	0.9513954206	0.4507646994
PRS: X20171017_M	1.085273778	0.4518114703
CDK4 amplification	1.252661485	0.4520271662
PRS: PGS000194_pl	0.9207601597	0.4536327676
PRS: PGS000195_pl	0.9207601597	0.4536327676
PRS: PGS000196_pl	0.9207601597	0.4536327676
PRS: PGS000197_pl	0.9207601597	0.4536327676

PRS: PGS000198_pl	0.9207601597	0.4536327676
PRS: PGS000199_pl	0.9207601597	0.4536327676
Lab value: MCV	1.012267503	0.4542981389
PRS: UKB_460K.dis	1.08430652	0.4548202703
MDM2 amplification	1.248432073	0.4557625292
SNV in ROS1	2.442877528	0.4571739809
PRS: PRSWEB_PHE	0.9188157453	0.4578563849
IKZF3 amplification	0.6053258359	0.4585442315
WHSC1 amplification	1.563680283	0.4591876629
SBDS deletion	0.486247859	0.4596616078
PPM1D amplification	0.6983609457	0.46033837
CYLD amplification	0.6003826911	0.4606137136
AXIN2 amplification	0.7015561816	0.4608124328
HABP2 amplification	0.009578735356	0.4613305723
CBFB deletion	0.6526433787	0.4621167953
JAZF1 deletion	0.04614446882	0.462192506
KLF4 deletion	1.662616415	0.4624839378
MAPK1 deletion	1.390076317	0.4625455931
PRS: UKB_460K.pig	1.124387197	0.4627762646
SH2D1A amplification	0.278016956	0.4645039993
HMBS deletion	0.677814291	0.4659621493
WT1 amplification	0.3190673664	0.4663146154
CDK5 deletion	0.06285669593	0.4663966792
HLA_DRB1_0401	0.7544641441	0.4668592594
PML deletion	0.5014907613	0.4675133608
HIST1H3B amplification	0.7325183135	0.4677048236
SNV in ARID1A	1.165697183	0.4680352196
RSPO3 deletion	0.752050842	0.4684456897
XPO1 amplification	0.6774288465	0.4696388592
TDG deletion	0.5467734124	0.4701329417
KDM6A deletion	0.2749417127	0.4727755253
TP53BP1 deletion	0.7064478194	0.4730749037
EXO1 amplification	0.7370747276	0.4742355682
ITK amplification	1.760467506	0.4744998009
ESR1 deletion	0.797282359	0.4761012958
FANCD2 amplification	0.6595407777	0.476131827
SLX4 amplification	1.707588021	0.4775936513
TERT amplification	1.215329243	0.4778936174
CD58 deletion	0.648788785	0.4779631186
ETV1 amplification	0.8252992991	0.4781860949
PRS: UKB_460K.blo	1.09666187	0.4782447703
MGA deletion	0.713228832	0.4787152665
MYB deletion	0.7989924415	0.4789478299

PRS: PMID27863252	0.9300409783	0.4794882964
DEPDC5 amplification	0.009277465758	0.4795708169
SNV in APC	1.303182924	0.4805563455
HLA_DRB1_0301	0.8469789734	0.480674541
FANCB deletion	0.2826160364	0.4815823902
SNV in TET2	2.123278272	0.4819772935
PHOX2B amplification	0.5830680177	0.482015225
NOTCH1 amplification	0.6162783957	0.4831254553
KEAP1 amplification	0.7025267022	0.4837355836
FLT1 deletion	0.7551756849	0.4839123044
TRAF3 amplification	0.1185543729	0.4845586594
Lab value: ABASO	16.23699443	0.4849639629
TRIM37 deletion	1.956431453	0.4853059064
SLX1A deletion	1.970505511	0.4860722389
LIG4 amplification	0.5750793387	0.4863785483
NTRK3 amplification	0.6150640731	0.4893593909
NEIL3 amplification	0.6308151731	0.4899612738
MEN1 deletion	0.591231799	0.4917849717
SMC3 deletion	0.7892933345	0.4920702843
PDCD1LG2 deletion	1.18681532	0.4932446322
HLA_C_1701	0.06511811093	0.4936692462
SUFU deletion	0.8070440657	0.4940441719
AKT3 amplification	0.8301198492	0.4975541126
PBRM1 amplification	0.442867119	0.4977732326
CEBPA deletion	1.469268012	0.4985805831
PRDM1 amplification	1.33074568	0.4991489037
PRS: Stratified_dist	0.9256840765	0.4993417516
GPC3 amplification	0.3961807265	0.4994061633
KIF1B deletion	1.347804612	0.5000028785
SLITRK6 deletion	0.6726222648	0.5001047769
RAD51 deletion	0.7239500187	0.5003619231
TSHR deletion	0.5916363549	0.5016684531
HLA_C_0501	1.249941374	0.5028720915
EXT2 deletion	0.6646085542	0.5031339424
NTHL1 amplification	1.613824471	0.5033676543
SOX9 deletion	2.044981267	0.5034108629
CDKN1B amplification	1.232709768	0.5037952382
TLX3 deletion	0.5974628962	0.5040226489
KMT2A deletion	0.7004692727	0.5045460356
SOCS1 deletion	0.6062023717	0.505273278
SRSF2 deletion	2.062162723	0.5063775333
MAP2K2 deletion	0.3553569386	0.5068916026
MRE11A amplification	0.4650936023	0.5100149378

DIS3 amplification	0.7145912364	0.5102303613
GATA3 amplification	0.6848014827	0.510373062
KDM5A deletion	0.5981454788	0.5111617684
RARA deletion	1.377430003	0.5118635414
PRS: GSCAN.Drinks	1.069156069	0.5123087978
SNV in BCOR	0.002869419024	0.5124516019
USP28 deletion	0.7160144998	0.5149284803
PTPRD deletion	1.283710955	0.5151089134
ASXL1 deletion	0.0003367107326	0.5160008858
PRS: PMID27863252	0.9270204622	0.5165610507
CSF3R deletion	0.7404095517	0.5185626933
DKC1 amplification	1.733808434	0.5188521368
AKT1 amplification	1.340243434	0.5188977072
HLA_C_0102	0.7629590591	0.5192547043
HLA_B_3501	0.7280163771	0.5192721784
PRS: PMID27863252	0.93789413	0.5196874083
NFKBIZ amplification	0.738063591	0.5197155167
PRS: UKB_460K.cov	1.072779234	0.5197595315
PPP2R1A amplification	0.629938108	0.5198541171
PRS: TRICL.sqc.HM	1.101116885	0.5201444425
LMO1 deletion	1.334484535	0.5202749122
MCL1 deletion	2.518404057	0.5220322437
SOX2 amplification	1.182657875	0.5227926601
AXL amplification	0.7670315458	0.5243993315
ERCC2 deletion	0.6654094424	0.5248004753
INSIG1 deletion	0.1079199324	0.5255097735
PRS: PRSWEB_PHE	0.9376562361	0.5258484823
MAF deletion	0.7165442534	0.5267266937
MAP2K1 amplification	0.6774841856	0.5278766873
NEIL3 deletion	0.5748475947	0.5301338164
XRCC6 deletion	0.5786658646	0.5307119204
MDM4 amplification	0.8521455334	0.5312310594
TCF7L2 deletion	0.80702615	0.5312815503
ATRX amplification	0.04433854743	0.5322049159
PRS: GSCAN.AgeOf	1.07894249	0.5324785012
FOXA1 amplification	1.395523417	0.5330693789
Lab value: CA125	0.9979316624	0.5334206721
MYBL1 deletion	1.570166191	0.5338429611
ENG deletion	1.551285115	0.5342022731
ZNF217 amplification	0.8239505158	0.5347124293
PRS: MEDS_PMI3	1.070955218	0.5352695118
Lab value: MALYM	1.938081042	0.5355580193
PRAME amplification	0.04765516035	0.5356273891

HLA_A_2402	0.8345949662	0.5356886036
IGF1R amplification	0.6692678808	0.5366177922
TAL2 amplification	0.6018361143	0.5373938214
SF1 amplification	0.0881491503	0.5374221784
Lab value: NEUT	0.9926974719	0.5376377104
MTOR amplification	0.6456125947	0.539514222
IKZF3 deletion	1.537603935	0.5403128788
RIF1 deletion	0.1614415145	0.5406804938
NR0B1 amplification	0.01998630971	0.5408549958
PRPF8 deletion	1.335992952	0.5411327122
BMPR1A deletion	0.8177301041	0.5415533143
PRS: Asthma.adults	0.9341774615	0.541598915
XRCC4 deletion	0.6837833174	0.5418443646
PRS: BRCA.ERNEG	1.069175946	0.5420088061
EPHA7 amplification	1.392389873	0.5443419458
STAG1 deletion	0.001259157264	0.5454174056
TDG amplification	1.383720319	0.5459963501
VHL amplification	0.7035537814	0.5463094039
ARHGAP35 amplification	1.582033396	0.5469783554
TMEM127 amplification	0.5912726364	0.5471562682
DMC1 amplification	0.6987509462	0.5474961872
PRS: PRSWEB_PHE	0.9361774136	0.5475959512
MAP3K1 deletion	1.219561182	0.5476721902
BRIP1 deletion	1.776377975	0.5480725707
PRS: MEDS_P MID3	1.077188726	0.5511773327
RIF1 amplification	2.17304831	0.5519262941
VHL deletion	0.7813170961	0.5526727993
PTEN deletion	0.823939506	0.5530535959
RAF1 deletion	0.7788948441	0.5535276066
PRS: PRSWEB_PHE	0.9286002573	0.5539864329
PRS: PMID27863252	1.068843782	0.5540805273
XRCC4 amplification	1.675292228	0.5545578215
PRS: PMID27863252	0.940589635	0.5548029795
PRPF40B deletion	1.664949875	0.5549296934
HLA_DPB1_0301	1.211583537	0.5549851569
MTA1 amplification	0.3007602258	0.5551459532
SLX1A amplification	0.01604681575	0.5555184618
DOCK8 amplification	0.5877092035	0.5556246063
MRE11A deletion	0.6791278829	0.556094356
PRS: UKB_460K.rep	1.076255101	0.5574767048
DMC1 deletion	0.5730363937	0.5600138486
FANCD2 deletion	0.7857687454	0.5614771179
RASA1 amplification	1.676347348	0.5629063157

PRS: PRSWEB_PHE	1.050689296	0.564728347
XRCC6 amplification	0.7041273681	0.5654386191
MTAP amplification	0.46297413	0.5660344763
KLF4 amplification	0.6472360984	0.5663772253
BRCA2 deletion	0.7987750693	0.5677069023
HLA_B_5301	0.002261315501	0.5680603323
PRS: UKB_460K.blo	0.9454199101	0.5684231884
INSIG1 amplification	1.299068151	0.5689994079
BCOR deletion	0.3055448326	0.5692694953
TNFAIP3 deletion	0.8355421096	0.5703460902
SDHAF2 deletion	0.6407202649	0.5706961886
Lab value: SGOT	0.9960510585	0.5723797929
SNV in ATR	1.598545501	0.5726649837
SUZ12 deletion	1.386199552	0.573595019
PRS: MEDS_P MID3	0.9429416836	0.5737514263
BCL2L12 amplification	1.308539083	0.5777694117
FANCB amplification	0.07999436792	0.5793568691
Lab value: BASO	1.18097913	0.5793570545
RASA1 deletion	0.7029870203	0.5793665297
FLCN deletion	1.166420778	0.5794130618
FGFR1 amplification	0.8151892573	0.579486554
YAP1 amplification	0.5638351617	0.5801170596
MED12 deletion	0.1552334262	0.5802466536
PTPN14 deletion	2.114441914	0.5803140077
Lab value: DBILI	2.528704847	0.5803973242
PRS: OVCA	0.947836938	0.5813243828
PMS1 deletion	0.7411398001	0.5816487613
PRS: MEDS_P MID3	1.064154726	0.5816681207
PRS: MEDS_P MID3	0.9466331133	0.5833074114
APC deletion	0.8134171332	0.5834306688
POLD1 deletion	1.409252665	0.5834338802
LMO2 amplification	0.3713357461	0.5841328628
ERG amplification	0.6097268583	0.586669524
CALR amplification	0.07016401241	0.587508988
ERBB2 deletion	1.289055745	0.5885701841
PRS: PMID2786325	0.9457671905	0.5909800076
HLA_B_0702	1.139810092	0.5912217736
NTRK2 amplification	0.6816333534	0.5914324733
Lab value: CA199C	1.013585751	0.5941240986
BCORL1 amplification	0.4072065752	0.5962584941
FGFR2 deletion	0.8463783559	0.5963784903
RUNX1 deletion	0.7346194973	0.5978012511
MSH2 amplification	0.7295212278	0.5981471989

PRS: UKB_460K.ca	1.071010618	0.5982883464
PPARG deletion	1.546433537	0.5996950656
HLA_DQB1_0201	0.8910561489	0.5998764778
PDCD1LG2 amplific	0.7929880988	0.6004427228
PRS: PMID2786325	0.9420663169	0.6004656114
BCL2 deletion	1.185030692	0.6005787358
FANCF deletion	1.281179346	0.6016080406
PRS: PMID2786325	1.055181513	0.6034929899
IGF2 amplification	3.044332531	0.605869979
Lab value: TSH	0.9737946027	0.6062001033
Lab value: CHOL	1.009974438	0.6074208365
H19 amplification	3.177488504	0.6075398865
FH amplification	0.8717710902	0.6087914722
SNV in ARID2	1.484151145	0.6096116912
PRS: UKB_460K.bo	1.062111741	0.6109504427
WRN deletion	1.1427041	0.6145724633
MEF2B deletion	1.316227464	0.615147737
MCM8 deletion	0.72962379	0.615352183
EPHA5 amplificati	0.6852613425	0.6155874019
Lab value: MBASO	1.508101926	0.6164176284
FANCI deletion	0.6904673223	0.6175168796
SRC amplification	1.281366429	0.617944181
SMAD2 deletion	1.176934702	0.6189084534
PRS: PMID2786325	0.9493058291	0.6205465949
PAXIP1 deletion	0.6466359186	0.6209912421
HLA_B_5701	0.8225744599	0.622189905
CSF1R amplificati	1.518201759	0.6247045196
FLT3 amplification	0.6338544172	0.6248942274
SF3B1 deletion	1.356353071	0.6265361141
Lab value: LYMPH	1.006285941	0.6281139903
CCND2 amplificati	1.162923072	0.6303667251
RAC1 amplification	0.8420082372	0.630942074
PRS: PRSWEB_PHE	0.9505951131	0.6322857822
SNV in KMT2A	0.6171373722	0.6330293361
HLA_B_4501	0.0004885550283	0.6340372446
ZNF708 amplificati	1.200685958	0.6346888338
Lab value: NRBC	0.5939603969	0.6361560435
COL7A1 amplificati	0.587359212	0.6372195151
NR0B1 deletion	0.2733920943	0.637294755
ARHGAP35 deletio	1.330262275	0.6380784007
KCNQ1 amplificati	2.720453921	0.6386904943
PRS: TRICL.ade1.HI	0.9466606529	0.640362277
FAH amplification	1.525510205	0.640811819

PRS: PRSWEB_PHE	1.05139931	0.6411449162
RBL2 deletion	0.7722444378	0.643035341
GLI2 deletion	0.6580090939	0.6436923047
PRS: MEDS_P MID3	1.049312694	0.6438673526
CRTC2 amplification	0.8649401883	0.6442297838
HLA_B_1801	0.8231449554	0.6445754453
PRS: CD_deLange2	1.061206252	0.6458796854
Lab value: AMONO	1.182327737	0.6463965072
MBD4 amplification	0.6916820046	0.6476777957
ZRSR2 amplification	0.6227799813	0.6483683384
PRKCZ amplification	1.507510064	0.6492185744
PRS: PRSWEB_PHE	1.046580651	0.6504872563
PRS: UKB_460K.br	0.9539435636	0.6506309036
XRCC2 deletion	0.6609422098	0.65197013
HOXB13 amplification	0.7827359667	0.6521909154
UBE2T deletion	2.01026691	0.6526984265
FANCI amplification	0.7006861495	0.6527687045
FAT1 amplification	0.7327094748	0.6535871052
PRS: PRSWEB_PHE	1.051161275	0.6548624488
CDKN1C amplification	0.3671148131	0.6572930394
SLITRK6 amplification	1.335235844	0.6578638352
MEF2B amplification	1.169569686	0.6589317564
BLM amplification	0.7586862965	0.6596722083
PRS: IBD_deLange2	0.9515871621	0.6609583495
WHSC1 deletion	1.29717279	0.6611449666
PRS: MEDS_P MID3	0.9503702673	0.6615677729
FLT4 deletion	0.8243292176	0.6632966159
PRS: PRSWEB_PHE	0.9518223736	0.6644948617
LINC00894 amplification	0.3369511917	0.6656455848
DKC1 deletion	3.048493258	0.6670356018
DNMT3A amplification	0.7576889491	0.6670749907
SETBP1 deletion	1.153361773	0.670982803
SNV in KMT2D	1.288485136	0.6711507356
JAK3 deletion	1.286776908	0.6712570922
PRS: ProstateCance	1.052283388	0.6714345861
TMEM127 deletion	0.2237694801	0.6718253888
ERCC6 deletion	0.8247096207	0.6719805155
FLCN amplification	0.04694641351	0.6721174424
PMS1 amplification	0.7917347025	0.6728555214
GNA11 deletion	0.7659437818	0.6734659829
PRS: PMID27863252	1.050506819	0.675306195
SNV in ARID1B	2.129565057	0.6761470761
BCL11B amplification	0.004864418212	0.6774663204

BRD4 amplification	1.154376841	0.6778628545
EXT2 amplification	0.6920793328	0.6780104179
SMARCA4 deletion	1.25707504	0.6782486948
WHSC1L1 amplification	0.7510682811	0.6791833483
ACVR1 deletion	0.3834228359	0.6800198988
CDKN2A deletion	0.9126743649	0.6807895337
Lab value: PTT	1.022739029	0.6810327876
HIST1H3C deletion	1.344432898	0.6813074369
XPA amplification	0.7420688765	0.6815074374
AURKB deletion	1.11472416	0.6821578402
MYCN amplification	0.7618841481	0.683209428
PDGFRA amplification	0.8198535838	0.6836534877
UIMC1 amplification	1.25182875	0.6844844436
SNV in STK11	1.295283482	0.6850582892
PRS: PRSWEB_PHE	0.9609630792	0.6860253773
SNV in TP53	0.8855354241	0.6865909235
GEN1 deletion	0.2794955832	0.6876137644
SERPINA1 amplification	0.3841481823	0.6896587117
PRS: UKB_460K.pig	0.9516588807	0.6899628246
CIITA deletion	0.7810141647	0.6925428379
KEAP1 deletion	0.7141079399	0.6928128401
PRS: TRICL.ade_s.H	0.9542215169	0.6930176275
MLH3 amplification	1.670753318	0.6941790145
RAD52 amplification	0.7706634452	0.6954413232
ID4 amplification	0.8438287415	0.6970021379
HELQ deletion	1.271790105	0.6972815555
PRS: PMID28067906	0.9375001177	0.698037036
PRS: PMID28067906	0.9375001177	0.698037036
PRS: PMID28067906	0.9375001177	0.698037036
TCF3 amplification	1.154645396	0.698815139
FANCE deletion	0.7537678646	0.6989583015
PRS: UKB_460K.dis	1.044975652	0.699382249
PRS: MEDS_P MID3	1.042946878	0.69975299
BABAM1 amplification	0.06283391301	0.7000429234
SRC deletion	3211.65304	0.7026017386
NPRL3 amplification	0.2465269501	0.7030356507
HIST1H3B deletion	1.33888702	0.7036132023
CREBBP amplification	1.243899388	0.7058989198
RBM10 amplification	0.2240182886	0.7061676285
PRS: TRICL.sma_s.f	1.044963443	0.7066468788
HRAS amplification	1.307184252	0.7099126796
Lab value: ALYMPH	1.063676091	0.710564752
Lab value: AEOS	1.385912906	0.7125144526

Lab value: URIC	0.9004774116	0.7137374941
KDM5A amplification	0.7811970939	0.7144143469
USP8 amplification	0.536963194	0.7153369179
PRS: GSCAN.Cigarette	0.9603401247	0.7154519392
VEGFA deletion	1.331224453	0.716039656
CTCF deletion	0.8222708059	0.7168969272
WT1 deletion	1.194158023	0.718865296
RHOA amplification	0.5867622208	0.7208358467
FLT1 amplification	0.7213293314	0.7209644275
KDR amplification	0.8372063149	0.721113837
SNV in PRKDC	1.219729527	0.7218359396
RNF8 deletion	1.33583999	0.7220494406
SOCS1 amplification	1.224581189	0.7221183483
GNB2L1 deletion	1.225746476	0.7222252183
PRS: UKB_460K.blocks	1.03226687	0.7231884638
Lab value: UPH	1.114338516	0.7233351249
RAD50 amplification	1.292170478	0.7235129125
PRS: PRSWEB_PHE	1.042148243	0.7241807996
JAK2 amplification	0.8617751235	0.724189751
FANCC amplification	0.7932402968	0.7244112742
RAC1 deletion	0.2901411207	0.7247421576
PIK3R1 deletion	1.130307537	0.7265721124
BCL2L1 amplification	1.121637586	0.7283363985
HLA_A_3201	1.177433997	0.7284706704
MUTYH deletion	0.8591873735	0.7290501547
Lab value: SQUAM	1.102033153	0.7291775201
CDKN1C deletion	0.8567196723	0.7295263478
Lab value: EOS	1.024214219	0.7310265939
ABCB11 amplification	0.6589230184	0.7310619151
Lab value: PHOS	0.8311406374	0.7317363956
TSHR amplification	1.972827906	0.7324556065
HLA_A_0301	0.9262468066	0.7329761769
CTNNB1 amplification	1.213719281	0.7378251478
BCL2L12 deletion	0.8560702434	0.7386647455
KCNIP1 amplification	1.31706179	0.7388373365
NRAS deletion	0.8652547688	0.7405484237
Lab value: FRT4	1.780479016	0.7410180065
NFKBIE deletion	1.298518641	0.7416984115
MYCN deletion	0.759519667	0.7452575621
XPC deletion	0.8735005062	0.746331173
Lab value: FRT3	0.7964095113	0.7471705187
DNMT3A deletion	0.7751389764	0.7497821758
GNA11 amplification	0.8887338265	0.751027718

PIK3C2B amplification	0.9212567589	0.7525092868
KMT2D deletion	0.7536753558	0.7536727773
LMO1 amplification	0.5904118965	0.7553863899
POLH deletion	1.278973793	0.7554206343
PRS: PRSWEB_PHE	0.9670779338	0.7559229143
EGFR amplification	0.9146065707	0.7566605721
CIITA amplification	1.123256704	0.7602264065
PRS: UKB_460K.bl	1.034378465	0.7609321143
HFE deletion	1.263876231	0.7631490579
IKZF1 deletion	1.278744385	0.7634026585
Lab value: PLCO2	1.014115876	0.7643091492
SNV in POLQ	1.68600881	0.7650683504
PRS: TRICL.all.HM3	1.036270307	0.7658563578
PRS: UKB_460K.oth	1.033992228	0.7663704859
Lab value: PNA	1.011881226	0.7666403903
HLA_C_0702	1.070911259	0.7670835421
SNV in COL7A1	1.623427521	0.7697495741
ETV6 deletion	1.127213122	0.7705220015
KAT6A amplification	0.8467717306	0.7709535027
PRS: MEDS_PMD3	1.031069377	0.7716958401
JAZF1 amplification	0.8951450483	0.7717601026
CDK1 amplification	0.0009070566823	0.7718593615
KRAS amplification	1.082230114	0.7733126534
CBFA2T3 deletion	0.8763763716	0.7772260771
MDM2 deletion	1.188180294	0.7781245686
PRKCI amplification	0.9224818759	0.7788111355
HLA_DPB1_0201	1.085159518	0.7815486517
HLA_B_4001	1.098570375	0.7826114107
FOXL2 deletion	0.8498883004	0.7851527751
CASP8 amplification	1.209774284	0.7863285838
PRS: UKB_460K.bl	1.033809738	0.7865076311
B2M deletion	0.9146839559	0.7874174506
AURKA amplification	1.082997683	0.7878114814
NEIL2 amplification	0.8138732241	0.7881837412
NBN deletion	0.7986906785	0.789526348
ERCC5 deletion	0.8887075397	0.789649342
CTLA4 amplification	0.8346163579	0.7899948324
RFWD2 deletion	1.455295927	0.790569485
MLH3 deletion	1.173435678	0.7921566288
BCL6 amplification	1.07650384	0.7927261047
ETV6 amplification	1.090748793	0.7928044278
PRS: PRSWEB_PHE	0.9709849928	0.7936519634
PRSS1 deletion	1.186748096	0.7952568224

U2AF1 deletion	1.161155282	0.7961987205
NPM1 deletion	1.12149267	0.7963640868
SNV in EP300	0.6747685896	0.7977906192
OGG1 deletion	1.222779221	0.79783618
HLA_DQA1_0301	1.060678624	0.7981214044
CCND2 deletion	0.8971887999	0.7984005272
Lab value: HCT	1.00571482	0.7987651132
SH2D1A deletion	0.5243336547	0.7991119367
ABCB11 deletion	0.5710032208	0.8010108837
FKBP9 amplification	0.8781421825	0.8018780209
GLI3 amplification	0.8749251203	0.8024278671
PIK3CA amplification	0.93158975	0.8029398425
POLB amplification	0.8671041847	0.8051507106
SNV in BRCA1	1.110440111	0.8053805931
MECOM amplification	0.9357377738	0.8074712842
STAT6 deletion	1.151166944	0.8075271937
CDK6 deletion	0.7982994302	0.8094470451
PRS: MEDS_PMI3	0.9712453767	0.8101408809
PRS: MEDS_PMI3	1.025847127	0.8101920595
LMO3 amplification	1.090639994	0.8102139086
MAP2K4 deletion	1.068317438	0.8110900234
PRS: PRSWEB_PHE	0.9741595436	0.8119883527
CRTC2 deletion	1.602940656	0.8120800306
ERG deletion	1.213684033	0.8121897937
RAF1 amplification	1.118919705	0.8122122179
ACVR1 amplification	1.229111016	0.8127713964
NRG1 deletion	0.9101364037	0.8129745947
Lab value: RETCP	1.829705071	0.814489402
PRS: PMID2786325	0.9705846162	0.814781847
MYC deletion	0.6760600359	0.8148164289
RFWD2 amplification	1.07501738	0.8154463049
RHOH amplification	1.225272086	0.8167458296
Lab value: MCH	1.010170846	0.8186534766
ERCC3 deletion	0.832612745	0.8209795257
SDHA amplification	1.081916424	0.82225106
Lab value: TBILI	0.9361569788	0.822768435
PRS: UKB_460K.dis	1.024860619	0.822943161
CTNNA1 amplification	1.18261966	0.8245444123
POLB deletion	0.9063899223	0.8254342312
REL amplification	0.9059714185	0.8257026731
PRS: UKB_460K.dis	1.023225441	0.8260880137
PRS: PRSWEB_PHE	1.02612489	0.8271195622
SERPINA1 deletion	1.147698705	0.8279569912

PRAME deletion	1.1358027	0.8286819105
PRS: PRSWEB_PHE	1.023231382	0.8292229184
PRS: PRSWEB_PHE	1.022409033	0.8293603064
CDKN2B deletion	0.9530909663	0.8312876928
TSC2 amplification	1.129639418	0.8314362934
CD274 amplification	1.078577475	0.8315159454
FAM46C deletion	1.094502507	0.8324043525
PRS: PMID27863252	0.9767397593	0.8336503845
PRS: UC_deLange2	1.023680353	0.8339470234
FGFR2 amplification	0.8445939477	0.8347988133
HELQ amplification	0.4589264876	0.8362505474
PPARG amplification	1.142344767	0.8374108158
CIC deletion	0.585136413	0.8375720232
SETD2 deletion	1.065609869	0.8411000272
PRS: Asthma.age_o	0.9766632843	0.841874855
PRS: PMID27863252	1.022948496	0.8418806835
SLC34A2 deletion	1.118750717	0.842183371
MTA1 deletion	1.135165829	0.8424067517
PRS: GSCAN.Smoki	1.021328075	0.8447288379
OGG1 amplification	0.8385040152	0.8448666823
KIT amplification	0.9196917123	0.8453269216
SDHA deletion	0.8912342783	0.8460030867
Lab value: MCHC	0.976061677	0.8460668845
DICER1 deletion	1.066390572	0.8467341975
PRS: UKB_460K.imp	0.9789487335	0.8479490512
FANCL amplification	0.9011988022	0.8480527711
Lab value: MAMON	1.409754077	0.8480608472
FOXA1 deletion	1.178205792	0.8483553745
RELA deletion	1.348990876	0.8499241248
PRS: MEDS_P MID3	0.9725226259	0.8502774654
PRS: UKB_460K.car	0.9782582745	0.8503620313
ELANE amplification	0.6878713428	0.850555612
DICER1 amplification	1.123631076	0.8511850109
GNAS amplification	1.057692587	0.8514664635
HLA_C_0602	1.052179743	0.8518722001
NPM1 amplification	1.077401312	0.851998235
PRS: MEDS_P MID3	1.021092307	0.8524344085
HLA_A_6802	1.369006682	0.8533779039
MAX amplification	0.8677412208	0.853625169
PRS: UKB_460K.dis	0.9775080202	0.8545168319
CADM2 amplification	0.6414549286	0.8546550838
TRAF3 deletion	1.121966603	0.8552981074
RECQL4 deletion	0.6794739592	0.8554282464

CRTC1 amplification	1.068625373	0.855900989
PRS: UKB_460K.dis	1.022015259	0.8559349979
MLH1 deletion	0.9381553603	0.8564322591
RAD51 amplification	1.296218774	0.8571125726
TET1 amplification	0.6641668475	0.8573197803
FAS deletion	0.9456473437	0.8575612224
SBDS amplification	0.9414353131	0.8581314583
PTCH1 amplification	0.8873606301	0.8583013815
RHOT1 deletion	1.177839824	0.8593048907
FAM175A amplification	0.5006545553	0.8614629797
GLI1 deletion	1.102111319	0.8614774198
HLA_A_6801	1.080708863	0.8620239844
PRS: MEDS_P MID3	1.020016145	0.8625851102
CDH4 amplification	0.9138193963	0.8626849048
PRS: UKB_460K.dis	1.02187455	0.863393788
GNAQ amplification	0.8876018341	0.8640882666
DIS3L2 amplification	0.8526820852	0.8646509686
PRS: UKB_460K.dis	1.019316646	0.8651448179
HLA_A_2601	1.086897663	0.8652625584
PALB2 amplification	0.8796065247	0.8661124616
PTK2 deletion	0.6810072686	0.8663291756
KAT6B amplification	1.157956781	0.8663664765
FANCM amplification	1.118554811	0.8666806243
SMARCA4 amplification	1.060414717	0.8671163273
KAT6A deletion	0.9292588306	0.8686345337
STK11 amplification	0.9429098537	0.8687540855
PIK3R1 amplification	1.121106562	0.8704065623
HLA_DRB1_0404	1.124991749	0.8720665595
MUS81 deletion	1.292039243	0.8720837655
ARAF deletion	0.6592663846	0.8742648112
EXT1 deletion	1.244611239	0.8758664195
CDK5 amplification	0.9343096315	0.8760113083
ARID2 deletion	0.9159036176	0.876060842
PRS: PRSWEB_PHE	0.979767746	0.8768666727
ERCC2 amplification	1.056650288	0.8804448185
TMPRSS2 amplification	0.9137962617	0.8807886415
DAXX deletion	1.132465665	0.8811471502
HLA_DQB1_0302	1.040485877	0.8828525726
PRS: PMID27863252	0.9842105236	0.8846694223
GREM1 deletion	0.9352296985	0.8851730902
CDH1 amplification	1.073817231	0.8853653053
ERCC4 amplification	1.081642513	0.8857412982
PRS: UKB_460K.me	1.016919267	0.8857901548

HLA_A_1101	0.944176739	0.8861528674
RAD21 deletion	0.7627852566	0.8878771864
PRS: UKB_460K.lun	1.017045761	0.889781711
DCLRE1C amplifica	1.122758262	0.8898736935
IKZF1 amplification	0.9580918318	0.8900404374
MPL deletion	1.060891152	0.8914886167
PRS: UKB_460K.rep	1.018078208	0.8923595428
PRS: UKB_460K.pig	1.016501719	0.8955980173
SOS1 amplification	0.9132156477	0.8963083235
FANCM deletion	1.114908499	0.8963466733
HLA_B_1302	0.9205037981	0.8966658671
RHPN2 amplificatio	0.9404668167	0.8967941771
BAP1 deletion	1.042145599	0.8980491607
FGFR3 amplification	0.9378618459	0.8984243793
PRS: Stratified_fem	0.9841052464	0.8989845937
CXCR4 deletion	0.8166517216	0.8993023653
GATA2 amplification	1.080101623	0.9000427566
TET2 amplification	1.117142207	0.9000695078
PRS: UKB_460K.bo	0.9852123008	0.9011296014
Lab value: PCL	1.004138976	0.9041233345
DOCK8 deletion	0.9586818551	0.9048523751
GATA4 deletion	0.9692712284	0.906660159
Lab value: USPG	49.89897742	0.9100286331
TP53 deletion	1.030132137	0.9105712917
MGA amplification	1.176580437	0.9111489718
TCF7L2 amplificatio	0.909634789	0.9119864744
TMPRSS2 deletion	1.100669571	0.9124427083
PRS: MEDS_P MID3	1.013905816	0.9128909341
PRS: TRICL.sqc_s.H	1.01549496	0.9132008442
CDK8 amplification	0.8852453463	0.9139687841
WHSC1L1 deletion	0.9552579876	0.9141132813
PRS: PMID27863252	0.9886818225	0.9151607652
AXIN2 deletion	1.103871686	0.9171141415
PRS: PRSWEB_PHE	1.01109454	0.9177487393
PRS: Asthma.childr	0.9866831645	0.9178051725
HLA_DQB1_0402	0.8822900064	0.9182607996
PRS: UKB_460K.bo	1.0109969	0.9186430515
PRS: UKB_460K.rep	1.01255359	0.9187849823
CARD11 amplificati	1.026882206	0.920559039
RINT1 deletion	1.109003559	0.9210333
PML amplification	1.111524354	0.9218438752
CXCR4 amplificatio	0.7977341388	0.9225179943
Lab value: HGB	1.005999533	0.9232369657

ERBB3 deletion	0.9454188693	0.9236397072
TFE3 amplification	1.212860534	0.9242402103
Lab value: ANION	1.006630782	0.9244927867
PRS: PRSWEB_PHE	0.9902563101	0.9245261871
PRS: UKB_460K.pig	0.988785433	0.9251329382
MYD88 deletion	0.9678321507	0.9258786039
Lab value: RDW	0.9956179122	0.9275528667
Lab value: RBC	1.016444942	0.9276385994
PTK2B deletion	1.035127667	0.927737634
PNRC1 amplificatio	0.9421724306	0.9277756897
XRCC3 deletion	1.058000615	0.9283064766
XPC amplification	1.044343031	0.928380255
Lab value: WBC	1.003233158	0.9292914297
EP300 deletion	1.04059046	0.9293436358
PRS: PRSWEB_PHE	0.9901162172	0.929489311
PRS: X25HydroxyVit	0.9867066137	0.929634423
HLA_B_2705	1.050157231	0.9302007918
TERT deletion	0.9601511187	0.9312546804
FAN1 deletion	1.041533464	0.9312626473
HLA_A_2501	1.064971934	0.9312940204
RSPO2 deletion	0.7788751325	0.9316568253
FUS amplification	0.9533883127	0.9330640406
XRCC1 deletion	0.8721804247	0.9346384082
FBXW7 deletion	1.03024272	0.9350180911
MAFB amplification	1.039796409	0.9368976229
LMO2 deletion	0.9602970199	0.9386807464
PTK2B amplificatio	1.060524203	0.9387134098
HLA_B_5501	0.9529822168	0.9388820296
CASP8 deletion	1.186006329	0.939147981
PRS: UKB_460K.dis	0.991839716	0.9410934955
ETV5 amplification	0.9805125387	0.9425076061
CDKN2C deletion	0.9722553525	0.9431604443
PIM1 deletion	1.050298212	0.9433692363
PRS: MEDS_PMIID3	1.007959765	0.9434872195
PRS: PMID27863252	0.9928799005	0.9443774613
MCM8 amplificatio	0.9523068509	0.9446426599
PRS: PRSWEB_PHE	0.9928907689	0.9455508489
WAS amplification	1.143779377	0.9461718757
NOTCH2 deletion	1.0327587	0.9462624285
BRCC3 deletion	0.8479509128	0.9472904566
PRS: PRSWEB_PHE	1.007008544	0.9475741129
GALNT12 amplificat	1.052871444	0.9484675007
ERCC3 amplificatio	0.9465802652	0.9490746485

ERBB4 amplification	1.046139216	0.9498103085
CDKN1A deletion	0.9572393461	0.9511647825
ROS1 amplification	1.037330267	0.952085043
TP53BP1 amplification	0.9086419426	0.953019076
HLA_DPB1_0401	1.01102774	0.9533150429
HLA_B_3801	0.9657659762	0.9534384333
LIG4 deletion	1.039169356	0.9545427461
FGFR4 deletion	1.022251565	0.9558034848
CRKL deletion	1.027761725	0.9561657938
HLA_C_1203	1.017811158	0.9572343143
DDB1 deletion	0.9017106886	0.9584762643
PRS: TRICL.sqc_ns	1.006422957	0.9588598321
PRS: PRSWEB_PHE	1.005413486	0.9609496517
TFE3 deletion	1.236337867	0.961256813
WAS deletion	1.236337867	0.961256813
ERCC5 amplification	0.9794591705	0.9622038461
JAK3 amplification	0.983489919	0.9623304233
SQSTM1 amplification	0.9727597252	0.9626838868
CD79B deletion	1.040727525	0.963176758
PRS: UKB_460K.dis	0.9937640441	0.9634619015
PRS: MEDS_P MID3	1.005431894	0.9634964093
FGFR3 deletion	0.9797652367	0.9642436164
NEIL2 deletion	0.9833653187	0.9653591837
SNV in MGA	0.8810024004	0.9660283411
PRS: PMID27863252	0.9957154121	0.9660345909
PRS: TRICL.ade1_s	1.005172127	0.9662163906
BRD4 deletion	1.028261243	0.9679296962
Lab value: DMANUT	0.9950376721	0.9679735419
PRS: PMID27863252	0.9949741607	0.9691883538
POLD1 amplification	0.9695343327	0.9706371056
AKT1 deletion	0.9878851725	0.9724581222
FANCA amplification	0.9757392811	0.9735522011
PBRM1 deletion	0.9890473518	0.9738792719
Lab value: ANEUT	0.9984341336	0.9740599929
QKI deletion	1.009683417	0.9747382126
BCL11B deletion	1.019066003	0.9761271058
PRS: GSCAN.Smoki	0.9968347461	0.9769677884
NRG1 amplification	0.9783910664	0.9780479073
STK11 deletion	1.013344112	0.9785940132
DIS3 deletion	0.9896211661	0.9790869234
DDB2 deletion	0.9871682522	0.9794243105
PRS: PRSWEB_PHE	0.9972161363	0.9796718144
CCND3 deletion	0.9801229889	0.9799068865

Lab value: PK	1.008492781	0.9802235491
SNV in CREBBP	1.01987343	0.9816829083
PRS: UKB_460K.blo	0.997840337	0.9831493676
PRS: UKB_460K.cov	0.9972730873	0.9834955395
PRS: TRICL.smoker	0.9977510042	0.9843790908
PRS: PRSWEB_PHE	0.9981591882	0.9864028363
RBM10 deletion	1.077440162	0.9864123903
HLA_A_2301	1.005499337	0.9899979977
PRS: PRSWEB_PHE	0.9986267771	0.990026711
CTLA4 deletion	1.029057733	0.9901551282
PRS: UKB_460K.dis	0.9988039266	0.9912128252
PHOX2B deletion	1.004834881	0.9916671588
CBLB amplification	1.003719273	0.9920268895
CTNNB1 deletion	0.9969669751	0.992889449
TAZ deletion	1.021980304	0.9929292481
NTRK1 deletion	1.011562655	0.9930403156
PRS: UKB_460K.blo	0.9991668495	0.9944127287
PRS: PRSWEB_PHE	0.9992649344	0.9946009711
SLC34A2 amplificat	1.005635564	0.9950440776
EPHA5 deletion	1.002364646	0.9958365143
ASXL1 amplificator	1.001288142	0.9969929254
AKT2 amplification	1.000996708	0.9976540872
SLC25A13 deletion	1.002809485	0.9978765417
Lab value: LIPASE	1.000025315	0.9985065475
MED12 amplificatio	0.7247086996	0.9992168184
LINC00894 deletion	0.3793687701	0.9994770059
SNV in STAG2	0.4685790378	0.9998049289
CSF1R deletion	0.9998719684	0.9998238112
AURKB amplificatio	0.6827227119	0.9998480575
GBA deletion	0.52536077	0.9998524322
AR amplification	0.8188294093	0.9999173731
RIT1 deletion	0.1809994975	0.9999200459
PVRL4 deletion	0.2007445671	0.9999781239

Search terms	Restriction of results
due to antineoplastic therapy	glucocorticoids and synthetic analogues
allergic reaction to drug	anemia
adverse effect	hepatitis c
toxic	immunosuppressive
autoimmune	infectious
drug-induced	anticoagulants
hepatitis	due to inhalation of food and vomit
endocrinopathy	insomnia
nephritis	constipation
pancreatitis	monitoring
uveitis	diagnostic agents
musculoskeletal	opium
carditis	opioid
cystitis	pancytopenia
arthritis	without complication
adrenal insufficiency	leukopenia
mucositis	agranulocytosis
myositis	clostridium difficile
pruritis	without esophagitis
sialadenitis	fever
bronchiolitis	non-steroid
myocarditis	malignant
ketoacidosis	nontoxic
colitis	chemo
pneumonitis	radi
dermatitis	chronic
neuropathy	cancer
hypothyroidism due to medication	nodule
hypothyroidism due to medication	history
	contact
	melanoma
	infection
	test
	cyst
	antibody
	viral
	bacteria
	noninflammatory